TECHNISCHE UNIVERSITÄT MÜNCHEN
Department Chemie
Fachgebiet Anorganische Chemie

Synthesis, Reaction and Deactivation Mechanisms of Copper Aluminate Spinel Hydrogenation Catalysts

Christoph Dörfelt

Vollständiger Abdruck der von der Fakultät für Chemie der Technischen Universität München zur Erlangung des akademischen Grades eines

Doktors der Naturwissenschaften

genehmigten Dissertation.

Vorsitzender:	Hon.-Prof. Dr. Richard Fischer
Prüfer der Dissertation:	1. Prof. Dr. Klaus Köhler
	2. Prof. Dr. Kai-Olaf Hinrichsen
	3. Prof. Dr. Moniek Tromp

Die Dissertation wurde am 08.02.2018 bei der Technischen Universität München eingereicht und durch die Fakultät für Chemie am 07.05.2018 angenommen.

Acknowledgements

First and foremost I want to thank **Professor Klaus Köhler** for giving me the opportunity to complete my PhD in his group. Amongst many things that I could list here, I want to particularly thank him for his continuously high interest in scientific problems, his open-mindedness to new ideas as well as his vast knowledge and experience in inorganic chemistry that I could rely upon.

The second group of people I want to thank are my old colleagues from the Köhler group at TUM, in no particular order: **Carmen Häßner, Florian Boch, Christoph Gnad, Patrick Bretzler, Oliver Thomys, Jian Zheng, Chenyang Wang, Xiaoqiao Zhao, Oliver Dachwald, Katharina Wussow, Andreas Wirth and Matthias Albert**. Thank you all for your help, the fruitful scientific discussions and for making the everyday life in our laboratory as entertaining as it was.

Thirdly, I want to thank all of my students, who contributed to this project. My two M.Sc. students **Alexander Wellmann** and **Clara Eisebraun**. Alexander's work was dedicated to model catalysts and catalyst stability. Clara's thesis focused on contributing to the reaction mechanism. My B.Sc. students **Matthias Feigel, Markus Schmidt, Steffen Sommer** and **Yean Man Tay** and of course thanks to all the students that accompanied this project for their lab-training en route to their M.Sc./M.Eng or B.Sc. **Lena Staiger, Moritz Eder, Christian Schneider, Christian Ladwig, Alexander Wellmann, Jonas Schlagintweit, Thomas Wylezich** and **Daniela Fey**.

The following people from Clariant Produkte (Deutschland) GmbH, our industrial partner, have to be thanked for their continuous effort within this project: **Manuel Pfanzelt, Frank Grossmann** and **Professor Richard Fischer**.

Our partners in Amsterdam (UvA) are thanked for their contributions to this project with XAS: **Michelle Hammerton, David Martin** and **Professor Moniek Tromp**.

I want to thank **Thomas Burger** for his help with ICP-OES and for his valuable input in catalyst characterization.

Carmen Häßner is acknowledged for measuring EPR samples and for her support with data evaluation and visualization.

Gabriele Raudaschl-Sieber is acknowledged for measuring MAS Al-NMR.

Ulrike Ammari, Petra Ankenbauer and **Bircan Dilki** are acknowledged for elemental analysis.

Many thanks to my best friends **Sebastian Eckstein** and **Johannes Wandt** for the serious discussions and hot noodle soup challenges at Onkel Lous soup kitchen to lift the spirits.

I want to thank **Melanie** for her continued support and patience while writing this thesis.

Last but not least I want to thank my parents **Sabine** and **Reinhart Dörfelt** for their continued and never ending support as well as my brothers **Matthias** and **Stefan**.

Abstract

Copper chromite ($CuO \cdot CuCr_2O_4$) hydrogenation catalysts have been successfully used for over 80 years. The production process using Cr(VI) containing raw materials and its possible residue raises concerns for workers and the environment. A possible, non-toxic alternative is copper aluminate ($CuO \cdot CuAl_2O_4$). While its catalytic activity is comparable to copper chromite, it suffers from stability losses in some applications.

At first, a catalytic test reaction and an activation procedure was developed with commercial catalysts. The liquid-phase batch hydrogenation of butyraldehyde in hexane (60 bar H_2, 120 °C, 1 h, 750 RPM) was used for benchmarking and all further experiments. Activation temperature for copper aluminates has to be higher (300 °C) compared to copper chromites (180 °C). 50 °C and pH 6.5 were identified as suitable co-precipitation parameters for copper aluminates from copper and aluminum nitrate with soda. An extensive promoter screening showed the beneficial effect of magnesium, likely due to smaller crystallite sizes and thus better interface/mixing between metallic copper and spinel. Promoters affecting the formation of spinel decreased activity. A good example is manganese, that was found to increase particle sizes and retaining copper in the spinel after activation.

Due to the introduction of sodium into the co-precipitates by using soda as a precipitation agent, its effect on catalyst formation was studied. Sodium content was controlled by variation of the washing procedure as well as by impregnation of sodium on regular catalyst ($CuO \cdot CuAl_2O_4$). Sodium was found to heavily interfere with copper aluminate spinel formation. Instead delafossite-like $NaAlO_2$ is formed. Moreover, copper oxide particles strongly agglomerate if sodium is present. The disintegration of spinel structure by sodium to form copper oxide and amorphous alumina was demonstrated for the first time.

The stability of copper aluminate can become an issue due to exposure to organic acids. Thus, the stability with regards to leaching and catalytic activity was investigated in the presence of carboxylic acids. Organic acids were found to inhibit the catalysts via competitive, reversible adsorption in the liquid-phase hydrogenation of butyraldehyde. Leaching of copper was generally low as expected for reducing conditons. Aluminum however was found to leach significantly (up to 2.4 wt-% of total Al) which is likely connected to the mechanic stability issues. Two methods to reduce leaching were identified. Silicon promotion did decrease leaching at the cost of catalytic activity. The co-feeding of ethanol decreased leaching even more while increasing activity. The *in situ* activation/reduction of the catalyst was shown under hydrogenation conditions with ethanol which could explain the increased activity but not the increased acid resistance.

Mechanistic studies with a wide range of model catalysts, characterization techniques and *in situ* experiments showed activated catalyst surface to consist of metallic copper, activated spinel and octahedrally coordinated Cu^{2+}. All obtained experimental data hint towards a reaction mechanism around a Cu^0/activated spinel interface, where the spinel acts as a Brønsted acid and metallic copper supplies electrons for the hydrogenation, which are subsequently replenished by hydrogen from feed.

Zusammenfassung

Seit ihrer Entdeckung vor über 80 Jahren sind Kupferchromite $CuO \cdot CuCr_2O_4$ bekannte Hydrierkatalysatoren. Ihre Produktion ausgehend von Cr(VI) ist problematisch bezüglich der hohen Toxizität. Eine mögliche Alternative stellen Kupferaluminat-basierte Systeme dar ($CuO \cdot CuAl_2O_4$), die in Ihrer katalytischen Aktivität der Chromitvariante ebenbürtig sind. Ein bekanntes Problem ist der Stabilitätsverlust in einigen Reaktionen.
Als katalytische Testreaktion wurde die Batch-Hydrierung von Butyraldehyd in flüssiger Phase (60 bar H_2, 120 °C, 1 h, 750 RPM) sowie eine Aktivierungsprozedur mit kommerziellen Katalysatoren entwickelt, die für alle weiteren Experimente benutzt wurde. Kupferaluminate benötigen eine höhere Aktivierungstemperatur (300 °C) als die Kupferchromitvariante (180 °C). 50 °C und pH 6.5 sind optimierte Syntheseparameter für Kupferaluminat-Katalysatoren, die man grundsätzlich ausgehend von Kupfer- und Aluminiumnitrat mit Soda fällen kann. Bei einer umfangreichen Untersuchung zum Einfluss verschiedener Promotoren auf die Aktivität wurde Magnesium als bester Promotor identifiziert. Die Kristallitgröße nimmt nach Magnesiumzusatz stark ab, wodurch eine höhere Durchmischung und Kontaktfläche zwischen Kupfer und Spinell erzielt wird, was sich wiederum positiv auf die Katalyse auswirkt. Alle Promotoren, die die Spinellbildung behindert haben, haben sich negativ auf den katalytischen Prozess ausgewirkt. Ein Besipiel hierfür ist Mangan, das größere Partikel begünstigt und Kupfer im Spinell nach Aktivierung zurückhält.
Durch die Co-Fällung mit Natrium wird dieses in die Katalysatorprecursoren eingebracht. Deswegen wurde der Effekt von Natrium auf die Bildung der Pre-Katalysatorphasen untersucht. Die Natriummenge wurde durch Veränderungen der Waschmethoden sowie gezielte Imprägnierung auf reine Prä-Katalysatoren kontrolliert. Dabei wurde ein starker Einfluss von Natrium auf die Bildung des Spinells identifiziert. Anstelle des Spinells bildeten sich Delafossit-artige $NaAlO_2$-Phasen. Hinzu kam die starke Agglomeration von Kupferoxidpartikeln. Des Weiteren wurde erstmals die Auflösung des Kupferaluminatspinells durch Natrium in Kupferoxid und amorphes Aluminiumoxid gezeigt.
Die Stabilität von Kupferaluminat-Katalysatoren kann zu einem Problem werden, falls diese Katalysatoren organischen Säuren ausgesetzt sind. Deshalb wurde die Stabilität bezüglich Leaching und Desaktivierung gegen Carbonylsäuren untersucht. Die organischen Säuren desaktivierten den Katalysator durch kompetitive, reversible Adsorption auf aktiven Zentren in der Hydrierung von Butyraldehyd. Das Leaching von Kupfer war,

wie unter reduzierenden Bedingungen zu erwarten, sehr niedrig. Überraschend war das hohe, gemessene Aluminiumleaching mit bis zu 2.4 % vom gesamten Aluminium, das höchstwahrscheinlich für die Stabilitätsprobleme dieser Katalysatoren verantwortlich ist. Zwei Methoden zur Verbesserung der Stabilität der Katalysatoren wurden gefunden. Erstens kann man durch Promotion mit Silicium eine Stabilisierung auf Kosten der katalytischen Aktivität erzielen, die durch die Bildung von Si-Al Mischoxiden erreicht wird. Zweitens kann durch das Zusetzen von Ethanol das Leaching bei gleichzeitiger Steigerung der Aktivität unterdrückt werden. Die Aktivitätssteigerung hängt höchstwahrscheinlich mit der *in situ* Reduktion des Katalysators unter Reaktionsbedingungen zusammen. Gründe für das reduzierte Leaching konnten nicht identifiziert werden.
Studien zum Reaktionsmechanismus am Beispiel von vielen Modellkatalysatoren und deren Charakterisierung, teilweise mit *in situ* Methoden, zeigen, dass die Katalysatoroberfläche nach Aktivierung aus metallischem Kupfer und Kupfer(II)-Ionen in oktaedrischer Koordinationsgeometrie besteht, sowie dem aktivierten Spinell. Alle Experimente deuten daraufhin, dass ein Grenzflächen-basierender Reaktionsmechanismus vorliegt. Die aktiven Zentren bestehen aus Cu^0 und aktivertem Spinel, der als Brønsted-Säure Protonen liefert, wohingegen metallisches Kupfer die Elektronen zur Verfügung stellt, die daraufhin von Wasserstoff regeneriert werden.

Contents

1 Introduction and Objectives

1.1 Hydrogenations and Standard Catalysts

Hydrogenations are among the most important reactions in industrial catalysis. Albeit losing to oxidation catalysis due to its sheer quantity (e.g. H_2SO_4), many chemical processes would not be possible without hydrogenation steps. These can range from a variety of hydrotreatments (HDT) such as desulfurization to avoid catalyst poisoning later in a process to hydrogenations for obtaining ingredients such as long chain alcohols for cosmetics [1].
The degree of complexity hidden in hydrogenation reactions is astounding. On paper however, a hydrogenation is a simple addition of a H_2 molecule to another, unsaturated molecule (see Fig. 1.1)

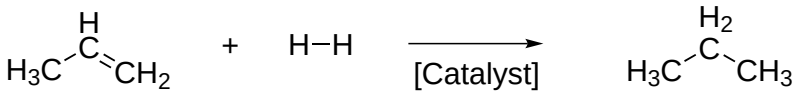

Figure 1.1: Simplified hydrogenation reaction.

Hydrogenation reactions are exothermic in the order of $\Delta G = -100\,\text{kJ/mol}$ and generally are reversible reactions. Due to its relatively high exothermicity, the reverse reaction, a dehydrogenation can simply be achieved by increasing reaction temperature. When the addition of hydrogen leads to the cleavage of a bond between for example A–B to form A–H and B–H, it is called a hydrogenolysis. The vast majority of hydrogenation reactions is conducted in the liquid phase. Fixed and trickle bed continuous operations make up the difference. In a liquid phase hydrogenation, usually a solid catalyst is immersed in a mixture of solvent and reactant, whereas hydrogen is supplied as gaseous hydrogen. For a successful hydrogenation, hydrogen gas would have to overcome several transportation barriers, diffuse into the pores of the catalyst, where the H_2 molecule is activated, typically to form surface M–H hydrides, which can then be added to the reactant to complete the hydrogenation. Any of the transport steps involved, which, for the sake of simplicity are only indicated here, can be the slowest, rate determining step of the process. A selective hydrogenation, i.e an addition of H_2 to a certain double bond in a multiply unsaturated reactant necessitates careful catalyst and reaction design. Finally, multiple degrees of complexity are added when one tries to understand a particular hydrogenation, i.e. reaction mechanism on a certain catalyst, which will be discussed within the scope of this work in later chapters.

Common hydrogenation catalysts typically consist of the platinum metals, nickel, copper or rhenium. The more expensive noble metals are usually immobilized on supports such as γ-Al_2O_3, whereas copper and nickel for example are used in bulk catalysts or even skeletal catalysts, which consist solely of the metal and possibly promoters [2]. Bulk catalysts are usually mixed oxides. They are synthesized via co-precipitation and thermal treatment. All catalysts have to undergo activation treatment either under reaction conditions (*in situ*) or with an extra activation step, where the active component (s. above) is reduced from its oxidic form to the metal, which is then able to cleave/activate the H−H bond. This work focuses on copper aluminate spinel catalysts, which have the idealized composition $CuO \cdot CuAl_2O_4$. These are known catalysts for hydrogenation [3, 4], methanol synthesis [5], oxidation [6], SCR of NO [7] and ethanol steam reforming reactions [8]. The following chapters will summarize the state of the art and demonstrate why these types of catalysts warrant further investigation.

1.2 Importance and Application of Copper Chromite and Copper Aluminate Spinel Catalysts

Copper aluminate ($CuO \cdot CuAl_2O_4$) and copper chromite ($CuO \cdot CuCr_2O_4$) catalysts share a similar composition. The chromite variant has been known and applied in commercial plants for quite a while (s. below). Due to stricter regulations by the European Union on 'substances with very high concern (SVHC)', Cr^{6+} (CrO_3) will be practically banned by September 22^{nd}, 2017. Manufacturers, suppliers and users will have to find alternatives before that date. For a copper chromite catalyst, an aluminate replacement could be the ideal solution. Thus, similarities and discrepancies of both catalysts, as far as they are known, are discussed below. Furthermore, it will be shown where and why further research is justified.

1.2.1 Copper Chromite as a Hydrogenation/Hydrogenolysis Catalyst

Mixtures of copper oxide and chromium oxide have been described as early as 1931 for being exceptional hydrogenation catalysts with high stability [9]. The so called Adkins catalyst has the following composition: $CuO \cdot CuCr_2O_4$. In a followup study, Adkins himself noted that the catalyst is neither a mechanical mixture of CuO and $CuCr_2O_4$ nor a simple chromite [10]. Adkins and Connor also noted that copper chromite was very active for the hydrogenation of aldehydes and ketones to their corresponding alcohols, as well as nitro-compounds to the primary amines. Benzene rings or in general C=C double bonds did not react. This selectivity is one of the features of using copper, and copper chromite in particular. These findings were supported in various studies throughout the years [11–13]. However, the preference for carbonyl groups changes in conjugated systems to an unselective hydrogenation [11] or to a preference of the C=C double bond [14]. Gallezot and Richard wrote an excellent review about the selective hydrogenation of α-β-unsaturated aldehydes with a chapter adressing copper chromite [15]. Due to the

selectivity issues in conjugated systems, copper chromite never found its way into large scale applications for such selective hydrogenations.

The largest field (industrial scale) of application for copper chromite catalysts is the hydrogenloysis of fatty methyl esters in the production of fatty alcohols, which are aliphatic alcohols with chain lengths of C_6 to C_{22}. Two thirds of fatty alcohols are used for surface active ingredients (surfactants). Cosmetics, polymers and other specialty uses make up the rest. Yearly production capacity is estimated to amount to 4.5 x 10^6 tons (2015) [16]. Depending on feed stocks, there are numerous synthesis routes to obtain fatty alcohols. The two largest feed stocks are petrochemical and natural sources. Natural sources are all plant and animal sources, which for example supply palm oil, consisting of C_{16} and C_{18} fatty acids. These fatty acids can be converted into the respective C_{16} and C_{18} fatty alcohols via a hydrogenation step. It can be done directly in a suspension hydrogenation, i.e. a copper chromite slurry. Alternatively, the fatty acids can be transesterified with methanol to the corresponding methyl fatty esters. These undergo hydrogenolysis in either gas phase fixed-bed or trickle bed reactors to form the fatty alcohols. Fatty methyl esters can be hydrogenated in milder conditions , while also seeing increased catalyst lifetime. Typical reaction conditions for the three process types are [17]:

1. Suspension hydrogenation: 250-300 °C, 25 MPa
2. Fixed bed (gas phase): 170-230 °C, 4-10 MPa
3. Trickle bed: 170-230 °C, 10-30 MPa

Synthesis routes (described in detail below) for the Adkins catalyst involve thermal decomposition of chromate precursors [18]. Incomplete decomposition results in leftover Cr(VI) in the catalyst, which is very problematic due to its properties. Cr(VI) is toxic, a carcinogen and hazardous to waters. This is why Cr(VI) is going to be a controlled substance in the EU, i.e. banned for the most part after the sunset date in 2017. Even in places where Cr(VI) is not as heavily controlled, its attributes will result in high costs for manufactures and users because of increased cost in occupational safety, transport and disposal. Thus, finding an alternative to chromite catalysts might not only offer a more sustainable alternative but also decreased cost.

1.2.2 Copper Aluminates in Catalysis

Possible chromium free alternatives to the Adkins catalyst are copper aluminates. Both share equivalent compositions of one part copper(II) oxide and one part copper chromite or aluminate spinel. The patent literature reveals a few attempts to replace chromium with aluminum and possible applications. Wegman et al. describe a vapor phase hydrogenation of esters and diesters catalyzed by a copper-aluminum catalyst promoted with a third metal. Their suggested calcination temperature of 300 - 550 °C however, is not sufficient to form the actual copper aluminate spinel phase [3]. Chen explicitly describes the development of a 'non-chrome catalyst for Cu/Cr catalyst applications' [19].

His proposed catalyst has to be calcined between 700-900 °C and thereby most definitely consists of $CuO \cdot CuAl_2O_4$ (see below). Applications range from hydrogenation of aldehydes and acids to hydrogenolysis of methyl laurate.

1.3 Catalyst Synthesis, Activation Procedure and Catalysis Reaction Mechanism

Over the years many synthesis routes have been established for both types of catalysts. Preferable routes usually go via precipitation steps, followed by washing, drying and calcination to obtain the oxidic spinel catalysts or pre-catalysts as they need to undergo activation/reduction. Copper chromite can be synthesized via precipitation of ammonium hydroxide, ammonium dichromate and copper nitrate [9]. Many chromite syntheses are described as thermal decompositions of precursors such as $[Cr_2Cu(NH_3)_2(OH)_6](NO_3)_2$, which are usually obtained with a prior precipitation/hydrolysis step [20].
Copper aluminate synthesis is conducted analogous for example by precipitation of copper nitrate and aluminum nitrate with sodium carbonate [3]. The necessity to wash the Cu-Al precipitates before thermal treatment has been mentioned [3, 19]. Calcination temperatures for both types of catalysts range from 400 - 900 °C [3, 9, 19, 20]. Temperatures of spinel formation vary for chromium and aluminum. Copper chromite spinel formation begins at lower temperatures compared to the aluminum variant [18, 21].
Both catalysts need to undergo reduction/activation treatment which is usually achieved in flowing hydrogen at elevated temperatures ($\leq$ 180 °C) [3, 19, 22]. While the formation of metallic copper on the spinel from copper oxide and spinel cupric ions is generally agreed upon, the reaction mechanisms as well as the existence and role of Cu(I) is controversially discussed. Yurieva et al. suggest that the spinel acts as a solid Brønsted acid and metallic copper supplies the electrons for the hydrogenation [23]. According to them the catalytic cycle is completed by regenerating Cu^0 with hydrogen from feed, which form protons located in the activated spinel structure. A second mechanism was proposed by Bechara et al., who where able to correlate Cu(I) amounts to hydrogenation activity and thus came to the conclusion that a Cu(I) species within the activated spinel is the active center [24, 25]. A mechanism involving the activation (i.e. dissociative adsorption) of hydrogen on metallic copper centers is also conceivable [26].

1.4 Scope of the Thesis

In this work, copper aluminate spinel hydrogenation catalysts ($CuO \cdot CuAl_2O_4$) were investigated and characterized with regards to their formation/synthesis, their hydrogenation reaction mechanism and their stability.

First of all, a test reaction was to be established including reactant and product analysis. The liquid-phase hydrogenation of butyraldehyde was used as a test reaction. Commercial catalysts (to eliminate possible errors of a synthesis step) are used for the benchmark to establish activation and test reaction procedure. Internal standards with a gas chromatography calibration enable a complete carbon balance.

The effect of synthesis and physico-chemical parameters for $CuO \cdot CuAl_2O_4$ catalysts were investigated in a next step, in order to identify possible correlations between these properties and catalytic activity. A large promoter-screening was conducted to help optimize catalyst composition. The influence of sodium ions, introduced by precipitation with soda (Na_2CO_3), should be identified.

Copper aluminate catalysts were described as less acid resistant in the literature, which is problematic with regards to processes that contain residual acids such as reactions with fatty acid methyl esters (FAME). A study about leachability of copper and aluminum as well as catalytic activity in the presence of carboxylic acids shall be conducted as a means to quantify and identify possible effects. Solutions to increase acid stability of these catalysts were found.

A contribution to the controversially discussed reaction mechanism should be made. Phase-pure spinel and varying supported copper model catalysts were to be synthesized, characterized and tested in the catalyt ic test reaction to identify the importance of the spinel phase and its interaction with copper in the activated catalyst. A mix of standard characterization tools such as TPR, XRD, N_2O-chemisorption were combined with *in situ* experiments (XRD, IR, EPR) to identify properties of the activated catalysts and thus deduce possible reaction mechanisms and active centers.

2 Liquid-Phase Hydrogenation of Butyraldehyde: A Catalytic Study of Spinel Catalysts

2.1 Literature Review and Motivation

An Adkins catalyst consists of equal parts copper oxide and copper chromite spinel. Promoter oxides usually account for $\leq$ 10 wt-% [22]. A typical x-ray diffractogram for an Adkins catalyst can be found in Fig. 2.1.

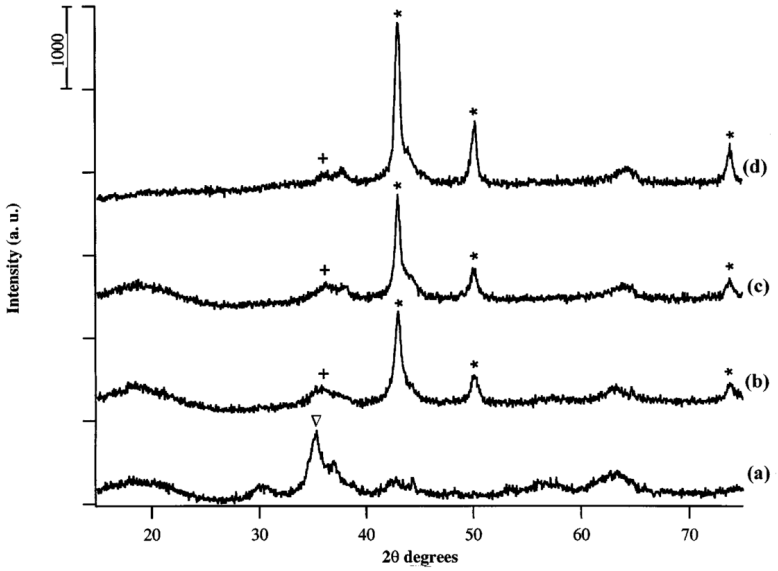

Figure 2.1: Typical x-ray diffractograms for Adkins catalysts before (a) and after reduction (b (473 K), c (573 K) and d (673 K)) with H_2 [27].

These catalysts are generally almost x-ray amorphous prior to reduction. Depending on thermal treatment, CuO can be completely amorphous as seen in Fig. 2.1. The reflex at 35.4° 2θ is indicative of the cupric chromite phase ($CuCr_2O_4$). After reduction, metallic copper particles are observed (43° and 51°) as well as a cuprous chromite ($CuCrO_2$) at 36.5° [28]. The reduction, also called activation, transforms the oxidic catalyst into a mixture of reduced and partially reduced phases. It is now ready to catalyze hydrogenation reactions.

For more details on the catalytic properties, synthesis and activation behavior one shall be referred to the general introduction (see Chapter 1). A literature review of possible

catalyic mechanisms as well as reduction behavior of spinels and cupric oxides can be found in Chapter 5.

2.1.1 Introduction to Spinels

Up to 50 mol-% of these catalysts consist of spinel phases ($CuCr_2O_4$ and $CuAl_2O_4$). Therefore, these types of crystal structures/minerals shall be introduced briefly. The name 'spinel' has its origin in the mineral $MgAl_2O_4$. It's crystal structure is a cubic close packing (ccp) of O^{2-} ions (s. Fig. 2.2).

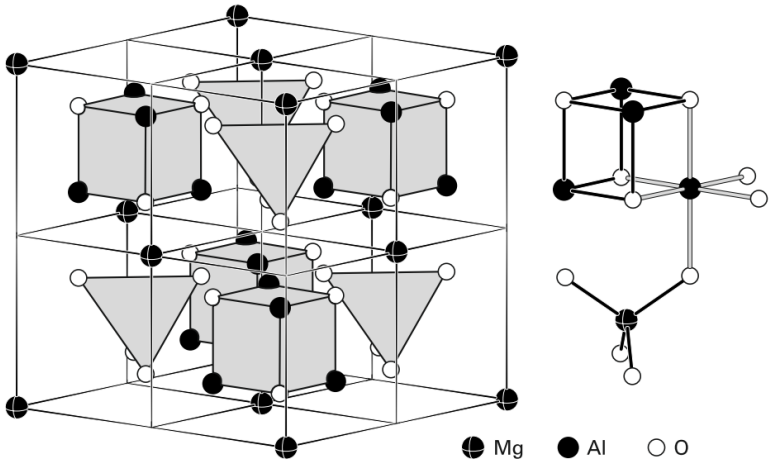

Figure 2.2: The spinel crystal structure [29].

½ of the octahedral sites are occupied by Al^{3+} and ⅛ of the tetrahedral sites are occupied by Mg^{2+}. Since the discovery of the mineral spinel, many more oxides with the composition AB_2O_4 have been found, that all crystallize in the same structure as $MgAl_2O_4$. Thus, the name spinel was given to the crystal structure itself. The most common spinels are aluminates ($Al_2O_4{}^{2-}$), ferrites ($Fe_2O_4{}^{2-}$) and chromites ($Cr_2O_4{}^{2-}$) with various A^{2+} ions from the first transition metal row offsetting the charge. An inverse spinel is formed, when A^{2+} and B^{3+} interchange positions, i.e. A^{2+} is located in the tetrahedral sites with half of B^{3+}, whereas the other half of B^{3+} is in the octahedral sites, resulting in a sum formula $B(AB)O_4$. The most common inverse spinel is magnetite (Fe_3O_4). Spinels with statistical distribution of A and B ions are called partially inverse. Another member of the spinel group are the defect spinels, where some of the octahedral and tetrahedral positions, that should be filled with either A or B, are empty. A typical example is γ-Al_2O_3, which is also a member of the partially inverse spinels, since Al^{3+} sits in both octahedral and tetralhedral sites [29, 30]. When one wants to predict the distribution of cations in the spinel crystal lattice, a variety of considerations can be made (such as charge, ionic radius). However, ultimately these considerations cannot accurately predict the distribution for all cases.

2.1.2 Motivation

In this first Chapter, a catalytic test reaction has to be developed to allow for all future syntheses to be benchmarked against copper chromite. As chromite should be replaced with aluminate, suitable activation and reaction parameters have to be identified. Physico-chemical properties are correlated to catalytic activity.

2.2 The Adkins Catalyst: $CuO \cdot CuCr_2O_4$

Commissioning and Benchmarking

For a comparative study of spinel catalysts, a benchmarking of a copper chromite catalyst as an established system was conducted. Benchmarking is an integral part of catalytic studies, offering the opportunity to repeat and reproduce the results by other research groups. Moreover the results can be put into perspective and be readily examined. For this work, an industrial $CuO \cdot CuCr_2O_4$ catalyst, promoted with manganese was used. These types of catalysts, regardless of promoter content, shall hereafter be abbreviated with 'CuCr'. A detailed description of the experimental setup can be found in chapter 7. Key points will be repeated here however, to display issues that had to be addressed. It should be emphasized, that the building and commissioning of the entire setup, with the exception of the autoclave, was part of this thesis. A successful experiment with these types of catalysts requires four basic steps:

1. Catalyst synthesis
2. Activation/reduction
3. Hydrogenation reaction
4. Product characterization

It is rather complicated to begin with all of these simultaneously hence the focus on an industrial benchmark to eliminate steps one and two. Step four, product characterization, is explained in detail in the experimental section (see chapter 7). The reaction that was studied over the course of this work, is the liquid-phase hydrogenation of butyraldehyde to butanol. In a first set of experiments, the temperature dependence of the reaction was measured. The results can be found in Figure 2.3. A typical curve for temperature dependence is obtained. At 90 °C only 12 % yields can be achieved. When the temperature is increased in a step-wise fashion, an exponential curve can be seen up to 50 % yield at 135 °C. Although the activation barrier for this reaction looks to be somewhat close to 90 °C, one should not speculate due to the complex nature of intrinsic kinetics, i.e. separation of transport phenomena such as product desorption. A simple experiment to check for transport limitations is a variation in catalyst mass. With only 50 % of the CuCr mass, yields of 16 % were achieved at 120 °C, which corresponds very well to the halved catalyst amount. It can be concluded, that the reaction is free of transport

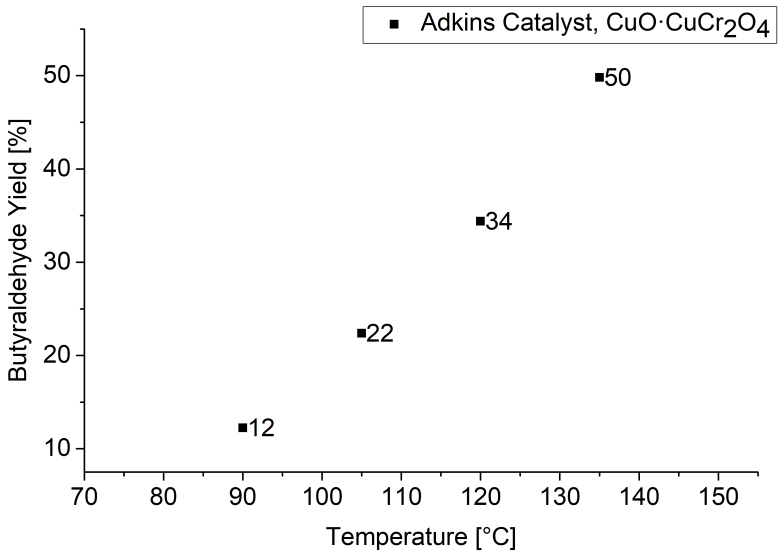

Figure 2.3: Butyraldehyde yields as a function of temperature with the Adkins catalyst [$p(H_2)$=60 bar, m(CuCr)=350 mg, 750 RPM].

limitations. Thus, a set of reaction parameters was determined for step 3, that allows for comparisons of different catalysts vs. the CuCr benchmark. This set of parameters is part of what is hereafter called 'the standard testing procedure'. An overview can be found in table 2.1.

Table 2.1: Paramters for the standard testing procedure for catalytic activity.

Reactant	Solvent	Temperature	$p(H_2)$	m(cat.)	RPM
Butyraldehyde	Hexane	120 °C	60 bar	350 mg	750

2.3 The Chromium Free Alternative: $CuO \cdot CuAl_2O_4$

Copper aluminate spinel is an industrially relevant, chromium-free alternative to copper chromite [3, 19, 31]. Its catalytic hydrogenation activities are described to be similar or better than those of copper chromite. Therefore, a commercial copper aluminate alternative was tested under the standard testing conditions (see table 2.1). It yielded only 10 % butanol compared to 34 % of the Adkins catalyst when in fact similar activities are expected. Two scenarios were identified, that could lead to this big discrepancy. First, an incomplete activation would result in activity losses, or second, reoxidation/passivation during catalyst transfer from the continuous activation reactor to the batch autoclave. The latter was addressed by modifying the transfer conditions with the implementation of Schlenk technique (comp. Chapter 7). Thus, reproducibility of these experiments reached very high levels for autoclave experiments (up to the first decimal). The first scenario however needed further investigation.

2.3.1 Catalyst Activation

Up to this point, a standard recipe for the reduction of copper chromite catalysts was used. Reduction was conducted in hydrogen flow (100 %, 40 mL/min) with a heating ramp of 15 K/min to 180 °C and holding for one hour. Since our catalyst was not as active as expected we could assume, that the activation conditions were too mild. A temperature programmed reduction experiment of the copper aluminate catalyst confirms the above hypothesis (comp. Fig. 2.4). TPR experiments were conducted with parameter constraints developed by Monti and Baiker [32] to ensure valid results. Further details are shown in the experimental section in chapter 7. The TCD-signal is equivalent to the hydrogen consumption on the y-axis when calibrated as such. On the x-axis the temperature progression is plotted. The reduction profile for this manganese promoted copper aluminate catalyst shows two overlapping peaks at 240 and 257 °C. An onset of reduction can be found beginning around 160 °C, where small copper crystallites form, which further catalyze the reduction of Cu(II). Thus, the reaction rate increases up to a maximum, which often coincides with a reduced copper fraction of 50 % ($X_{Cu} = 0.5$). Since the catalyst consists of two different oxidic phases, $CuO \cdot CuAl_2O_4$, which means different Cu(II) positions, one in CuO lattice the other in the spinel lattice, multiple reduction peaks are expected. An overlay of both peaks, albeit the very different lattice positions, can again be explained due to the catalytic nature of already formed metallic copper, which facilitates further reduction. To summarize, an activation temperature of 180 °C does not seem appropriate for experiments conducted on the laboratory scale. The scale has to be emphasized here, as a handful of differences to an industrial activation are present in these experiments. First of all, the catalysts activated in our experiments are powdered catalysts, whereas on an industrial scale tablets or shaped catalysts are used. The major differences are of course heat transfer and diffusion when one is working with shaped catalysts. The heat transfer of oxidic tablets is relatively low, thus local hotspots can increase the temperature above what is set to the reactor. Secondly, water diffusion from the tablets core can hinder reduction. Due to these issues, an industrial scale reduction is often extended over an entire week at low temperatures and low H_2 concentrations to avoid heat buildup or in the worst case a runaway of the reactor itself. Hence, it makes perfect sense to use higher reduction temperatures on the laboratory scale. The heat transport is much better with small powdered catalyst beds. Furthermore, the reduction was conducted in pure hydrogen flow, which in itself has a much better heat capacity than inert gases that are typically used to dilute the hydrogen, such as nitrogen, to avoid heat buildup during the highly exothermic activation.

Activation Paramter Study

Verification of the TPR results (Fig. 2.4) was done via an investigation of activation parameters such as heating rate, temperature and hydrogen concentration. In this fashion, an optimized parameter set for comparable catalyst activations between chromites and aluminates was obtained. The influence of heating rate during activation procedure with

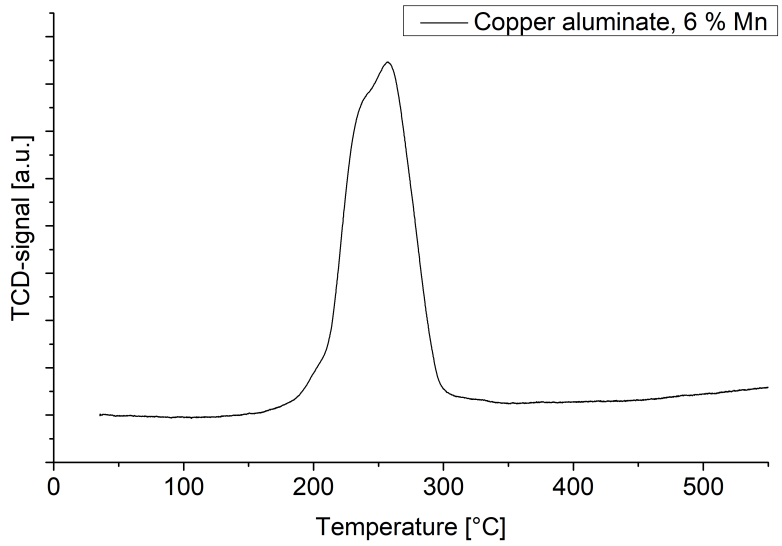

Figure 2.4: TPR profile of a manganese promoted copper aluminate catalyst.

adjusted, final activation temperatures is shown in Figure 2.5. Copper aluminate shows excellent yields of 30 % at 1 K/min and 300 °C. Higher ramps fare significantly worse, down to 15 % yields. On the other hand, copper chromite appears to be relatively stable over the wide range of heating rates tested. The experiment at 15 K/min and 180 °C however, exhibits the highest activity obtained. The biggest influence on catalyst activation has the activation temperature. Just how much it affects activity can be seen in Figure 2.6. These tests were conducted at rates of 15 K/min, which are disadvantageous for the aluminate variant as established above. Autoclave reaction temperatures were increased to 150 °C to vizualize the effects. At 180 and 240 °C not even 10 % yields are obtained. However, at 300 °C activation temperature catalytic yields suddenly jump up to 75 %.

Chromite catalysts give yields of about 95 % under the same reaction conditions, which can be explained by the 15 K/min rates being superior for Cr-containing catalysts.

Thus, an optimized set of parameters for the activation of both catalysts was found and verified. Copper chromite catalysts are readily reduced at 15 K/min and 180 °C with one hour hold time. Copper aluminate on the other hand, requires 1 K/min and 300 °C with one hour hold time. Using these conditions, the influence of hydrogen concentration was investigated. Diluting hydrogen from 100 % down to 25 % in nitrogen did not affect activity at all.

Active Structures

With the activation parameter studies we were able to confirm that both types of catalysts indeed are on similar levels regarding the catalytic properties in an aldehyde hydrogenation reaction. Nonetheless, the notably different reduction parameters give an interesting insight in possible discrepancies between both catalyst systems. If one thinks about he-

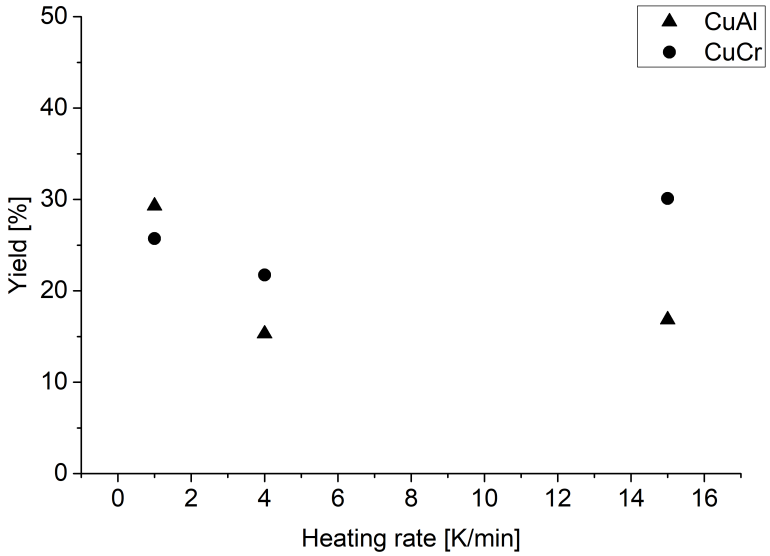

Figure 2.5: Effect of heating rate during activation on catalytic activity. Activation temperatures 300 °C for CuAl and 180 °C for CuCr.

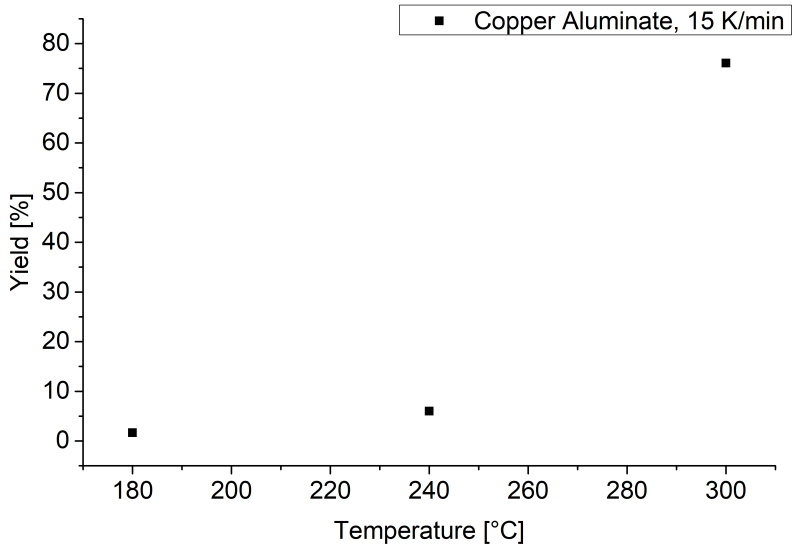

Figure 2.6: Effect of activation temperature for copper aluminate with 15 K/min (reaction temperature increased to 150 °C to visualize effect).

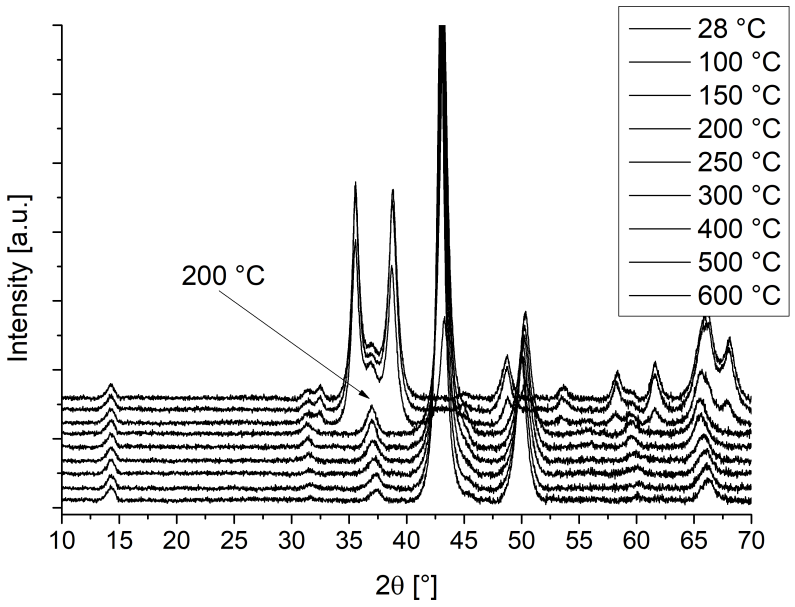

Figure 2.7: XRD patterns during *in situ* reduction of $CuO \cdot CuAl_2O_4$ catalyst in 5 % H_2 in N_2 (increasing temperature from top to bottom).

ating rate in terms of time since the isothermal zone was kept constant at one hour, then it is apparent that a fraction of the copper aluminate catalyst is reduced much slower than the Adkins catalyst. On the one hand, the Adkins catalyst is effectively reduced over the course of 72 minutes, whereas the copper aluminate catalyst on the other hand needs 5 hours and 35 minutes of reduction time. Higher activation temperatures would also hint towards higher activation barriers that need to be overcome, although a clean separation of kinetic and thermodynamic phenomena is of course not possible with these experiments. Regardless of what exactly happens during reduction, active structures of both catalysts must be similar, because of the similar catalytic behavior.

The actual catalysts not only consist of the spinel phase but excess CuO. To understand the role of CuO, which should be reduced at much lower temperatures compared to the spinel and thus offer catalytically active, metallic copper to catalyze reactions within the spinel, *in situ* XRD with an unpromoted $CuO \cdot CuAl_2O_4$ catalyst was conducted (Fig. 2.7). The diffraction pattern before reduction (28 °C) confirms the catalyst consists of two phases CuO and $CuAl_2O_4$. At 150 °C the intensity of the largest CuO reflexes at 35.5 ° and 38.8 ° is diminished. The formation of metallic copper at 43 ° and 50.4 ° occurs simultaneously. Beyond 200 °C, a sharp increase in the intensity of metallic copper reflexes is observed. CuO is not present and thus completely reduced at 200 °C. A cleaned up view is presented in Figure 2.8 with ICDD phase references. As expected, the reduction of copper oxide occurs at low temperatures. As early as 150 °C the reduction leads to notable changes in phase composition. The most intense reflex for the aluminate spinel can be found at 36.9 °. If one follows this reflex throughout this series up to 600 °C, it is apparent that the reflex shifts to 37.4 °. Similarly, the second and third most intense spinel reflexes at 31.3 ° and 65.3 ° respectively, also show this shift in angles 2theta to

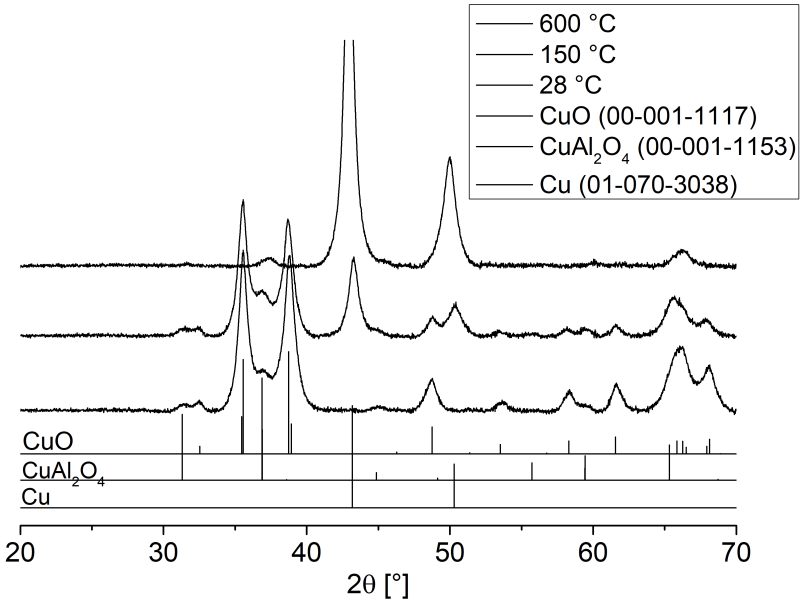

Figure 2.8: Detailed *in situ* XRD during reduction with references from the ICDD database (600 °C sample on top due to large reflex intensities).

higher angles. For this to be observed, constrictions of the spinel lattice must occur, thus shifting diffraction plane distances from eachother. Plyasova et al. were attributing this to the removal of copper from the spinel itself [33], which is the logical conclusion to draw when one considers the size of a Cu^{2+} ion that is removed and replaced by protons [33]. Furthermore, Plyasova and co-workers described aluminum to as well move within the spinel between octahedral and tetrahedral positions. In light of these findings, the shift in spinel diffraction reflexes due to constrictions of the unit cell during reduction can be explained. This means, that the same phenomena described by Plyasova et al. occur in the catalyst with excess CuO. Metallic copper from the copper oxide reduction thus does not hinder, i.e. via blocking of surface, the reduction of cupric ions from the spinel lattice.

Further proof of this phenomenon was collected in temperature programmed reduction experiments. The integral of the curve is equivalent to the consumption of hydrogen (compare Figure 2.4) which has to be calibrated with a known quantity of cupric oxide for example. If one looks at the stoichiometry of copper reduction (shown in equation 2.1), the theoretical amount of reduced copper can be quantified.

$$\mathrm{CuO} + \mathrm{H_2} \longrightarrow \mathrm{Cu} + \mathrm{H_2O} \tag{2.1}$$

In these experiments, copper reduction degrees of up to 96 % were found. Considering the catalyst consists of equal parts copper oxide and copper aluminate spinel and thus 50 % copper inside of the spinel lattice, it can be concluded that almost the entire amount of copper is reduced from the spinel itself (92 % of spinel Cu). Moreover, our experiments are in complete agreement with the findings of Plyasova et al., who conducted pioneering work on this field. They investigated the reduction of both spinels in question without

excess CuO as present in the catalyst. For copper chromite spinel, they found copper to be reduced from the spinel itself [34] and concluded the growth of epitaxially bonded, flat copper particles on the surface. Copper was also partially reduced to Cu(I) within the lattice, which is consistent with other literature describing $CuCrO_2$ as a side product of reduction [29]. Thus, a cation deficient spinel is obtained. The missing charge is offset by protons, which migrate into the lattice to form OH groups. Furthermore, the spinel is able to absorb hydrogen, which has been previously described by Jalowiecki and co-workers [5]. With neutron diffraction Plyasova et al. were able to locate the absorbed hydrogen in octahedral lattice positions close to tetrahedral Cu^{2+}. Overall, they attribute a high stability to the chromite spinel structure, that, in its entirety, resists reductive dissolution i.e. via formation of water.

Copper aluminate spinel showed very similar effects when reduced above 270 °C [33]. Cu^{2+} ions left the spinel structure, first from tetrahedral then from its octahedral positions, to form metallic, hemispherical particles on the surface. Again, the cation deficient spinel structure was stabilized via formation of lattice OH groups as well as by absorption of hydrogen. Two large discrepancies between both spinel types were found. As described, the authors proposed different shapes of metallic copper particles (flat, epitaxially bonded on chromite, hemispherical on aluminate) on top of the spinel surface after reduction. The second difference was found in reactivity of lattice oxygen. The chromite spinel was stable against lattice disintegration, aluminate spinel, however, was found to be attacked by hydrogen, which would form water with parts of the lattice oxygen, thereby creating a porous but partially disintegrated spinel structure. Surface metallic copper particles were found to be randomly oriented single crystals attached to the spinel. Above 400 °C the metallic copper particles separated from the spinel and agglomerated.

Therefore it can be concluded that their proposed mechanism of reduction for the pure spinel extends to the catalyst itself. Plyasova's results also shed light on why copper aluminate catalysts would need higher activation temperatures. Metallic copper surface, as per our results, is already available at 200 °C due to reduction of copper oxide (comp. Fig. 2.8) and very likely also reduction of spinel-Cu(II). However, this does not seem to be sufficient to give an active catalyst. Only at higher temperatures, when the spinel lattice itself participates in the reaction, a highly active catalyst is obtained. This could be due to re-organization of Al^{3+} within the cation deficient spinel, but more likely the reduction of spinel via removal of lattice oxygen (forming H_2O) to increase pore volume and therefore, in the process, active surface of the reduced catalyst.

The catalytic results (comp. Figure 2.6) against the findings of Plyasova and co-workers do raise one question however. If all copper is reduced prior to an increase in pore size it should not affect the active surface area because this additional surface would be limited to the activated spinel phase. The constricted surface area of the oxidic catalyst precursor ($CuO \cdot CuAl_2O_4$) would have all copper metal particles on its surface after reduction. This reduction as proposed by Plyasova occurs before the disintegration of the spinel and thus before creating additional pore volume. This doesn't mean that new pores would not affect the activity at all, since they can easily increase access of

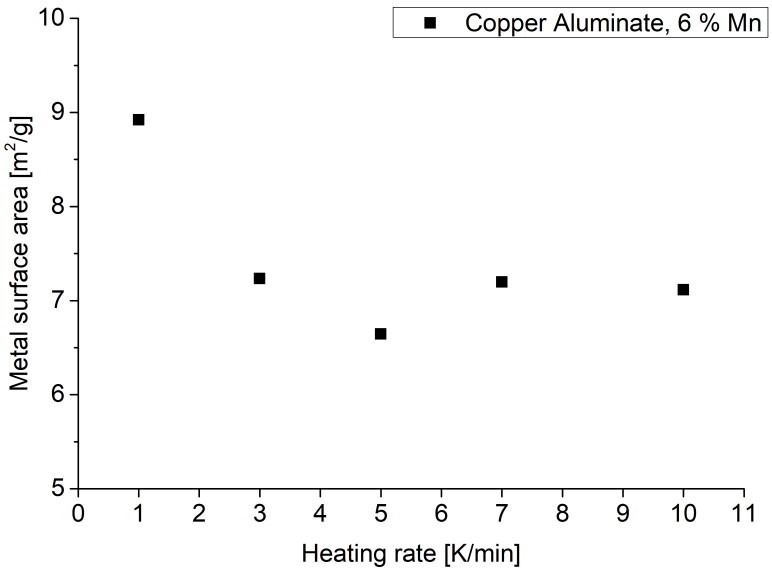

Figure 2.9: Metal surface area of $CuO \cdot CuAl_2O_4$ with 6 % Mn determined by N_2O-chemisorption after activation at 300 °C with varying heating rates.

reactant to active surface or even increase active surface indirectly via removal of spinel underneath copper metal particles. Nonetheless the drastic increases in activity cannot simply be explained if the two effects 1) reduction of copper and 2) creation of new pores, i.e. increasing pore volume occur consecutively. To investigate whether these effects could be linked or are in fact occuring consecutively, the effect of heating rate on metal surface was determined by N_2O-chemisorption. The results can be found in Fig. 2.9. As it can be seen, the copper surface hovers around 7 m^2/g for heating rates between 3 - 10 K/min. After reducing the rate to 1 K/min a sharp increase to 9 m^2/g is obtained. This is congruent with an increase in activity of the catalyst by a factor of two (15 $\longrightarrow$ 30 % yield). Just to reiterate that a change of heating rate is always a change in terms of time. Even though the activation temperature is set to 300 °C, the reaction time is kept relatively short at higher heating rates, compared to the 5 hours and 35 minutes for 1 K/min with 1 h isothermal zone. So at longer reaction times, something happens to the catalyst, which cannot be explained merely by the increase in active surface, when one proposes copper metal to be the active surface. The activity jumps by a factor of two and active surface only by 1.29. When one follows the reaction pathway throughout the TPR experiments (e.g. Fig. 2.4), it can be seen that the reduction process ends abruptly around 300 °C, although the signal never fully returns to the baseline. Therefore it must be proposed, that higher temperatures and reduction times are necessary to activate the spinel itself, which seems to be an integral part of the catalyst. This activation consists of the reduction of lattice Cu^{2+} and possibly aluminum migration as well as oxygen removal from the lattice as proposed by Plyasova et al.

Summarizing this section, it can be concluded that, based on the results and literature presented, aluminate-type catalyst activation includes a mechanism that affects/modifies the spinel phase, which in turn strongly influences the catalyst's activity. Chromite ca-

talysts reportedly undergo similar reduction of lattice Cu^{2+}, without reductive dissolution of the spinel lattice. Thus, an interesting followup study would have to have a focus on copper particle shape and distribution after reduction. For the pure spinel, Plyasova et al. proposed hemispherical copper particles on the surface of the spinel. However, how the excess CuO, which is reduced earlier than the spinel, influences this is still unknown. The activation conditions for both catalysts, that were determined in this work, are given in Table 2.2.

Table 2.2: Summary of optimized activation parameters for both catalysts.

Catalyst	Heating Rate [K/min]	Temperature [°C]	Hold time [h]
$CuO \cdot CuAl_2O_4$	1	300	1
$CuO \cdot CuCr_2O_4$	15	180	1

2.3.2 Synthesis and Optimization of $CuO \cdot CuAl_2O_4$ Catalysts

With the reaction and activation parameters having been established, further work was put into the synthesis of catalysts. Generally, these types of catalysts are synthesized via co-precipitation of metal nitrates with soda. Ageing, washing and drying are all necessary steps before the precursors can be calcined and the oxidic catalyst $CuO \cdot CuAl_2O_4$ is obtained. The patent literature offers insights into the industrial operations [3, 19, 31]. The precipitation is usually conducted around neutral pH and temperatures between 25 and 90 °C. Ageing is an integral part to control crystallite sizes and possibly remove undesired anions from the precipitate such as nitrates. Kinetics of metal nitrate precipitation are usually faster than hydroxides and carbonates. During ageing hydroxides and carbonates can form [35]. These are usually a preferred precursor since carbonates completely transform into the respective oxides while also increasing the pore volume due to CO_2 evolution. Washing removes undesired ions, which are often akalimetals and/or leftover nitrates.

In a first set of experiments, the influence of varying the precipitation pH was investigated at 50 °C. The results are shown in Figure 2.10. A general trend is an increased activity at higher pH values. The catalyst precipitated at pH 7.4 achieves 37 % butanol whereas the catalyst at pH 6.5 yields only 29 %. The titration curves of the copper and aluminum nitrate solutions as well as its mixture used for co-precipitation are shown in Figure 2.10. Both ions exhibit equivalence points according to their charge as expected. Copper has two and aluminium three equivalent points. The last one is around pH 7.5 for both solutions. The co-precipitation mixture Cu/Al is a combination of both single curves. At low pH values it follows the copper curve, then switches to aluminum and finally shows an interaction of both ions above pH 5. Its last equivalence point is located at pH 7.5 as well. Thus at higher pH, more aluminum and copper will have precipitated which could explain the better performance in catalysis. Crystallite sizes (calculated from XRD) and temperature of reduction as well as reducible amount of copper calculated from TPR for these experiments are summarized in Table 2.3.

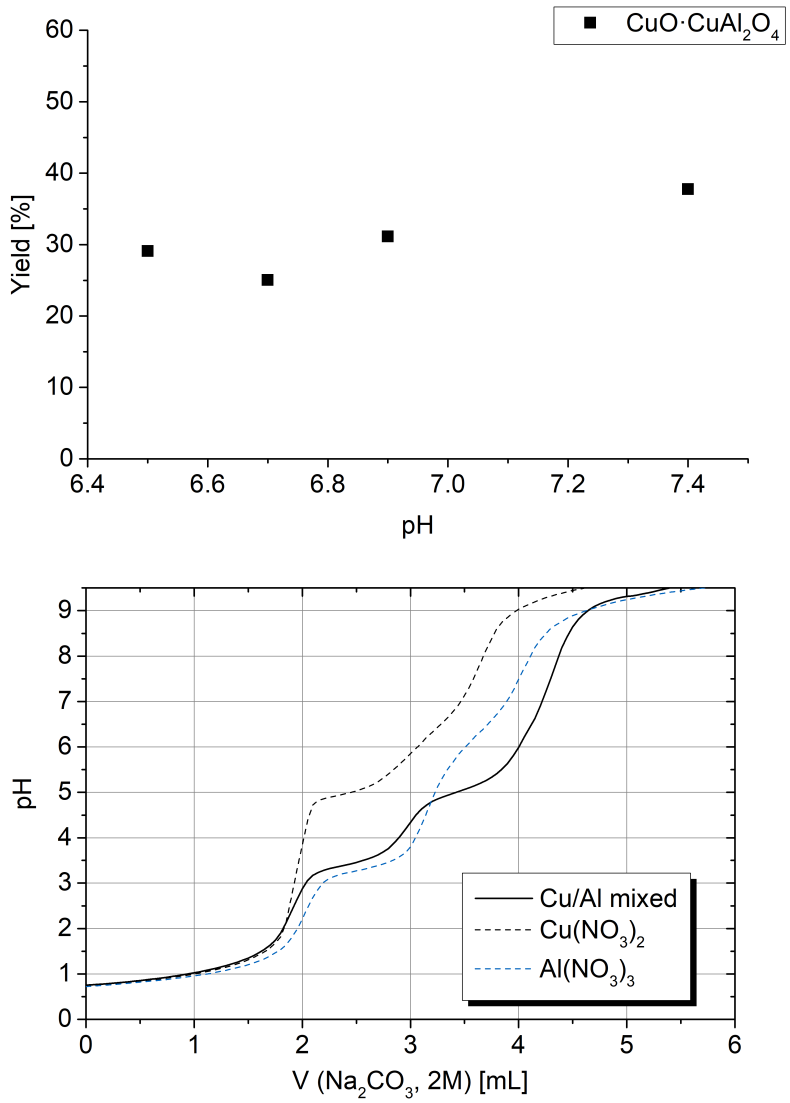

Figure 2.10: Influence of co-precipitation pH on catalyst activity (top) and titration curves for the catalyst and its separated nitrate solutions respectively (bottom).

Table 2.3: XRD and TPR results for catalyst precursors precipitated at different pH.

Precipitation pH	T_M	Reducible Cu [%]	d CuO [nm]	d $CuAl_2O_4$ [nm]	Yield [%]
6.5	257	65.7	16.2	12.5	29
6.7	275	69.8	16.1	12.6	25
6.9	315	85.4	13.2	11.0	31
7.4	277	81.9	10.8	11.5	38

The TPR experiments show, that an increase in pH generally leads to a higher temperature of maximal reduction speed (T_M) but also to more reducible copper. At pH 6.5 only 65.7 % of copper in the entire catalyst can be reduced. Increasing the pH to 7.5 during co-precipitation enables 81.9 % of copper to be reduced. Although in the previous section (compare section 2.3.1) it was already established that not only the metallic

copper surface but also the spinel takes an important part in the catalysis, an increase this large in reducible copper will most likely lead to more active surface. This hypothesis is further supported by the smaller particle sizes calculated from the XRD. Both copper oxide and copper aluminate spinel crystallites decrease with increasing precipitation pH. CuO, as shown previously, is completely reduced. The spinel follows with very high percentages of reducible copper. However in the case of the spinel, copper has to migrate through the Al-O lattice to reach the surface and form metallic copper clusters/particles. Thus, when one thinks of a model to account for this behavior, a core-shell model can be used as a simple tool, which then favors smaller particles for a more complete and faster reduction. A higher T_M does not necessarily affect catalysis. Once this is known, an activation procedure can be modified accordingly. In these experiments a higher T_M even correlates with higher activity.

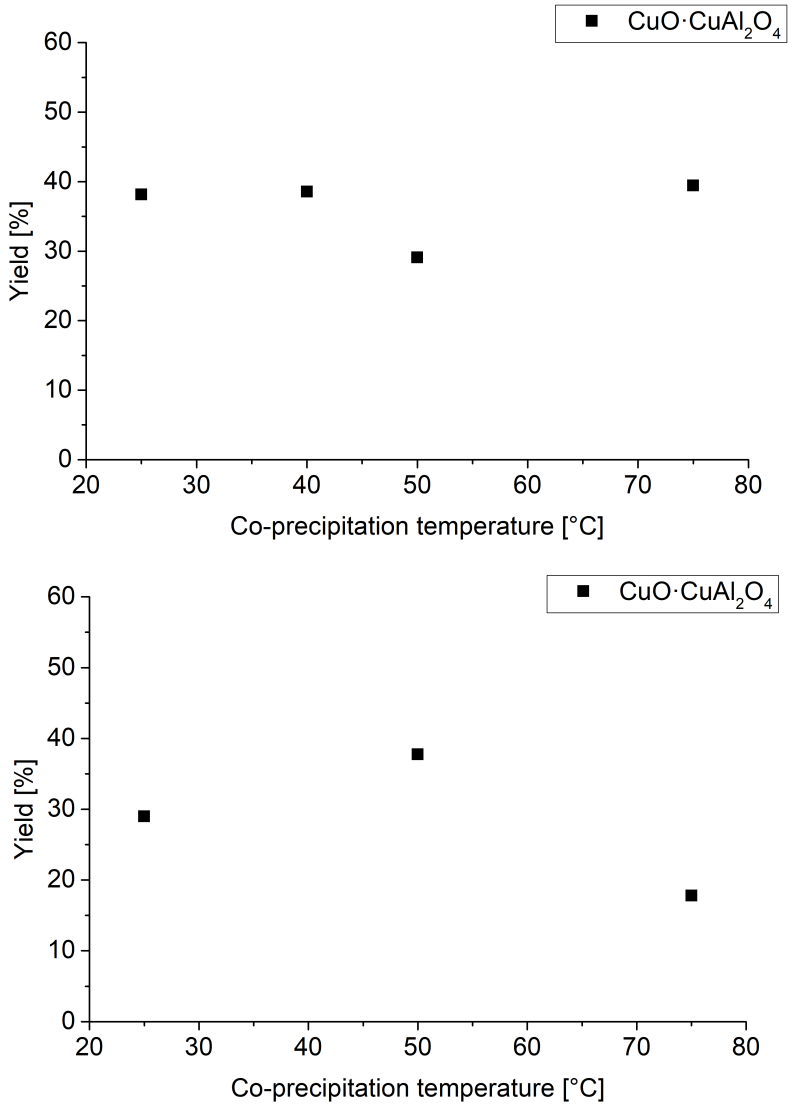

Figure 2.11: The effect of co-precipitation temperature at different pH (6.5 (top) and 7.4 (bottom)) on catalyst activity.

Table 2.4: XRD and TPR results for catalyst precursors precipitated at different temperatures.

Temperature (pH) [℃]	Reducible Cu [%]	d CuO [nm]	d $CuAl_2O_4$ [nm]	Yield [%]
25 (6.5)	68.5	14.3	12.5	38.1
40 (6.5)	81.1	13.1	11.3	38.5
50 (6.5)	65.7	16.2	12.5	29.1
75 (6.5)	92.8	11.5	9.3	39.4
25 (7.4)	77.5	13.8	12.4	29.0
50 (7.4)	81.9	10.8	11.5	37.1
75 (7.4)	81.3	16.9	11.7	17.8

In a next step, the influence of temperature during co-precipitation was investigated. Since it could be shown, that precipitation pH does have an effect on catalytic activity, the effect of temperature was investigated at pH 6.5 and 7.4 respectively. The results are shown in 2.11. At pH 6.5 the influence of temperature is relatively small, as constant yields were achieved from 25 to 75 ℃. The data point at 50 ℃ drops off compared to the others by up to 9 % yield. That data was gathered within the pH variations experiments and the other temperatures were a separated, newer set of experiments. Therefore an improvement in the reaction system could be the sole reason for this and not necessarily a chemical change of the catalyst at exactly pH 6.5 and 50 ℃. At pH 7.4 on the other hand, the effect of temperature is relatively pronounced. 25 and 75 ℃ fall off significantly compared to 50 ℃. Supplementary data calculated from XRD and TPR (as presented above) is shown in Table 2.4. The data for the pH 6.5 series looks very interesting. As explained previously, the data point at 50 ℃ falls off compared to the rest. It has a relatively low amount of reducible copper with only 65.7 % but that is also the case for 25 ℃, where 38 % butanol yields were achieved. This experiment really is an outlier however, when the particle sizes are considered. CuO and $CuAl_2O_4$ crystallites are 16.2 and 12.5 nm respectively. All other experiments exhibit significantly smaller particles. Copper oxide particles for example are smaller than 14.3 nm for all other samples. Reducible copper by itself does not appear to be a good parameter to predict catalyst activity. The 25 ℃ sample has similar amounts of reducible copper compared to the 50 ℃ experiment (65.7), but its activity is a quite a bit higher with 38.1 %.
The particle size hypothesis also holds true for the series of experiments at pH 7.4, where the 50 ℃ experiment has the smallest crystallites for both CuO and $CuAl_2O_4$ and at the same time the highest activity. Similarly, the amount of reducible copper hovers around 80 % for all samples at pH 7.4, whereas the activity is significantly different. This supports the hypothesis that particle sizes of the oxidic precursors are much better for predicting activity of the final catalyst compared to all other parameters presented.

2.3.3 The Influence of Manganese

Manganese is a standard promoter for a variety of industrial catalysts. Often it is not really understood in what ways manganese actually promotes the catalyst. Therefore,

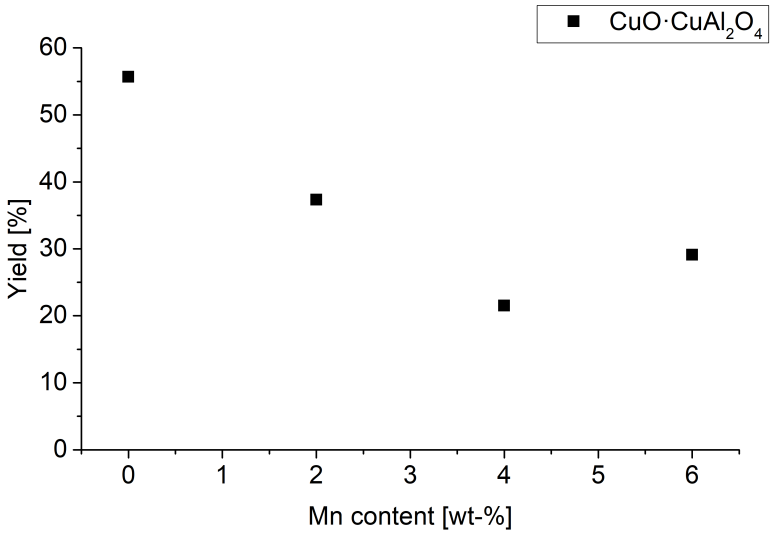

Figure 2.12: Influence of manganese content on catalyst activity in the hydrogenation of butyraldehyde.

in this chapter the influence of manganese with regards to catalyst activity and precursor attributes shall be investigated. In Figure 2.12 the yields of butanol are plotted over manganese content in the catalyst. At 0 %, an unpromoted catalyst ($CuO \cdot CuAl_2O_4$) can achieve about 55 % yields. Upon increasing the manganese content to 4 %, the activity decreases linearly down to 21 %. At 6 % Mn content, the obtained yields increase slightly to 29 %. Thus it can be concluded, that any amount of manganese is detrimental to catalyst activity. This is actually a really interesting finding since catalysts are rarely poisoned on purpose. Most likely, manganese must bring other benefits at the cost of catalyst activity. There are several possible effects of manganese, that we could not investigate in the course of this work, which could explain the need for manganese. First of all, manganese could improve mechanical stability of the catalyst. On the laboratory scale all catalysts were tested as granulates but industrial scale operations do not have this luxury. Large reactors would suffer from gigantic pressure losses or clog completely when filled with small granulates. Therefore catalysts are pressed as tablets, which need to be stable against the pressure inside of the reactor, temperature and the pressure exercised by the catalyst mass above the tablet. Secondly, industrial feeds are nowhere near as pure as what can be used on the laboratory scale. Fatty alcohols are produced from aldehyde feeds, that can contain up to 2 wt-% of the corresponding acids (compare Chapter 1.2). A high chemical resistance to this acidity is then required to reduce leaching to prevent impurities in the products as well as catalyst dissolution. A third reason for the addition of manganese could be as a selectivity promoter. Since the test reaction was the hydrogenation of butyraldehyde to butanol, selectivities were not an issue. No carbon-carbon cleaving or acetal formation was observed. Aldol-condensations and Tishchenko reactions were not observed either. More information can be gathered from the x-ray diffractograms as well as the temperature

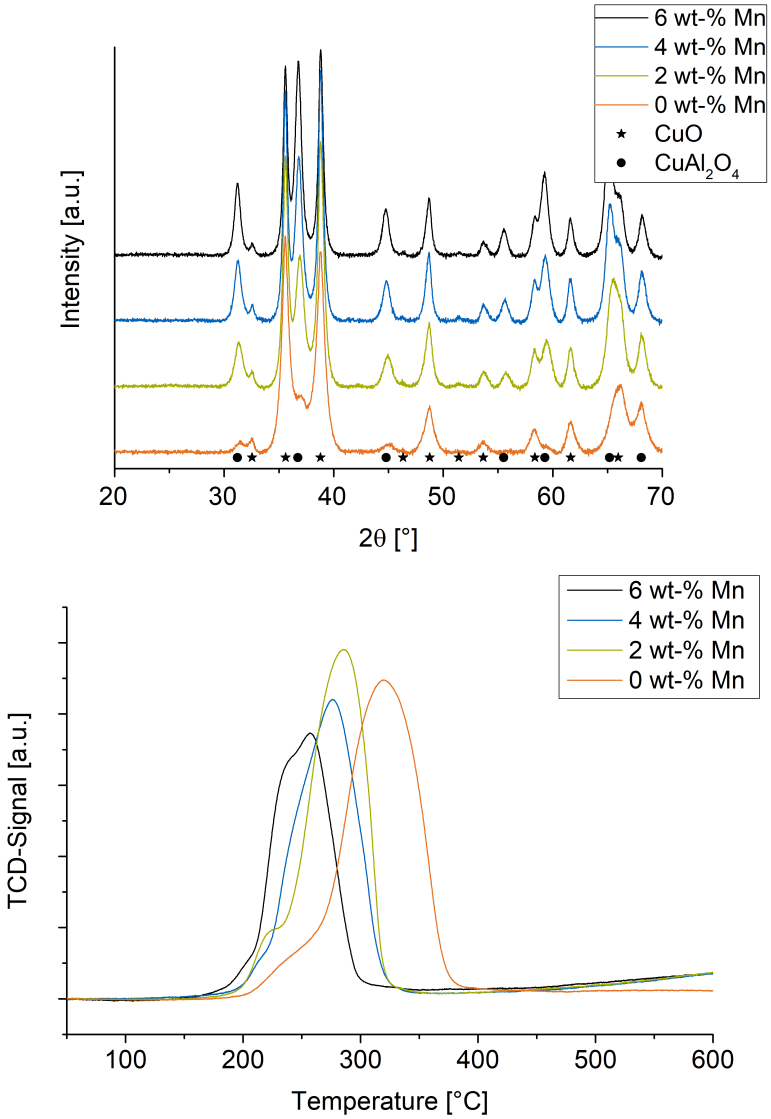

Figure 2.13: XRD (top) and TPR (bottom) of precursors with varying amounts of manganese.

programmed reduction experiments, which are shown in Figure 2.13. With increasing manganese content, the XRD reflexes become sharper and more intense for both CuO and $CuAl_2O_4$. This is indicative for larger particles. Hence manganese increases particle size of both phases, which can be calculated via the Scherer-equation (see Table 2.5). As shown above, the particle size is the main parameter correlating with activity. Smaller particles in the precursor drastically increase yields. Unpromoted copper aluminate catalyst (0 % Mn) yields 55.7 % butanol with CuO particles being as small as 9.4 nm. The spinel is calculated to be 7.3 nm but the reflexes are overlapped by CuO so the error for this value can be assumed to be quite large. On the other hand, 6 % manganese content leads to 16.2 nm and 12.5 nm particles for CuO and $CuAl_2O_4$ respectively. This catalyst only yields 29.1 % butanol. TPR experiments (comp. Fig. 2.13) give insights into the reduciblity of the catalysts. A shift of the TPR curves occurs to lower temperatures with

Table 2.5: Data calculated from XRD and TPR experiments for Mn-promoted catalysts.

Mn [wt-%]	Reducible Cu [%]	T_M	d CuO [nm]	d $CuAl_2O_4$ [nm]	Yield [%]
0	97	319	9.4	7.3*	55.7
2	86	286	13.3	9.1	37.3
4	78	276	16.0	11.0	21.5
6	66	257	16.2	12.5	29.1

*XRD reflexes too small for reliable crystallite calcultation

increasing manganese content. The onset of reduction, which is located around 200 °C for all catalysts, is shifted in the same manner. More importantly however, the slope of this onset is flat without manganese, meaning the reduction kinetics are slow, and steep (fast reduction rate) for high manganese contents. It can thus be concluded, that manganese facilitates the reduction of Cu^{2+} to metallic copper, which is further supported by the shift in T_M to lower temperatures with increasing Mn content. Interestingly, the amount of reducible copper linearly decreases with Mn amount. At 0 % almost the entire Cu^{2+} can be reduced (97 %), whereas 6 % Mn retains one third of the copper as Cu^{2+}. Apparently, manganese hinders the migration of Cu^{2+} through the spinel lattice. This raises the question, how exactly Mn is incorporated into the catalyst. First of all, manganese could form an aluminate spinel ($MnAl_2O_4$) by itself [36, 37]. Thereby a manganese promoted catalyst would consist of three solid phases: CuO, $CuAl_2O_4$ and $MnAl_2O_4$. In the previous experiments it was already established, that CuO and $CuAl_2O_4$ are, with the exception of minor fractions, completely reducible with regards to copper content. Therefore, it is very unlikely, that manganese aluminate spinel forms seperated from the other two phases because the effect of Mn on copper reducibility is too pronounced. It not only retains Cu^{2+} in the spinel but also facilitates the reduction of the copper that is reducible. Thereby an incorporation of $Mn^{2+/3+}$ into the copper aluminate spinel is more likely [38]. Surface-Mn would be able to speed up the reduction of Cu^{2+} and manganese incorporated deeper in the spinel lattice could block channels, that are needed for copper migration, thus inhibiting reduction of Cu^{2+}.
To summarize, manganese as a promoter is detrimental to catalyst activity, which is caused by an increase in crystallinity especially for the CuO phase. Furthermore, it inhibits Cu^{2+} reduction because $Mn^{2+/3+}$ is most likely incorporated in the copper aluminate spinel phase itself. At the same time Mn facilitates copper reduction on the spinel surface. Thus, it can be proposed that Mn is added for other reasons, which could be promoting selectivity and/or stability of the catalyst.

Other Promoters

A large variety of promoters were tested with regards to their respective activity when added to $CuO \cdot CuAl_2O_4$. A 6 wt-% promoter content was aimed for. Due to the vastly different precipitation behavior of some promoters, it cannot always be guaranteed to be exactly 6 %. Promoter compounds used for these experiments and methods of prepara-

tion as well as addition to the co-precipitation are described in detail in the experimental section 7. All promoters are listed in Table 2.6. The activities of the promoted catalysts are summarized in the form of a periodic table in Figure 2.14. Activities are colorized by activity levels. As it can be seen, most promoters achieve 30-50 % yield (blue). A few are on the lower end of activities with less than 30 % (red), while six promoters achieve above 50 % yields (green).

Table 2.6: List of promoters tested with $CuO \cdot CuAl_2O_4$ in the hydrogenation of butyraldehyde.

Earth akali metals	Mg, Ca, Sr, Ba
1^{st} row transition metals	Sc, V, Cr, Mn, Fe, Co, Ni, Cu, Zn
2^{nd} row transition metals	Y, Zr, Nb, Mo, W, Re
Lanthanides	La, Ce, Pr, Nd, Sm, Gd, Tb, Er, Tm

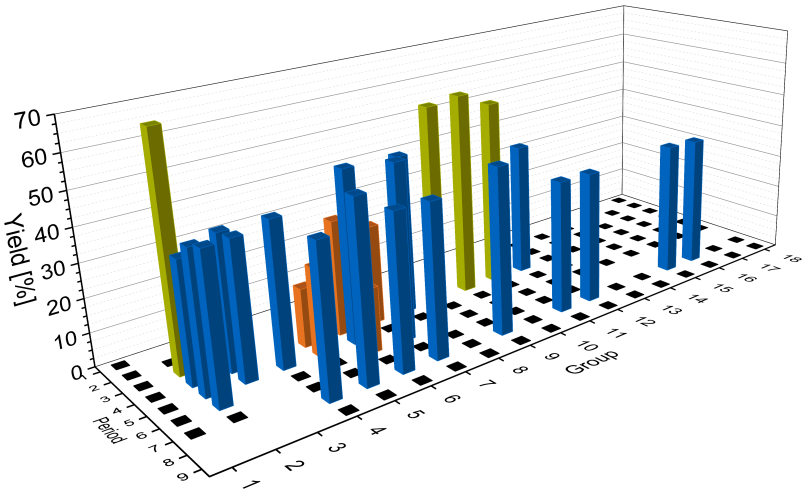

Figure 2.14: Overview for all promoters tested with $CuO \cdot CuAl_2O_4$ in the butyraldehyde hydrogenation. Promoter content was targeted to be 6 %.

At 6 wt-%, vanadium, chromium, manganese, niobium and tungsten have to be considered inhibitors, only achieving yields $\leq$29.1 %. Attributing the causes for these rather harsh drops in activity is not trivial. Vanadium for example forms crystalline oxides next to the copper oxide and spinel phase. Albeit not being incorporated in either copper phase, it drastically affects reduction behavior (measured by TPR) of the catalyst. Similar phenomenons can be observed for molybdenum, but a Mo-promoted catalyst achieves close to 40 % yield, whereas vanadium promoting decreases activity to 19 %. This overlap between different promoting/inhibiting effects makes a deduction of how the catalyst should be optimized rather complex. Based on these experiments, an inhibiting effect per se cannot be identified. It has to be considered however, that the 6 % promoter amount was a direct replacement for 6 % Cu in the original $CuO \cdot CuAl_2O_4$ catalyst. Thus, it is here suggested that higher copper and therefore copper oxide and copper aluminate

amounts are crucial for high activities. More insight for this hypothesis can be gathered from the best promoter: magnesium. It increases yields by more than 10 % compared to $CuO \cdot CuAl_2O_4$, again with less overall copper. However, magnesium drastically decreases particle sizes of both copper oxide (7.3 nm) and copper aluminate (7.2 nm). This leads to high copper surface areas after reduction and also to an increased interface between metallic copper and cation deficient spinel. Apparently, this interface is crucial for the catalytic reaction. Maximizing it thus leads to an improved catalyst. Unpromoted $CuO \cdot CuAl_2O_4$ has larger crystallites with 9 nm for copper oxide and 7 nm for copper aluminate. However, the higher copper content seems to offset, at least to some degree, the loss in interface. The metal surfaces of the unpromoted and magnesium promoted catalyst are shown in Table 2.7. As it can be seen, magnesium promotion increases copper surface to 10.74 m^2/g, although up to 6 % magnesium was used to replace copper, meaning this catalyst has a higher copper surface with less copper. Therefore, due to smaller particles sizes of metallic copper to cause such a surface increase, the interface between metallic copper and spinel must be larger.

Table 2.7: Comparison of copper surfaces in relation to catalytic activity.

Catalyst	Cu surface area [m^2/g]	Yield [%]
$CuO \cdot CuAl_2O_4$	9.11	55.7
$CuO \cdot CuAl_2o_4$, 6 % Mg	10.74	68.4

An extended study of these promoters to look for physico-chemical properties unfortunately did not reveal single or combinations of parameters to predict catalyst activity. Data and diagrams are partially shown in this chapter but due to the sheer quantity without correlations to catalytic activity, the full amount is not shown in this work.
Crystallite sizes in the pre-catalyst have to be small, which is why magnesium is such a good promoter. Copper metal surface area is a good indication but does not work as a tool to predict catalytic activity when chemical composition, i.e. promoter and promoter content, are modified. All these experiments do however, point towards the importance of the spinel phase and the interface to metallic copper being crucial for catalysis. We were unsuccessful in developing combination tools of chemisorption and physisorption measurements as a measurable attribute to predict catalytic activity, i.e. in quantifying the size of the interface.

2.4 Conclusions

In this Chapter it was shown that copper aluminates and copper chromite catalysts are similar in terms of activity in the liquid-phase hydrogenation of butyraldehyde. However, the activation of copper aluminates has to be conducted at higher temperatures (300 °C) compared to the chromite variant (180 °C). *In situ* XRD experiments showed that an activation of the spinel phase occurs, i.e. reduction of curpric ions from the spinel phase.

The charge is offset by the incorporation of protons within the spinel.
Activity of copper aluminates was not dependent on pH of precipitation between 6.5 and 7.4. However, precipitation temperature effects were shown to be important. Synthesis conditions at 50 °C and pH 6.5 are suggested.
A large scale promoter sreening revealed that only three promoters are able to outperform $CuO \cdot CuAl_2O_4$, which are magnesium, nickel and cobalt (in the order of decreasing activity). Promoter fractions were calculated as a direct replacement of copper and to be 6 wt-% of the catalyst.
An analysis of physico-chemical properties revealed that small copper oxide and aluminate spinel particles in the pre-catalyst $CuO \cdot CuAl_2O_4$ lead to highly active catalysts in the test reaction (liquid-phase hydrogenation of butyraldehyde). Moreover, promoters that affected the formation of spinel phase were detrimental for catalytic activity. These findings allow for two conclusions, namely the importance of the spinel phase and copper amount for active catalysts.

3 The Strong Influence of Sodium

3.1 Literature Review and Motivation

Copper aluminates have been described as catalysts for various applications, e.g. hydrogenation of esters [3] and aldehydes [4], oxidation of aromatic compounds [6], SCR of NO [7] and ethanol steam reforming [8]. Usually, these types of catalysts are synthesized via co-precipitation, followed by drying and calcination. The calcined precursors have to be reduced to obtain the active catalyst. A typical precipitation agent is sodium carbonate [3]. Calcination temperatures range from 300 to 900 °C, determining the pre-catalyst's composition. At temperatures above 600 °C copper aluminate spinel forms, whereas at temperatures below 600 °C, alumina and copper oxide are the dominant phases [39, 40]. Likewise, copper oxide supported on alumina can react to form copper aluminate spinel at higher temperatures [21].

Copper aluminate spinel based catalysts are industrially relevant hydrogenation [3] and hydrogenolysis [41] catalysts. While precursor composition is generally agreed upon, active species and reaction mechanisms are still reported controversially. Early descriptions find Cu^+ to be the active species in the hydrogenation of dienes [5] and allylic alcohols [14]. On the other hand, Plyasova et al. proposed the direct formation of Cu(0) (as opposed to Cu^+) from copper aluminate spinel during reduction with H_2 [33], which would eliminate a possible role of Cu^+ as active center. Research conducted by Yurieva and co-workers on copper chromite catalysts showed similar results [23]. They found a direct conversion to metallic copper and a cation deficient chromite spinel that was subsequently stabilized by two different hydrogen species: protons and absorbed hydrogen. Moreover, during an investigation into the reaction mechanism of the hydrogenation of acetone over copper chromite, they measured catalytic conversion of acetone in the absence of hydrogen on pre-reduced chromite catalyst. Thereby, they could pinpoint the hydrogen species participating of the hydrogenation reaction to be the protons in the cation deficient spinel. Electrons necessary for charge compensation would be delivered from Cu^0, which would then migrate back into the cation deficient spinel as Cu^{2+}. The reaction rates with and without hydrogen were measured to be very similar further supporting their proposed reaction mechanism. These findings imply, that an active center is a metallic copper (Cu^0) atom. However, it has to be in close proximity to reduced/cation deficient chromite spinel, that is loaded with protons, basically making it a solid acid. Upon reacting with a carbonyl (C=O) group, the cupric ion has to be regenerated. Yurieva et al. suggest hydrogen (H_2) from the reaction medium to reduce copper ($Cu^{2+} \longrightarrow Cu^0$), which then migrates back onto the surface, switching positions

with the protons. Several research papers support these findings for copper chromites [23, 42, 43]. These observations have interesting implications for catalysts of the spinel type, which usually have excessive amounts of copper present such as $CuO \cdot CuCr_2O_4$. Copper oxide would supply the catalyst with a lot more metallic copper, which is integral part of the catalytic mechanism. However, this metallic copper is not necessarily in close proximity of the spinel, thus wouldn't participate in the catalysis or could even block the spinel surface, thereby inhibiting the catalytic cycle. A composition with higher copper content must thus focus a lot more attention on the synthesis to maximize the $Cu/H_2Al_2O_4$ interface and not block it, for example with large copper crystallites. It is quite interesting, whether these proposed mechanisms are similar for copper aluminate catalysts. A few research papers were published for copper aluminates [5, 33]. The authors agree that the reduced spinels act as a hydrogen reservoir, providing H^+ and/or hydride ions for the hydrogenation after which they are replenished by H_2 from the reaction atmosphere. Plyasova et al. proposed a cation deficient spinel, analog to the copper chromite described above, due to reduction of Cu(II) from the spinel itself, which is then stabilized by the incorporation of protons. At this point, it makes sense to assume a similar catalysis mechanism for copper aluminates as was proposed for chromites (s. above). Therefore a maximization of the $Cu/H_2Al_2O_4$ interface would lead to the best catalysts and any interference with such interface would cause a loss in activity. With this in mind, an investigation into the effects of sodium, which is known to increase CuO crystallites [19] and form delafossite-like $NaAlO_2$, could reveal a negative effect of sodium, which would in turn strengthen the argument for a reaction mechanism described by Yurieva et al. [23]. Selim and Youssef investigated the effect of thermal treatment on the Na-doped $CuO\text{-}Al_2O_3$ system [44]. They were able to follow spinel formation at high temperatures (800 °C) and subsequent disintegration to $CuAlO_2$ at 1000 °C. Sodium contents larger than 5 wt-% resulted in large CuO crystallites, whereas $CuAl_2O_4$ crystallinity as well as $CuAlO_2$ crystallinity was severely decreased.

A wide range of promoters has been mentioned for copper aluminate, e.g. Mg, Zn, Ti, Zr, Sn, Ni, Co [3, 4], Mn [31] and Na [45]. For most of these promoters, the actual effect of promotion has not been investigated for the above mentioned type of catalyst. Out of all promoters mentioned here, sodium has a somewhat special role as it is the only element not introduced deliberately but via precipitation with Na_2CO_3. Most patents reveal that a washing step is included in the synthesis of $CuO \cdot CuAl_2O_4$ catalysts. Chen et al. investigated the effect of residual sodium on the leachability of copper and aluminum from $CuO \cdot CuAl_2O_4$ catalysts [19]. They found that higher sodium content increases leached copper and aluminum. Further, they reported sodium to increase reduction temperature of copper oxide and to retard copper aluminate formation. Moreover, they were able to correlate lower sodium content in the catalyst with higher activities in the hydrogenolysis of coconut oil fatty acids. However, the authors did not identify the cause of these phenomenons. Koritala and co-workers reported sodium poisoning of copper chromites in the hydrogenation of soy bean oils [46]. Since there is barely any literature on Na^+ affecting either $CuAl_2O_4$ or $CuCr_2O_4$, a look into similar catalyst types and reactions

is worthwhile. Kondrat et al. investigated the effect of sodium during the formation of Cu/ZnO catalysts from zincian georgeite [47]. They found pre-catalyst stability to heavily depend on sodium content, as higher sodium contents lead to different precursor compositions. Further, the higher sodium content samples (up to 2.1 wt-%) exhibited larger CuO crystallite sizes and lower copper surfaces after reduction/activation. Moreover, the authors showed a vastly negative effect of sodium on the catalytic activities for both the low-temperature water-gas shift reaction and methanol synthesis from syn-gas. A blocking of active sites by Na^+ was postulated. Similar to copper catalysts, a poisoning effect of sodium was reported for V_2O_5/TiO_2 SCR catalysts [48]. The authors attributed the negative effects to quenching of surface acidic sites by sodium. If a similar effect could be relevant for aluminate spinel catalysts remains questionable. Aluminates are of course Lewis acidic, their Brønsted aciditiy outside of Al-Si mixtures such as zeolithes is rather low however. For Al-Si dehydrogenation catalysts this exact quenching of acidic sites by sodium was described by Figueras et al. [49].
On the other hand, various sodium salts did not affect Raney-nickel in the liquid-phase hydrogenation of vegetable oils [50]. Interestingly, the exact opposite was reported for alumina supported nickel methanation catalysts, where even small sodium impurities decreased activity significantly [51]. The authors reported, that nickel surface areas only slightly changed after exposure to sodium. Now it is unlikely that the metallic nickel surface is blocked by Na^+, because this effect should affect measured nickel surface area by N_2O. This leaves three possible effects that should be considered. On the one hand, sodium ions could alter the electronic properties of nickel metal partices and thus inhibit the reaction. The same is true, if sodium modifies nickel particle strucutre. This is unlikely however, since metal surfaces remained the same. On the other hand, Al_2O_3 or Ni-Al_2O_3 mixed oxides could engage in an active role in the catalytic cycle, thus making it part of the active site, that is usually only attributed to metallic particles. If this holds true, any precipitated metal/alumina mixture should be heavily poisoned/affected by sodium, when used as a hydrogenation catalyst, since sodium will be incorporated in the alumina phase during temperature treatment and drastically change its attributes.
Therefore, this work attempts to identify the cause of these effects by investigating the influence of sodium on phase development during thermal treatment as well as catalytic activity of sodium poisoned catalysts in the hydrogenation of aldehydes.

3.2 Results and Discussion

3.2.1 Hydrogenation Activity in the Presence of Sodium

To investigate the effects of residual sodium, copper aluminate catalyst precursors were exposed to different washing procedures after co-precipitation. The washing step removes sodium and nitrates from the co-precipitates, which are introduced by soda as a precipitating agent and the metal nitrate precursor solutions. The drastic effect of sodium is demonstrated after washing, calcination and activation of the catalysts and its activity in

the hydrogenation of butyraldehyde. The correlation of sodium content in the pre-catalyst and catalytic yields is shown in Figure 3.1. An unwashed catalyst, containing 16 wt-% sodium, is almost completely inactive with less than 5 % butanol yield. Improving the washing procedure, where the filter cake is flushed with distilled water, diminishes sodium content to 10 wt-% while increasing yields to 15 %. Further enhancing the washing procedure, i.e. dispersing the precipitates in freshly distilled water three times in a row, drastically improves catalytic yields up to 36 %. Simultaneously sodium content drops below 0.5 wt-%. These experiments clearly establish the detrimental effects of sodium on the liquid-phase catalytic hydrogenation of butyraldehyde, because the magnitude of the effects goes way beyond the reduction of catalyst components when 16 % of the catalyst consists of sodium instead of copper and aluminum.

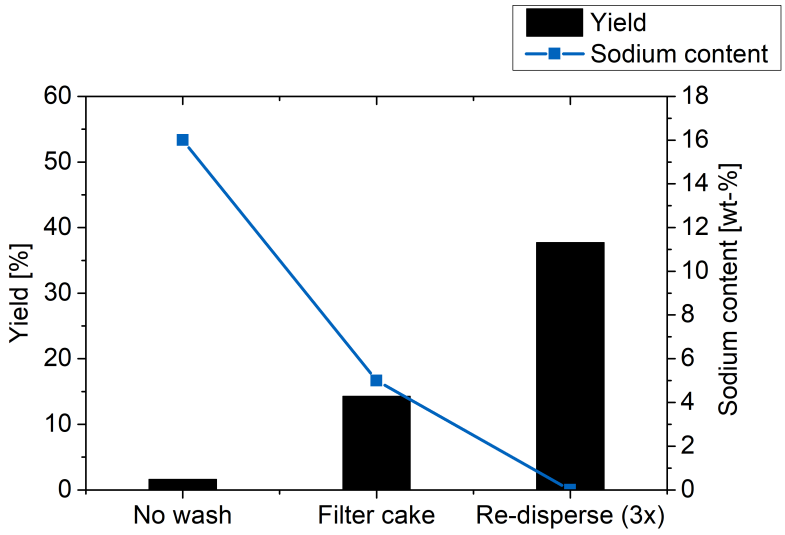

Figure 3.1: Catalyst activity in relationship to sodium content in the pre-catalyst ($CuO \cdot CuAl_2O_4$) in the hydrogenation of butyraldehyde [120 °C, 60 bar H_2, 1 h, 750 RPM].

3.2.2 Pre-Catalyst Composition With Varying Exposure to Sodium

A comparison crystal structures of pre-catalysts ($CuO \cdot CuAl_2O_4$) compositions after thermal treatment is shown in Figure 3.2. Right away the vast influence of sodium on aluminate-phase formation becomes obvious. The bottom (blue) diffractogram shows the oxidic catalyst precursor ($CuO \cdot CuAl_2O_4$) without sodium. Both phases, copper oxide and copper aluminate, are present in equal parts, which was confirmed by ICP-OES analysis. The crystallite sizes for both phases are relatively small being $\leq$ 20 nm. Such a catalyst achieves 35 % yield of butanol (comp. Chapter 2). The black x-ray diffractogram shows the unwashed pre-catalyst with 16 wt-% sodium. Intensity and crystallinity of copper oxide becomes much higher than that of a sodium-free pre-catalyst. With sodium present, copper oxide particles grow to 26 nm calculated from XRD reflexes via the Scherer equation (comp. 35.5 and 38.7 °). Furthermore, the copper aluminate spinel

phase is not observed in the sodium rich sample. Copper aluminate's most intense peak at 36.8 ° is completely absent. Instead, crystalline sodium aluminate ($NaAlO_2$) and cuprous aluminate ($CuAlO_2$) phases develop during thermal treatment (e.g. 33.2, 34.3 and 34.9 °).

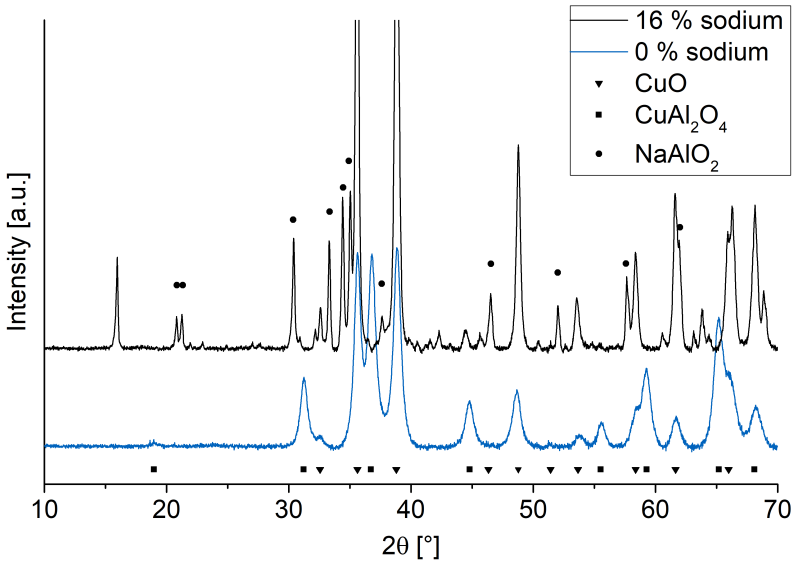

Figure 3.2: X-ray diffractograms of an unwashed (black) vs. thoroughly washed pre-catalyst (blue), which were used after activation (300 ℃ in flowing H_2 in the hydrogenation of butyraldehyde [120 ℃, 60 bar H_2, 1 h, 750 RPM].

The effectiveness of sodium in destroying the catalyst during thermal treatment can thus be explained by the very strong interaction of sodium with the pre-catalyst phases and its high affinity towards alumina phases at higher temperatures. A reduction in metallic copper surface areas that is most probably accompanied by the large increase in copper oxide particles must cost catalytic activity. A complete lack of copper aluminate spinel phase, even though its participation/function in the catalytic cycle is still discussed controversially, would further hurt catalytic activity. All these effects must play a combined role as to why the activity suffers in a high sodium content catalyst. These findings confirm some older reports on the interaction with sodium on copper aluminates, like the increase in CuO particle sizes [19] and complement the work of Selim and Youssef, that at high sodium contents, the spinel is not formed at all because all alumina forms sodium aluminate [44]. Even without aluminum present, a similar disturbance of precursor phase composition was found for Cu/ZnO catalysts [47]. The results here complement, extend and explain what is described in the literature.

3.2.3 Reduction Behavior of Pre-Catalysts Exposed to Sodium

One important question, that is left unanswered, is the exact mechanism of sodium poisoning at lower sodium loadings, where catalyst precursors consist of the required phases (CuO and $CuAl_2O_4$) but suffer from activity losses. One method to gain further insight is temperature programmed reduction. The results are shown in Figure 3.1. A

regular, unpromoted $CuO \cdot CuAl_2O_4$ catalyst is shown in black. It is not uncommon for their TPR curves to exhibit a small shoulder at higher temperatures. This essentially means, that there are two non-equivalent reducible species present. The peak's onset resembles the slow initial reduction which then speeds up in an autocatalytic reaction, which was further explained in chapter 2.

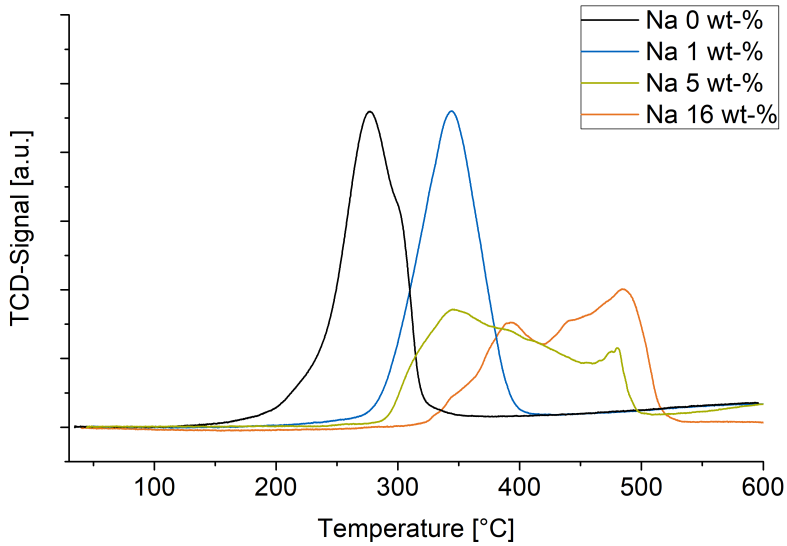

Figure 3.3: Effect of sodium content on reduction behavior of $CuO \cdot CuAl_2O_4$ precatalysts. 0 and 16 % sodium samples prepared by varying washing methods after precipitation, washing, drying and calcination. 1 and 5 % samples were synthesized with an additional impregnation step of sodium formate.

When 1 wt-% sodium is deliberately added to this catalyst via impregnation of sodium formate and different calcination at 400 °C applied, the TPR curves change quite drastically (see blue curve). The temperature of maximum hydrogen consumption (T_M) shifts to higher temperatures by 100 K. Further, the reduction curve becomes symmetrical, losing its high temperature shoulder. Thus, the two different Cu^{2+} species observed without sodium turn into one, that is more difficult to reduce. At higher sodium loadings (5 and 16 wt-%), the reduction curve completely loses its resemblance with the unpoisoned catalyst. Moreover, the reduction is shifted to even higher temperatures and becomes relatively slow as the maximum hydrogen consumption stays almost constant compared to the formerly mentioned TPR curves throughout the TPR experiment. Maciejewski described a change of this magnitude as proof for changes in the reaction mechanism [52]. It can be concluded that the mechanism of the reaction of hydrogen with copper oxide changes drastically at sodium contents of 5 wt-% and more. Instead of a direct reduction ($CuO + H_2 \longrightarrow Cu + H_2O$) that is usually observed under industrially relevant conditions [53], pathways via Cu_2O are possible alternatives to explain the observed effect of sodium. A stabilization of Cu(I) could also explain the higher temperatures necessary for the reduction, i.e. $CuAlO_2$ or Cu_2O as shown by Kato et al. [54]. How sodium achieves this strong of a change is still unclear however. The blocking of copper sites by Na^+ as

described for Cu/Zn catalysts [47] could happen analogous on CuO and thus interfere with the reduction of copper by physically blocking the surface. If this was true, how could the shift in reduction temperature be explained. A blocking of surface sites by sodium ions is not suddenly removed at higher temperatures to enable CuO reduction. Instead, a change of electronic properties induced by sodium in close proximity or doped into the CuO phase would be a reason for the drastic changes in the interaction of hydrogen with CuO that are observed when sodium is introduced into the system. From the data presented here, no conclusions about a direct interaction between sodium and copper can be drawn. The XRDs do not reveal a mixed Na-Cu phase, which could of course be amorphous. Only crystalline sodium aluminates are found next to copper oxide in the highly contaminated sample (16 wt-% Na). At the time of writing this chapter, the available literature does not offer further insight into the interactions of sodium with copper oxide under these or comparable conditions. Therefore, while we can demonstrate the strong influence of sodium on the electronic properties of CuO, it is not possible to pinpoint its exact mechanism with these experiments.

3.2.4 Sodium Impregnated Pre-Catalysts - The Effect of 'Surface Sodium'

Further insight can be gathered from the the phase composition of the impregnated samples (see Fig. 3.4). At the bottom of the diagram the unpoisoned pre-catalyst (0 wt-% Na) is shown for reference. 1 and 5 wt-% sodium were impregnated on the blue and black sample respectively. Since sodium formate was used, the samples were calcined again at 400 °C to remove organic residues. The first observation that can be made is that CuO XRD reflexes become sharper due to particle agglomeration. Moreover, copper oxide reflexes become more intense even if sodium is introduced to an already existing $CuO \cdot CuAl_2O_4$ pre-catalyst (comp. green diffractogram). Both effects appear to be proportional to sodium content. In this regard, the samples behave exactly the same as when sodium is introduced in the precipitation step. Interestingly, when one follows the copper aluminate peak intensity, a sharp decrease with higher sodium contents is observed. This means that the amount of copper aluminate spinel phase decreases relative to the other samples. To draw this conclusion it is important to emphasize that the green sample was used as the basis for these impregnation experiments and that is why the relative intensity of CuO to $CuAl_2O_4$ within one sample and in comparison to the other two, gives a very decent indication of relative phase compositions. Of course it should be mentioned that the phases here were not quantified absolutely since neither internal standards nor Rietveld methods were used. However, both of these methods experience difficulties with nanocrystalline/amorphous samples whose discussion go beyond the scope of this chapter. Since the basis (green sample) stays the same for all impregnation experiments, these samples suffice to show a relative increase or decrease of single components in the pre-catalyst.

In the washing experiments, that were described previously, it was shown that sodium inhibits the formation of copper aluminate spinel phase if not removed before thermal tre-

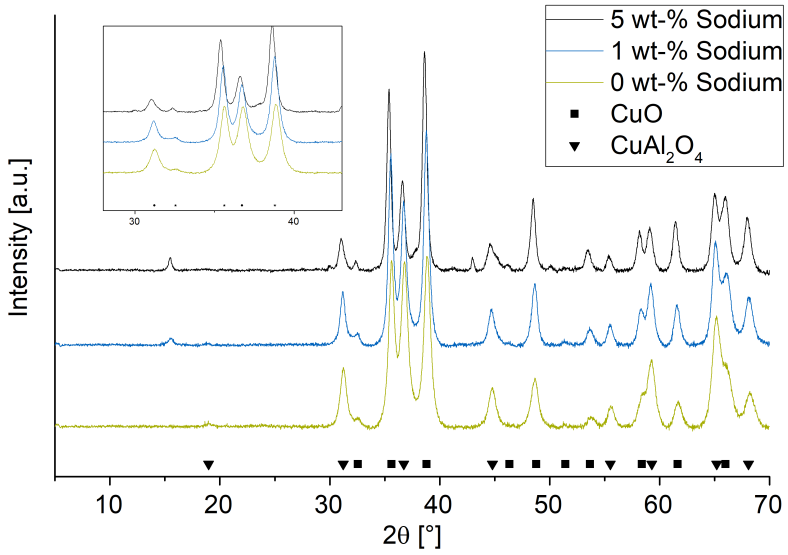

Figure 3.4: Phase composition of impregnated sodium samples (blue and green) against a clean precursor (black) after a second calcination (400 °C).

atment. Obviously, sodium is also capable of destroying copper aluminate spinel when put in contact with eachother at 400 °C. Reaction products between $CuAl_2O_4$ and Na^+ cannot be specified, since only a few new reflexes appear with regards to sodium content. At 15 ° a new peak is found that increases with higher sodium content (from blue to the black sample). Such a peak is indicative of Diaoyudaoite ($NaAl_{11}O_{17}$). However, that phase should exhibit more reflexes e.g. a very low intensity peak at 20 ° which is absent. Most of the other reflexes would be underlying the very broad CuO or $CuAl_2O_4$ peaks. This reflex could also proof the formation of delafossite-like $CuAlO_2$. This would mean that sodium stabilizes cuprous rather than cupric ions. Another new reflex at 43 ° could either be from Diaoyudaoite or sodium aluminate ($NaAlO_2$), which was to form during the washing experiments with high sodium content (see above). These experiments confirm the necessity to entirely remove sodium from the catalyst precursors. Surface sodium added via impregnation as opposed to structural sodium, which is located throughout the precipitate and thus will be able to migrate into any phase during thermal treatment, has the same effect on pre-catalyst phases as bulk sodium: It destroys copper aluminate spinel and agglomerates copper oxide. In the catalytic test reaction, these catalysts perform much better than the unwashed (16 wt-%) sodium precursor, which is only logical considering that they still partially consist of the necessary phases CuO and $CuAl_2O_4$. Nonetheless, 1 and 5 wt-% sodium precursors suffer from deactivation.

3.2.5 Effect of Sodium on Pure Copper Aluminate Spinel and Pure Copper Oxide

The most pronounced effect of sodium is its destructiveness with regards to the copper aluminate spinel phase. Thus far, the working hypothesis is a disintegration of spinel in the presence of sodium to form CuO and mixed Na/Al phases. The direct decomposition

into CuO has never been shown. Thus, purified $CuAl_2O_4$ spinel was impregnated with sodium and exposed to thermal treatment at 750 °C. The results can be found in Figure 3.5.

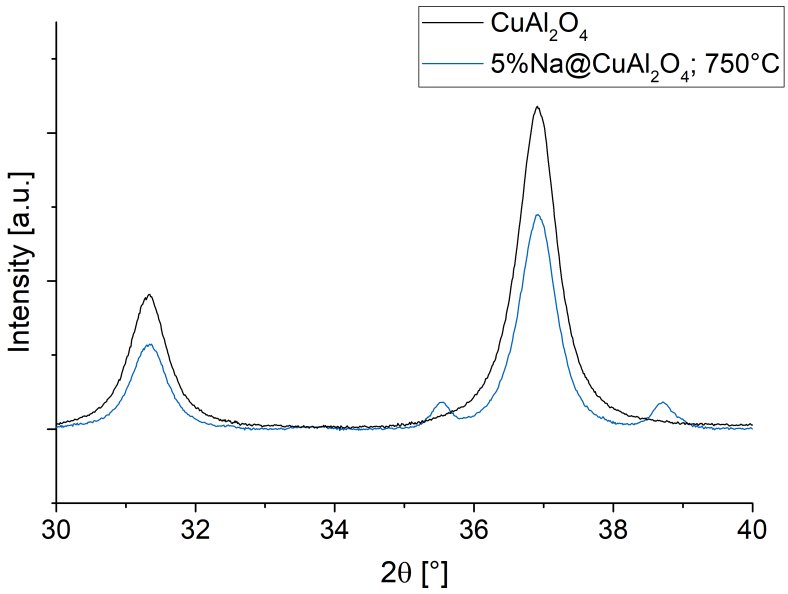

Figure 3.5: Effect of sodium on copper aluminate spinel during thermal treatment.

For simplicity, the diffractogram is zoomed in to show the two largest peaks of both CuO (35.6 °, 38.8 °) and $CuAl_2O_4$ (31.3 °, 36.9 °). The black diffractogram shows a clean copper aluminate spinel. After exposure to sodium, a crystalline CuO phase is found in the blue diffractogram. Thus, for the first time, this sodium induced disintegration of spinel was proven to form CuO. The relatively sharp drop in intensity of the spinel phase could mean that some x-ray amorphous phases such as sodium aluminates have been formed next to copper oxide. From the observations gathered in these experiments, the spinel disintegration can be proposed as follows:

$$2\ CuAl_2O_4 + Na^+ + e^- \xrightarrow{\Delta} NaAlO_2 + CuAlO_2 + CuO + Al_2O_3$$

Figure 3.6: Proposed disintegration of spinel after exposure to sodium.

It has to be emphasized that $NaAlO_2$ in this case must be treated as the simplest representative for all sodium aluminate mixed oxides, that could form under these conditions, as $NaAlO_2$ was only observed at very high sodium loadings and hints for other phases such as $NaAl_{11}O_{17}$ were obtained (comp. Fig. 3.4). Traces of cuprous alumina were also found (see Figs. 3.2 and 3.4), but generally speaking a disintegration of spinel could also form copper oxide as the sole product to contain copper next to sodium aluminates and alumina phases. To summarize, the effect of sodium is very pronounced not only on copper oxide, where an agglomeration of particles and changes in electronic properties was demonstrated, but also on copper alumina spinel, which was shown to not form in the first place or be disintegrated at temperatures as low as 400 °C. However, the strength of

the effect depends on the timing and temperature at which sodium is introduced. During washing experiments, drops in catalytic yields down to 0 % where observed, but how do the catalysts with impregnated, surface-sodium fare? The results are summarized in Table 3.1.

Table 3.1: Activities of sodium impregnated samples vs. an unpoisoned pre-catalyst that was calcined twice (750 °C, 400 °C) to account for a second heat treatment.

Sodium content [wt-%]	Butanol yield [%]
0	26.5
1	22.5
5	15.2

Similar to the washing experiments, surface sodium added via impregnation inhibits the catalytic activity. For reference, the clean precursor (0 %) was calcined again to account for a second heat treatment. As it can be seen (comp. Table 3.1), the catalytic activity is decreased by this heat treatment already (down from 36 %, see Fig. 3.1). Particle agglomeration and losses in BET surface area are likely responsible. Adding 1 wt-% sodium further decreases activity (22.5 %), which reaches its lowest point with the addition of 5 wt-% sodium at 15.2 % butanol yield. A similar sodium content in the washing experiments (compare Fig. 3.1) gave very similar results with just below 15 % yield. Albeit different starting points of sodium, in a bulk co-precipitate vs. on the surface of a clean precursor, its deactivation strength is comparable. One has to keep in mind however, that the second calcination already deactivates the catalyst quite a bit. Nonetheless, the same effects are observed for bulk sodium and surface sodium. A reason for this could be the high mobility of Na^+. It likely migrates into the bulk phases even if its added as surface sodium via impregnation. This is especially obvious for the copper aluminate spinel phase, which becomes sodium aluminate and which interestingly coincides most with the losses in catalytic activity. Thereby, the experiments here produce further evidence that the aluminate spinel phase could play a much more active role in the catalysis than that of a mere support to dilute valuable metal catalysts as discussed for nickel supported on alumina in the state of the art section (comp. section 3.1). A hydrogenation mechanism as described by Yurieva et al. remains within the scope of possible reaction mechanisms [23]. It remains questionable, if a solid state reaction, i.e. the migration of Cu^{2+} into the alumina phase, subsequent regeneration to metallic copper and another migration back to metallic copper particles, is quick enough to be part of the catalytic and not of a regenerative cycle.

After the effect of sodium on pure $CuAl_2O_4$ was examined and found to be rather pronounced, an effect on pure CuO, i.e. a change of electronic properties or phase composition/particle growth has to be investigated. The results can be seen in Figure 3.7.

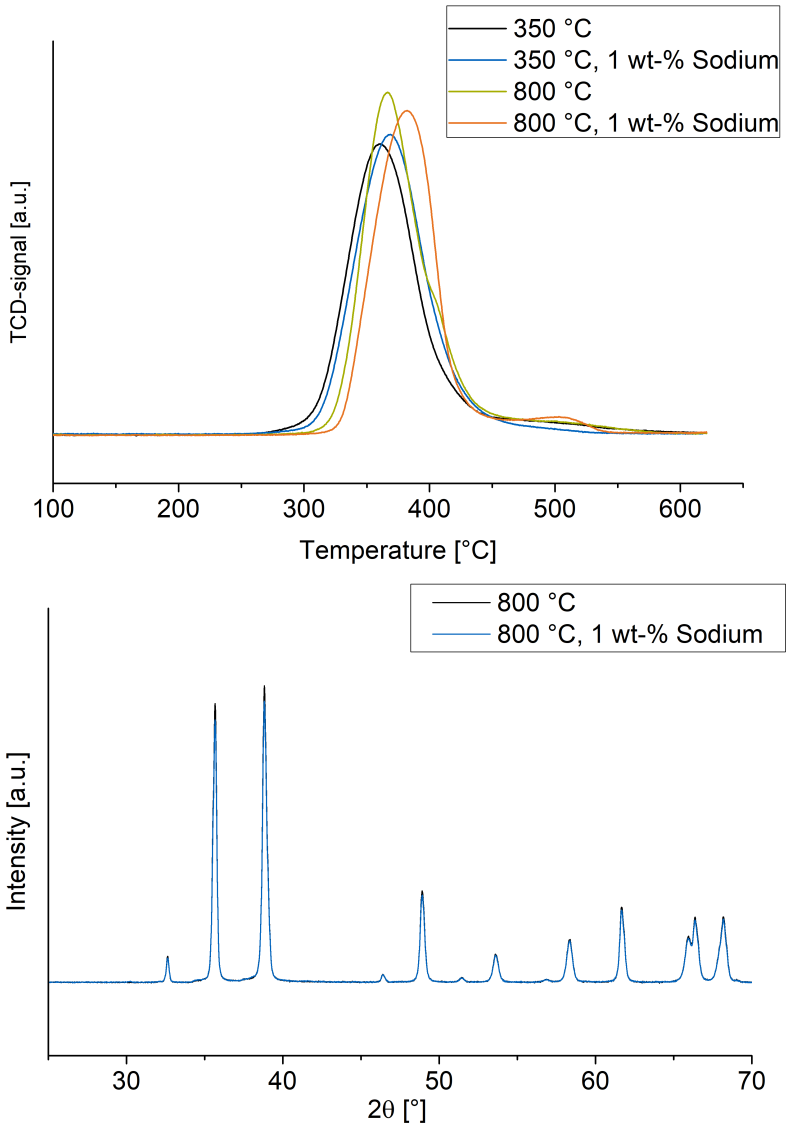

Figure 3.7: TPRs of fresh CuO synthesized at various temperatures and its sodium impregnated counterparts (top) and representative XRDs for the 800 °C samples (bottom, overlapping due to high similarity of the samples).

The temperature programmed reduction diagrams (Fig. 3.7 (top)) show a comparison of two sets of samples, namely freshly synthesized copper oxide at 350 and 800 °C and their sodium impregnated (1 wt-%) counterparts. Both sodium-free samples (black and orange) show the typical curves for pure copper oxide with an early onset. The 800 °C sample exhibits a high-temperature shoulder. Upon contact with sodium and another temperature treatment, both samples show a very minor shift to higher reduction temperatures (5 K for the 350 °C samples and 17 K for the 850 °C samples). The 800 °C sample loses its high temperature shoulder once in contact with sodium and instead a small peak around 500 °C is observed. For the sake of simplicity, only the 800 °C temperature XRDs are shown on the bottom in Figure 3.7, since all XRDs are essentially the same. Upon contact with sodium, the crystallite size of CuO marginally grows. Moreover, the addition of sodium does not lead to phase changes as was observed for the copper

aluminate spinel. Overall it has to be emphasized that sodium barely affects pure copper oxide. Qualitatively the effects go into the same direction as for the spinel, e.g. shift to higher reduction temperature and particle growth upon contact with sodium, however the magnitude of these effects is barely visible. Thereby, it was shown that similar to the actual pre-catalyst ($CuO \cdot CuAl_2O_4$), the effects of pure single phases were similar in trend but the extent of the effects was very different, which is most pronounced for copper oxide especially in its reduction. Thus it has to be considered for the catalyst ($CuO \cdot CuAl_2O_4$), that copper aluminate spinel not only takes part in the catalysis itself (or regenerative cylce as discussed above), but further modifies the properties of copper oxide in the manner similar to strong metal support interactions (SMSI). In light of these findings, the loss in activity that coincides with the destruction of copper aluminate spinel, can be explained very well.
On the other hand, metallic copper appears to be an integral component for the active hydrogenation catalysts. Without the reduction step (activation), the oxidic pre-catalysts ($CuO \cdot CuAl_2O_4$) are completely inactive. Of course this reduction includes the spinel itself, so a clean separation of which phase is responsible for the catalysis is difficult based on this merit alone. The data collected thus far puts heavy emphasis on the importance of reduced spinel, which results in metallic copper and cation deficient spinel phase. These findings fit very well to the observations by Yurieva et al. [23]. To maximize a catalytic activity thus means to maximize the interface between CuO and $CuAl_2O_4$. Hereby, copper surface area would not be a suitable measure to predict catalytic activity, since a large metallic copper surface area could just mean that large parts of the spinel are blocked by copper or that copper particles are not connected to the spinel and thus would not be able to complete a catalytic cycle as proposed by Yurieva.

3.3 Conclusions

In this chapter, the strong influence of sodium on pre-catalyst ($CuO \cdot CuAl_2O_4$) phases was demonstrated, which negatively influences reduction behavior and catalytic properties. Hence, it is necessary to completely remove sodium in a washing step after the co-precipitation. Sodium has a very high affinity towards the alumina phase, inhibiting copper aluminate spinel formation. Instead sodium aluminate ($NaAlO_2$) is formed. It further promotes copper oxide particle agglomeration and changes its properties during reduction/activation. A stabilization of Cu(I) occurs (as $CuAlO_2$), which is more difficult to reduce than Cu(II) and could explain the higher reduction temperature necessary. When pre-catalyst ($CuO \cdot CuAl_2O_4$ was impregnated with sodium, the same trends as with bulk, precipitated sodium were observed albeit being less pronounced. When the catalyst precursor phases were separated, the effects of sodium were the strongest on the copper aluminate spinel. Copper oxide was barely affected. The magnitude of effects on the pure spinel was comparable to that on the catalyst, ultimately resulting in its disintegration. Thereby, $CuAl_2O_4$ must play an integral part in the catalysis, either via

a $Cu^{2+} \longrightarrow Cu(0)$ regeneration step or via strong metal support interactions that are destroyed due to sodiums high affinity to the aluminate phase. For all these reasons, the catalyst is strongly deactivated when sodium is not properly removed.

4 Stability of Copper Aluminate Spinel Catalysts

4.1 Motivation and Literature Review

The leaching of catalyst components is one of many issues that cause catalyst deactivation due to the loss of active components that dissolve in reactants and/or solvents. In this chapter the leaching of copper is presented under various circumstances reported in the literature.

Oxidation Catalysis

An increased strain is put on copper containing catalysts during oxidation reactions. Reaction 4.1 shows a simplified leaching mechanism, which shows the oxidative leaching of metallic copper from, for example, a catalyst surface.

$$\mathrm{Cu}^0 \longrightarrow \mathrm{Cu}^{2+} + 2\,\mathrm{e}^- \tag{4.1}$$

Santos et al. investigated copper leaching during wet oxidation of phenol on CuO(67-77 %) · $CuCr_2O_4$(20-30 %) catalysts [55]. They found an increase in copper leaching if the pH dropped below 4 and if phenol-based organics were present in the aqueous media. Strong complexing agents such as oxalic acid were able to form complexes with copper which eventually precipitated as copper oxalate. The same group also reported leached copper to be an active component in the catalysis [56]. Similar observations were made by Miró and co-workers, who also found rapid catalyst deactivation by copper leaching on silica and alumina supported catalysts [57].
The effect of acetic acid on the wet oxidation of benzene was investigated by Kanzaki et al. [58], who found it to strongly increase copper leaching up to 74 % leached on various supports at 20 wt-% acetic acid. When acetic acid is present in higher concentrations (80 %) copper leaching was suppressed. Copper was then found to precipitate as copper acetate. An effect on the catalysis itself could not be found due to their catalysts exhibiting very low activity. Álvarez and co-workers measured copper leaching when recycling 5 % CuO on activated carbon in the wet air oxidation of aqueous phenol and attributed the leaching to the interactions of acetic (carboxylic) acid with CuO on the interface [59, 60]. Many other researchers reported copper leaching in various CuO-based catalysts in wet oxidation reactions [61–68].
On the other hand George and Sugunan reported barely any leaching in the oxidation of

ethylbenzene over nickel substituted copper chromite when organic solvents were used [69].

Hydrogenations and Reduction Reactions

Hydrogenation reactions rely on metallic copper which does not directly leach and needs to undergo oxidation first (at any sort of process). As per reaction 4.1 copper leaching in reductive environments will therefore be suppressed because by Le'Chatelier's principle the reaction will be shifted to the left. This theory has been supported by investigations into hydrogenolysis reactions [70] and hydrogenations [71], where only very small quantities (<6 mg/L) of leached copper were reported. Even the hydrogenation of acetic acid in continuous reactors was demonstrated without apparent deactivation by complexation or leaching [72]. For fatty alcohol production, the patent literature does not consider metal leaching under reaction conditions with the exception of Schneider et al., who report up to 280 mg metal leaching per 10 g catalyst in the liquid-phase batch hydrogenation of laruic acid [31]. The leachability of each single catalyst component (Cu/Al/Mn) is not further specified. However, those 280 mg only represent 2.8 wt-% of the catalyst, thus leaching seems generally very low. More insight can be gathered from a publication by Ladebeck and Regula [73], who contrast the leaching of copper and aluminum in slurry vs. fixed-bed applications. In the slurry hydrogenation of fatty acids (not specified), they reported up to 18 mg/L copper and 2 mg/L aluminum leaching. Since neither the amount of catalyst used nor liquid volume was reported, the total leachable components cannot be computed. The only known quantity is the volume of the autoclave (2 L), which suggests that the liquid volume was 1 liter or less. Leaching in the fixed-bed operation was reportedly less (2.5 mg/L Cu and 1 mg/L Al). This changed drastically for copper when water was present in the ester feed, which resulted in higher acid concentrations. However, their catalysts were only calcined at 600 °C. Spinel formation ($CuAl_2O_4$) can begin at that temperature, but they describe their catalyst as copper supported on alumina without showing XRD data. It has to be assumed that they in fact did not investigate a spinel catalyst.

To summarize, the leaching of copper has only very scarcely been investigated and mostly for catalytic wet oxidation (CWO) reactions, which can be considered as very harsh in terms of reaction conditions due to high acidity and temperatures. For hydrogenations and reducing environments, copper leaching appears not to be a point of concern. The few studies conducted on this field all report very low quantities of leached Cu (single digit mg/L). This changes in the presence of organic acids, where higher copper leaching was reported. Aluminum leaching was never found to be a point of concern.

4.2 Results and Discussion

4.2.1 Activity Study in the Presence of Organic Acids

To investigate the stability of copper aluminate spinel catalysts ($CuO \cdot CuAl_2O_4$), the liquid-phase batch hydrogenation of butyraldehyde (the test reaction, see Chapter 7) was extended to include carboxylic acids such as acetic and caprylic acid. The results can be found in Figure 4.1. To better understand the influence but also the amount of acid present in the catalytic reaction, the data are plotted as TOF over molecules acid per surface copper atom (or active center). The amount of surface copper atoms, which was also used to calculate the TOF, was determined by chemisorption of N_2O and calculated from the space requirements for a copper atom ($1.47 \cdot 10^{19}$ atoms per square meter).

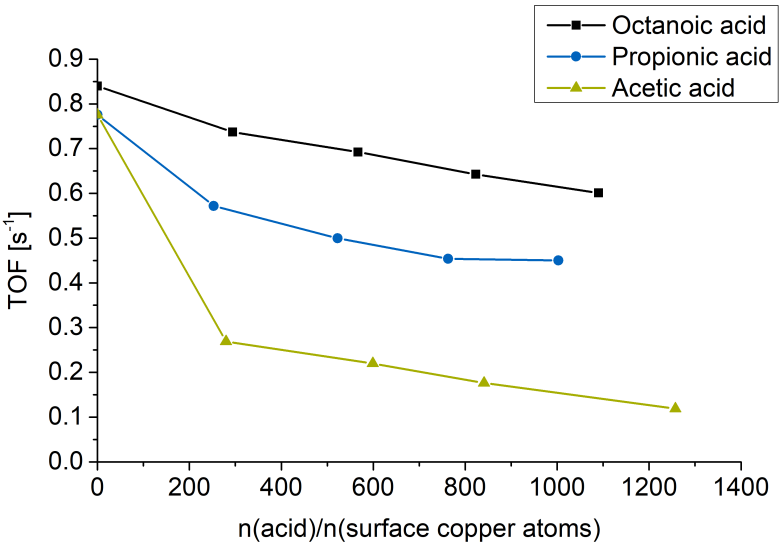

Figure 4.1: Observed deactivation depending on carboxylic acid addition to liquid-phase batch hydrogenation of butyraldehyde [120 °C, 60 bar H_2, 750 RPM, 1 h].

The small gap between the 0 % acid data points for caprylic and propionic/acetic acid stems from the fact that caprylic acid was interfering with the internal standard during gas chromatography. Therefore, the yields were calculated from the gas chromatography integrals alone. This method is very precise, but in terms of accuracy puts the results just a few percent higher than the true value because it does not account for evaporation-condensation losses in the autoclave.

As it can be seen, acetic acid (C_2) causes a very strong deactivation of the catalyst, followed by propionic (C_3) and caprylic acid (C_8). These experiments clearly establish the deactivation strength with regards to the chain length. At larger excess ratios of carboxylic acids per surface copper atom, all three deactivation trends become linear with the same slope. Thus, the deactivation graphs can be split into two parts. The first being the difference between no acid and the first data point with acid. This part shows the deactivation strength. The second part is the linear trend followed right after the

initial drop. For all three acids it is essentially the same, showing that the deactivation mechanism is probably similar with varying degree of strength based on chain length. The second part in particular is indicative of the mechanism. To achieve a flatting off into a linear deactivation trend as observed here, the mechanism must be dependent on an underlying equilibrium, where the addition of further excess acid slightly shifts the equilibrium towards the more deactivated state. Another possible deactivation mechanism that has to be considered is a possible demixing of liquid components in a stationary liquid film around catalyst particles. Liquid components can be separated into two groups. Hydrophobic components such as hexane and dodedance and hydrophilics such as butyraldehyde and carboxylic acids (depending on chain length). If this was the case, hydrophilic compounds would be enriched in the stationary liquid film close to the polar catalyst surface. A deactivation would occur simply by replacing reactants with other hydrophilic components that would induce a slower diffusion of reactants to active centers. This hypothesis would also explain the strength of deactivation depending on chain length of the carboxylic acid since their polarity varies with the length of its alkyl chain.

To investigate this issue a new set of experiments was conducted with acetic acid. In these experiments the amount of acetic acid was lowered to achieve molar ratios as low as one for the ratio of acetic acid to surface copper atoms. Thereby, a demixing cannot possibly cause the deactivation since the amount of carboxylic acid molecules is not high enough to form liquid films around catalyst particles. The results can be found in Figure 4.2. The acetic acid series was expanded by four catalysis experiments between 0 and 280 n/n on the x-axis. At molar ratios of 2.6, which is equivalent to 5 µL acetic acid in 110 mL liquid phase volume, a relatively harsh drop from 0.78 s^{-1} to 0.69 s^{-1} can be observed. Increasing the molar ratio of acid to surface copper atoms leads to the flattening off into the linear trend that has been discussed above. This clearly indicates that the deactivation mechanism of carboxylic acids can be attributed to a reversible blocking of active sites with an underlying adsorption-desorption equilibrium (comp. Fig. 4.3). A small sample calculation can help illustrate this point. If one assumes spherical particles of 15 nm diameter without pore volume to be covered by a 1 nm thick layer of demixed liquid, then 5 µL acetic acid would cover $1.665 \cdot 10^{15}$ of such particles. The catalyst particles have a density of roughly 2 kg/L, which means 47 mg of catalyst particles could be entirely covered by a 1 nm thick acetic acid layer with the assumptions made prior. In the catalysis itself, 700 mg of catalyst were used and the pore volume was not even considered. Of course some of the surfaces of the 15 nm particles that were used for this sample calculation, will be covered by other crystallites to form primary particles. However, this loss of surface is offset multifold by the pore volume that was not accounted for. By any means, this consideration should clarify, why a demixing cannot be considered for the deactivation mechanism and instead a reversible blocking of active sites by carboxylic acids (see Fig. 4.3) must be the cause.

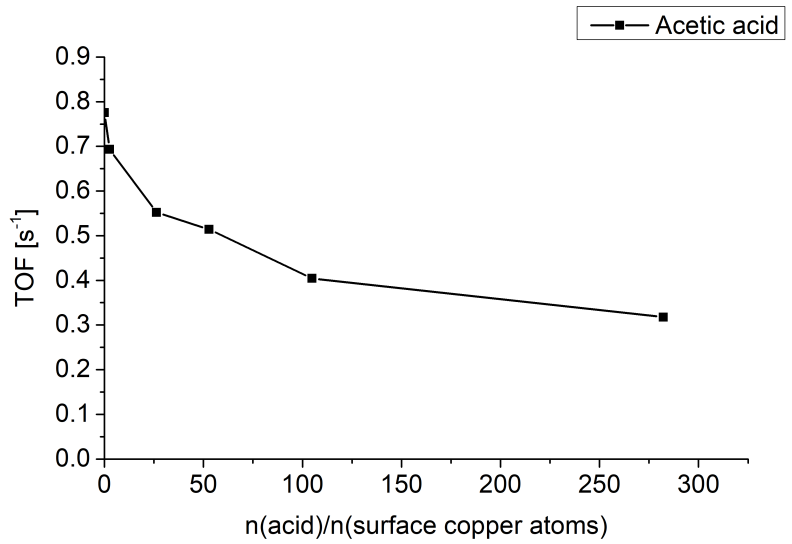

Figure 4.2: Activity at lower acetic acid amounts, as low as 5 µL in 110 mL reaction medium [120 °C, 60 bar H_2, 750 RPM, 1 h].

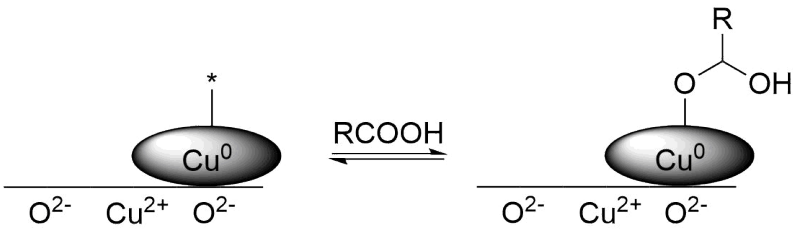

Figure 4.3: Suggested blocking of active centers by carboxylic acids without deactivation due to de-mixing.

4.2.2 Phase Composition Changes Induced by Carboxylic Acids

Investigation of the catalyst phase composition after exposure to carboxylic acids is a simple way of measuring the catalyst's bulk stability. Thus, the phase compositions of pre-catalysts ($CuO \cdot CuAl_2O_4$) was compared to spent catalyst with and without exposure to carboxylic acids. After the liquid-phase batch hydrogenation of butyraldehyde the catalysts were filtered from the organic phase and subsequently measured by XRD. The results can be found in Figure 4.4. The phase composition of spent catalysts with and without exposure to caprylic acid (C_8) shows up to three crystalline components, which are Cu(0), $CuAl_2O_4$ and Cu_2O. Metallic copper and coppper aluminate are expected, as they are the products after reduction of the oxidic pre-catalyst ($CuO \cdot CuAl_2O_4$). Further, metallic copper is produced from the spinel phase itself by reducing Cu^{2+} from the spinel lattice which migrates to the spinel surface and forms metallic copper particles. The now cation-deficient spinel is stabilized by incorporation of protons. These findings by Plyasova et al. were discussed in Chapter 2. Cuprous oxide is the natural re-oxidation product.

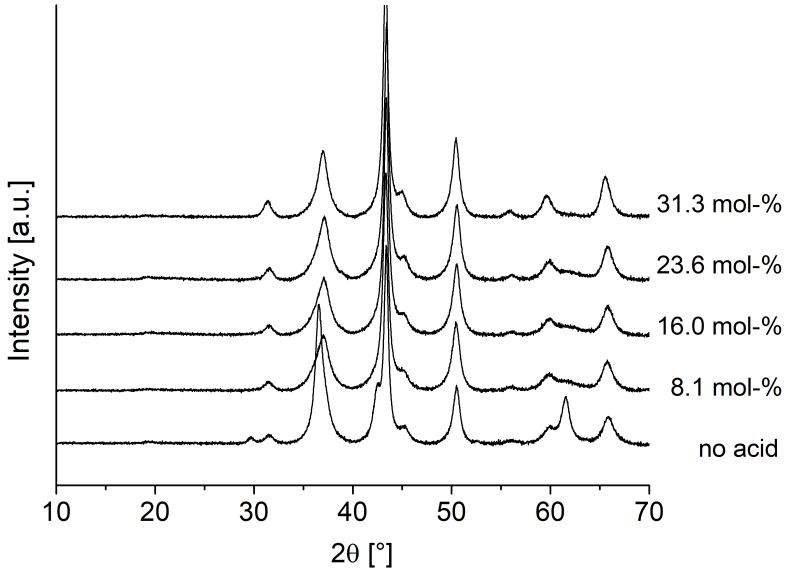

Figure 4.4: Phase composition of spent catalysts after the test reaction with increasing amounts of caprylic acid. Mol-% calculated against butyraldehyde amount [120 °C, 60 bar H_2, 750 RPM, 1 h].

Unlike the reduction reaction, that skips Cu_2O on the way from Cu^{2+} to Cu(0) under industrially relevant conditions, the re-oxidation kinetically favors cuprous oxide as its sole product. Due to air contact, re-oxidation to Cu_2O is observed with respect to how long the samples were exposed to oxygen. The regular, spent catalyst ('no acid') for example has the highest and most crystalline cuprous oxide content. That sample was significantly older (about 2 weeks) than the others, where no reoxidation product is observed. Two conclusions can be drawn from these experiments. First of all, the influence of caprylic acid, as a representative for longer chain carboxylic acids, does not extend to the bulk phases. It only affects the catalyst surface by competitive adsorption during catalysis and leaching of components into the reaction mixture. Thus, only the two expected phases Cu(0) and $CuAl_2O_4$ are observed. Secondly, the activated but spent catalysts seem to benefit from a passivation, because the re-oxidation is very slow. Possibly, adsorbed carboxylic acids prevent passivation layers to form and enable oxidation from more angles. Freshly activated catalysts that are exposed to air are pyrophoric. Their re-oxidation is very fast and exothermic.

The experiments with acetic acid, shown in Figure 4.5, draw a different picture. The three previously mentioned phases Cu_2O, $CuAl_2O_4$ and Cu(0) are all present and make up the bulk of the catalyst. However, cuprous oxide reflexes, e.g. at 42.4 °, are higher in intensity, which means the fraction of crystalline Cu_2O is increased.

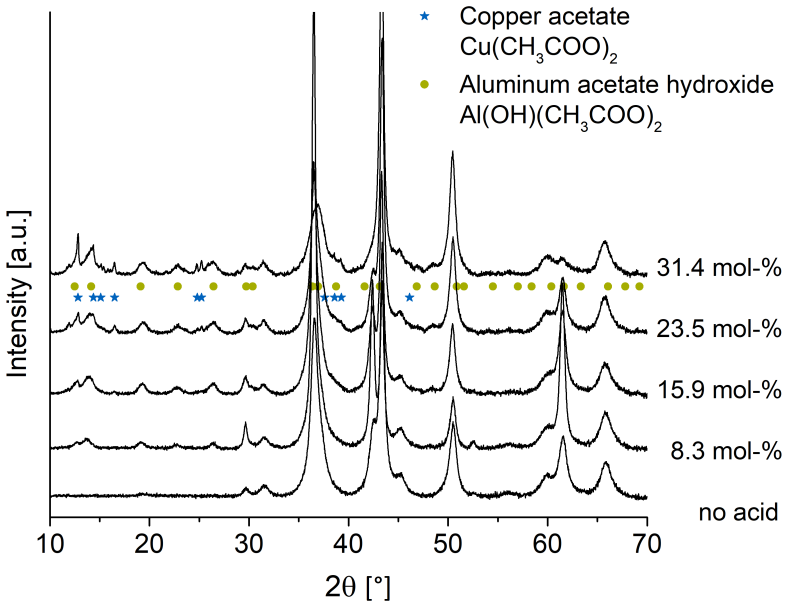

Figure 4.5: Phase composition of spent catalysts after the test reaction with increasing amounts of acetic acid [120 °C, 60 bar H_2, 750 RPM, 1 h].

Furthermore, two new phases can be detected in the diffractograms namely copper acetate and aluminum acetate hydroxide. Both phases are low in intensity and have rather broad peaks, meaning the fraction of product and its crystallite size is rather low. Nonetheless, it must be concluded that acetic acid causes large scale restructuring of the surface since a mere single layer of copper and aluminum acetate would not be visible in an x-ray diffraction pattern as a bulk analysis method. The mechanism of formation must occur via a dissolution-crystallization mechanism, to enable the formation of crystallites large enough to be detected by XRD. A diffusion of a rather large molecule such as acetate into solid copper metal or cation-deficient aluminate can be excluded. This would also explain why the deactivation strength of acetic acid is much larger than the other two acids tested (comp. Fig. 4.1). Not only does the acid block active centers (as discussed above) but it further destroys active centers by the dissolution of copper and aluminum. A re-precipitation on top of the catalyst surface could further block active centers completely.

4.2.3 Metal Leaching under Acidic Conditions

Leaching during industrial catalysis is an undesired process with regards to catalyst activity, stability and purity of the product. As a surface phenomenon, leaching can remove active components from the catalyst, which would cause a decrease in catalyst activity while contaminating reaction products. A loss of stability will be observed when structurally important surface components are removed. Therefore, leaching under reaction conditions was investigated in this work. Right after the reaction, the autoclave was opened and a filtered liquid sample taken to avoid oxidation processes influencing the results, i.e. to avoid modification of copper dissolution by oxidation processes. Copper

and aluminum leaching was measured by ICP-OES. More information can be found in Chapter 7.

The concentration of leached copper against a variety of carboxylic acids is plotted in Figure 4.6. For pentanoic and heptanoic acid it was not possible to determine the catalytic activity because the acids heavily interfered with the product gas chromatography integrals. Nonetheless, leaching samples were withdrawn and are presented here. It can be seen that C_2 - C_7 acids cause minor copper leaching $\leq$ 4 mg/L. Under reaction conditions caprylic acid (C_8) has up to 12 mg/L leached copper which is equivalent to 0.3 wt-% of total copper. The fact that copper leaching was found could also be attributed to the fact that at some point during sample workup, the spent catalysts are exposed to oxygen and could potentially undergo leaching after oxidation by air. However, as it will be shown in Chapter 5, Cu^{2+} is a part of the activated spinel phase. While it is interesting to observe copper leaching under reducing conditions, these experiments show very small leaching regarding the total copper of the catalyst as expected. Furthermore, there seems to be a threshold in chain length after which Cu^{2+} is sufficiently stabilized in the solvent to be leached from the surface (comp. heptanoic acid) with the exception of acetic acid. Acetic acid seems to play a somewhat special role that extends beyond the sole phenomenon of varying hydrophobic attributes by chain length as will be further discussed below. The amount of leached copper is so low (max 0.3 wt-%), that this could be attributed to unreacted Cu^{2+} during the activation (or formed during the reaction). However, when the exact mechanism of leaching is considered, this might not be the best explanation. Leaching is a surface phenomenon. During activation, especially the copper on the surface would be reacted to metallic copper which we would not expect to be leached under reducing conditions as it has to undergo an oxidation to Cu^{2+} first. For reference the electrode half cell potential of $Cu^{2+} + 2\,e^- \rightleftharpoons Cu$ is 0.35 V. While this is nowhere close to noble metals such as Pt (1.2 V), it does show that copper is not easily oxidized in an atmosphere of 60 bar hydrogen.

Such a reduced copper surface should thus be relatively inert against leaching unless something oxidizes copper. This exact oxidation step is proposed in the hydrogenation reaction mechanism by Yurieva et al. [23], where metallic copper centers are oxidized while transferring electrons to a carbonyl group. It should also be mentioned at this point, that ligands can heavily affect the oxidation potential (electrode half cell potential) via stabilization of oxidation states, which for example is used during the production of gold among other things. Therefore, the electrode half cell potential should not be over emphasized as a standalone property. These considerations and findings support a reaction mechanism via Cu^{2+} but are by no means proof of such a mechanism.

With respect to catalyst stability, leaching of aluminum has to be considered as well. The amount of aluminum leached is shown in Figure 4.7 (corresponding data points to copper shown in Fig. 4.6). It is instantly clear, that aluminum leaching is a much larger issue than one would anticipate. While alumina supports are definitely not considered to be as stable against acidic attacks as silicates for example, one would assume that a dissolution would only occur slowly under very acidic conditions.

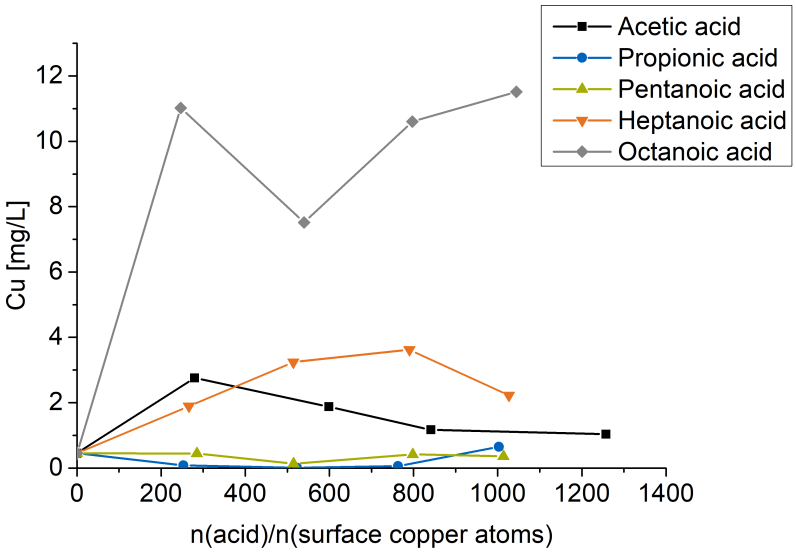

Figure 4.6: Leaching of copper after one hour under reducing reaction conditions during the hydrogenation of butyraldehyde with a variety of carboxylic acids [120 °C, 60 bar H_2, 750 RPM, 1 h].

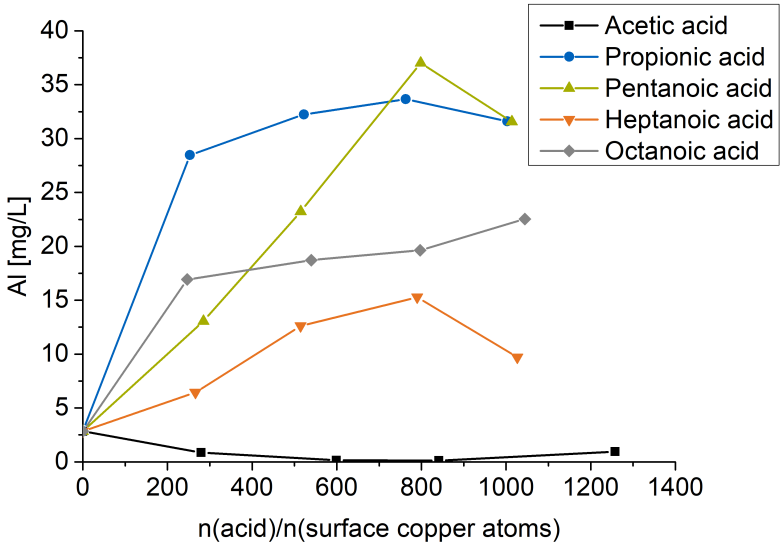

Figure 4.7: Aluminum leaching after one hour under reducing reaction conditions during the hydrogenation of butyraldehyde with a variety of carboxylic acids [120 °C, 60 bar H_2, 750 RPM, 1 h].

Here a dissolution of up to 37 mg/L Al^{3+} can be measured, which is equivalent to 2.4 wt-% of total aluminum in the catalyst. This is an amount that exceeds mere surface leaching. An erosion of catalyst structures has to be assumed at this point or at the bare minimum a dissolution or large fractions of the surface. The implications are of course a strong decline in stability. In catalyst tablets, that are used in industrial applications, they would lose a significant amount of side crush strength, a test that measures how much pressure the tablets can withstand before crumbling. These tablets would crumble inside of a real reactor which would lead to high pressure drops or even blocking of the reactor. But why

do these catalysts exhibit such high aluminum leaching? The explanation for this has to be connected to the activation procedure. All Al^{3+} ions that are present in the catalyst are located in the spinel phase. However, after activation this spinel phase is very cation deficient. XAS results (not shown here) find some Cu^{+} and leftover Cu^{2+} in the spinel, but the vast majority ($\geq$ 75 %) of Cu^{2+} is reduced to form metallic copper particles on the surface. To offset the loss of charge, protons are incorporated in the spinel phase. Small protons replacing large cupric ions lead to lattice tension and constrictions that make the activated spinel lattice vulnerable to acidic attack, which then leads to destruction of said cation deficient spinel by carboxylic acids. It is not really possible to find trends based on chain length in these experiments.

In section 4.2.2 it was shown that acetic acid forms crystalline acetates of both copper and aluminum during catalysis. A dissolution-precipitation mechanism was proposed due to the crystallinity of the particles, that extend surface precipitates to be visible in the XRD. In the leaching experiments with acetic acid, copper leaching is increased compared to the catalyst that was not exposed. It goes through a maximum of 3 mg/L and at higher concentrations stabilizes around 1 mg/L. Thus, higher acid concentrations lead to reduced amounts of leached copper and, as shown in the XRD, more precipitated copper acetate. Although crystalline copper acetate only appears in the 23.5 mol-% sample, it can be assumed that $Cu(Ac)_2$ crystallites are x-ray amorphous in the lower samples and only grow to detectable sizes at higher excesses of acid. These findings fit very well into the proposed dissolution-precipitation mechanism, that would allow the formation of large copper acetate particles. This would be a second mechanism to reduce catalyst activity as opposed to reversible blocking of active centers at higher carboxylic chain length.

After exposure to acetic acid, aluminum leaching is decreased and crystalline aluminum acetate hydroxide appears (comp. Figs. 4.5 and 4.7). Thus, the solubility product of aluminum acetates must be rather small. This becomes especially obvious when one compares the amounts of leached aluminum with other carboxylic acids. For example, pentanoic acid has as much as 35 mg/L of leached aluminum. Due to the above mentioned effects, acetic acid stands out in this reaction system. Other reactions than the mere blocking of active sites are involved and the bulk structure of the catalyst is affected. Thereby, using acetic acid as an example carboxylic acid to measure acid stability of these types of catalysts cannot be recommended.

Some open questions remain that will need further investigation regarding the leaching behavior. In the experiments for leached copper, all acids show very low amounts of leached copper species without a recognizable trend based on chain length for example. Caprylic acid then triples the maximum of previously measured copper. The reason for this behavior is still unclear, although it must be related to stabilization of $Cu^{1+/2+}$ in solution for example via micelle formation. Another topic for further research could look into the vastly different copper and aluminum leaching for pentanoic and propionic acid. Both do not dissolve copper under reaction conditions and instead exhibit the highest aluminum leaching. How is it possible, to selectively dissolve a cation deficient copper

aluminate spinel while not affecting copper at all?

4.2.4 Catalyst Stabilization against Acidic Attacks

As it was demonstrated, the presence of carboxylic acids is very detrimental to copper aluminate spinel catalysts ($CuO \cdot CuAl_2O_4$). Acids not only decrease activity by adsorption on active centers, but partly dissolve catalyst structures. Especially the cation deficient spinel phase is prone to losing aluminum in large quantities, which can decrease stability of catalyst tablets. Two strategies to circumvent these issues are possible. First of all, the chemical properties of the alumina phase can be altered, for example its acidity by incorporation of substituents such as silicon. On the other hand, if one considers the proposed reaction mechanism by Yurieva et al. [23] that includes a regeneration step from Cu(II) to Cu(0) and that leaching requires metallic copper to oxidize first, then modifying the reduction potential of the environment can be helpful in preventing leaching. Moreover, by affecting the regeneration step it could also proof useful in the catalysis itself.

The effect of 6 wt-% silicon promotion is shown in Figures 4.8 and 4.9. It can be seen that silicon promotion is an effective tool to reduce leaching. Aluminum leaching is reduced from 1.25 wt-% of total aluminum down to 0.79 wt-%. Copper leaching is decreased from 0.16 wt-% to 0.11 wt-%. Unfortunately, silicon promotion also decreases catalytic activity from 67 % yield to 47 % without acid and 65 % to 39 % with 8 mol-% octanoic acid (comp. Figure 4.9). Thus, the stabilizing effect which is responsible for a decrease in leaching also hinders catalytic activity. X-ray diffractograms confirm, that crystalline phases CuO and $CuAl_2O_4$ remain intact upon silicon promotion. They become more amorphous. Considering that Si^{4+} ions cannot be built into the spinel due to their charge, one can assume that amorphous Al-Si mixed oxides form which are known for their acidity. Thereby, the better acid stability can be explained. The loss in activity could also be traced back to this mixed oxide, since the catalyst contains less copper than the unpromoted one and due to mixed oxide formation also less spinel, which, as it was shown time and time again in this work, is detrimental for catalysis. A very interesting observation can be made from the leaching of pure spinel which barely shows any leaching without acid and rather high copper leaching in the presence of octanoic acid compared to the catalyst $CuO \cdot CuAl_2O_4$. This confirms that leached Cu^{2+} does not necessarily stem from the reaction cycle but is rather confined to residual cupric ions from the spinel phase. Pure spinel is leaching more copper because in those experiments there was 700 mg of spinel present as opposed to only 50 mol-% in the reactions with catalyst ($CuO \cdot CuAl_2O_4$). Furthermore, excess CuO (and after reduction metallic copper) will potentially block spinel sites which, if they were exposed to the carboxylic acid, would then be a source for leached Cu(II). These findings further prove the hypothesis of spinel being the source of leaching.

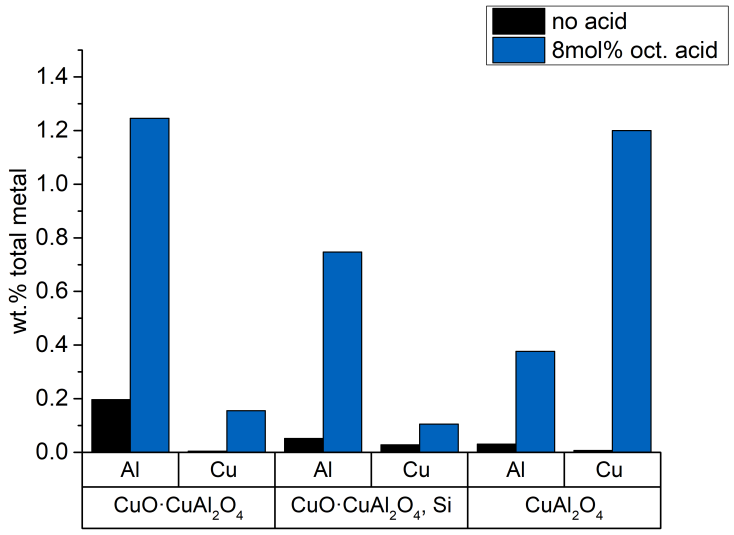

Figure 4.8: Leaching of copper and aluminum from a standard catalyst ($CuO \cdot CuAl_2O_4$) compared to a silicon promoted (6 wt-%) catalyst and pure copper aluminate spinel plotted as fraction leached of each composite [120 °C, 60 bar H_2, 750 RPM, 1 h].

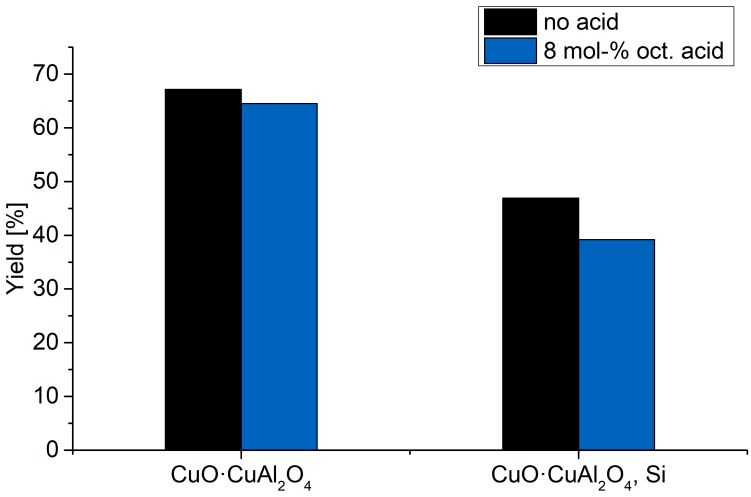

Figure 4.9: Activity of a standard catalyst ($CuO \cdot CuAl_2O_4$) compared to a silicon promoted (6 wt-%) catalyst with and without addition of octanoic acid [120 °C, 60 bar H_2, 750 RPM, 1 h].

The second method for stabilization involves the modification of the reaction medium by variation of redox potential. To test this hypothesis, methanol was added as a reducing agent to the liquid-phase hydrogenation of butyraldehyde. This proved unsuccessful, as transport phenomena such as chemical vapour deposition were observed [74], where copper was deposited on the autoclave walls. To avoid chemical vapour transport by methanol, that would have uncontrollable side effects on the catalysis and would contaminate the autoclave, ethanol was used as a replacement. Ethanol is a weaker reducing

agent but most importantly should not exhibit CVD with copper. First of all, the effect of ethanol was tested without the addition of carboxylic acids. The results are shown in Figure 4.10.

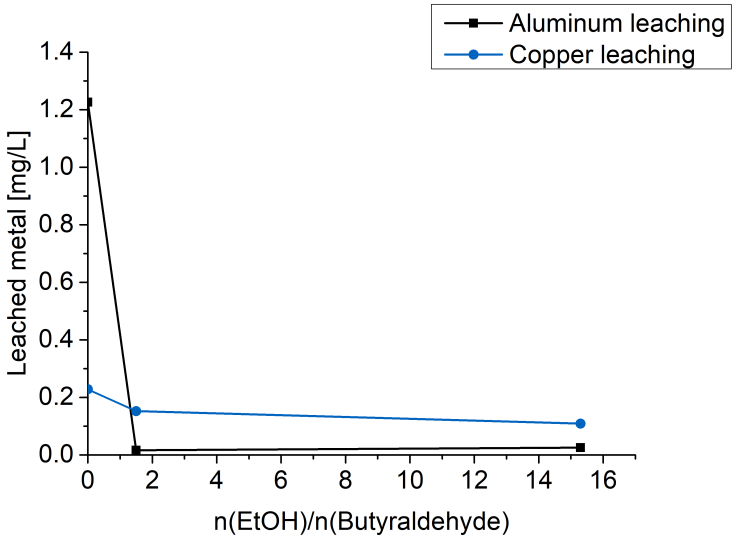

Figure 4.10: Aluminum and copper leaching after one hour under reaction conditions during the hydrogenation of butyraldehyde without EtOH compared to EtOH as an additive and solvent [120 °C, 60 bar H_2, 750 RPM, 1 h].

On the left hand side (marked 0), the leaching data for the standard experiment without additives is shown. 1.25 mg/L aluminum was leached and 0.25 mg/L copper. With the addition of 10 mL ethanol, aluminum leaching is suppressed to only 0.016 mg/L. Copper leaching decreases slightly (0.152 mg/L). When hexane as a solvent is replaced with ethanol (100 mL), aluminum and copper leaching are similar to ethanol as an additive (0.025 and 0.108 mg/L respectively). Thus, ethanol works in agreement for the hypothesis that reducing agents would prevent leaching of copper. Interestingly, aluminum leaching also seems to decrease but the data points below 0.5 mg/L are outside of the calibration curve and most definitely close to the lower detection limit in these ICP-OES experiments. In a next step, this method has to be tested with carboxylic acids present. For this, ethanol was used as an additive and solvent in the presence of caprylic acid (comp. Fig. 4.11).
For reference the metal leaching with 8 mol-% octanoic acid is shown without the addition of ethanol. 17.26 mg/L aluminum and 11.19 mg/L copper leaching was found which was discussed above in detail (see Figs. 4.6 and 4.7). With the addition of 10 mL ethanol, the leaching of both $Cu^{1+/2+}$ and Al^{3+} is strongly reduced down to 8.62 mg/L and 5.86 mg/L respectively. This effect becomes even more pronounced, when ethanol is used as a solvent (2.85 mg/L Cu and 0 mg/L Al). Thus, the hypothesis of influencing the reductive environment is a working strategy in reducing metal leaching.

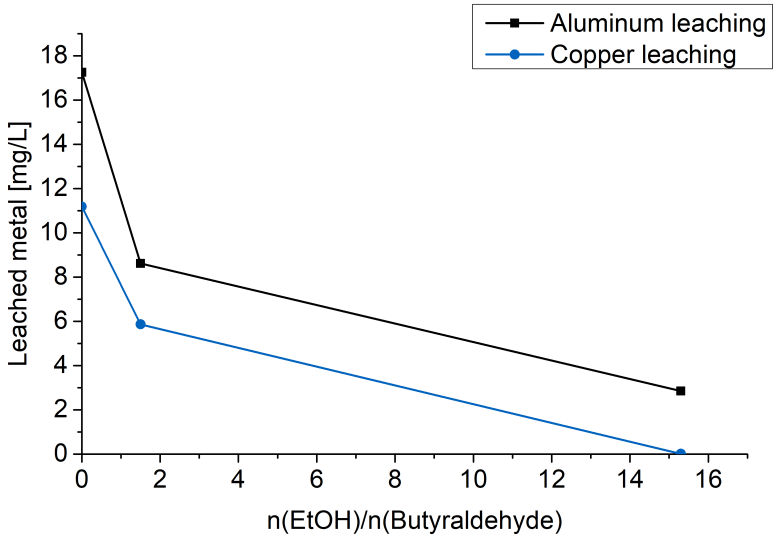

Figure 4.11: Metal leaching with exposure to octanoic acid without ethanol compared to EtOH as an additive and solvent [120 °C, 60 bar H_2, 750 RPM, 1 h].

Surprisingly, this extends to aluminum as well which should not be part of the oxidation-reduction cycle. When copper is leaching from the surface, unsaturated aluminum is exposed to acids. Furthermore, aluminum from the cation deficient spinel will be destabilized due to a lack of charge in the spinel. Thus, aluminum leaching by itself is not surprising. The fact that ethanol prevents this is. At this point multiple effects could be the reason and they have to be considered as speculative. On the one hand ethanol could modify solubility of the aluminum carboxylates or affect the formation of those, on the other hand an influence on the carboxylic acid itself, preventing it from forming aluminum surface carboxylates that would subsequently leach is possible. Nonetheless, with this method the negative influence of acids on catalyst stability can be completely offset. A co-feeding of ethanol in an industrial reactor could thereby solve stability issues caused by leaching.

Catalytic Activity in the Presence of Ethanol

While testing the effect of ethanol on metal leaching in the hydrogenation of butyraldehyde, catalyst activity was also monitored. The results are shown in Table 4.1. With 8 mol-% octanoic acid, the initial activity of the catalyst drops from 95.8 % to 85 % due to competitive adsorption on active centers as established above. When ethanol is used as an additive or even as the solvent, the activity increases to 88 % and 99.4 % respectively. The negative effects of acids on catalyst activity can thus be offset by ethanol. To illustrate the positive effect of ethanol on catalyst activity, the yields without octanoic acid and halved catalyst masses are shown in the third column in relation to the amount of ethanol added. Without any modifications of the standard hydrogenation test 45.7 % yield are achieved. Once 10 mL ethanol were added, the yields jump as high as 81.5 %. Ethanol as the solvent achieves 99.4 % yield.

Table 4.1: Catalytic activity of $CuO \cdot CuAl_2O_4$ in the presence of ethanol and 8 mol-% octanoic acid [120 °C, 60 bar H_2, 750 RPM, 1 h].

n(Ethanol)/n(Butyraldehyde)	Butanol yield [%]	Yield with 50 % catalyst, no acid
0 (no acid)	95.8	45.7
0	85.0	
1.5	88.0	81.5
15.3	99.4	99.4

After addition of only 10 mL ethanol (to ca. 110 mL liquid volume), the yields are almost doubled, showing the strong influence of ethanol on catalyst activity. The hypothesis that adding modifieres to the redox properties of the system must influence the catalytic activity holds true. A reducing agent which can increase the regeneration rate of Cu^{2+} to Cu(0) would benefit activity such as displayed here.

EtOH: Mechanistic Studies

To investigate the mechanism of effect of ethanol, reactions were conducted with the pre-catalysts ($CuO \cdot CuAl_2O_4$) without prior activation (comp. Fig. 4.12). In the first experiment (bottom of Figure 4.12), ethanol was added to the reaction mixture and the reaction was run without hydrogen pressure under an inert, argon atmosphere. The catalyst was filtered after the reaction was completed and measured by XRD. A regular pre-catalyst consisting of CuO and $CuAl_2O_4$ can be seen. A CuO reference pattern was added below as a line diagram. No phase change occurs. This experiment did not yield any butanol either. However, when not only ethanol but hydrogen are added to the pre-catalyst in the reaction mixture (top of the XRD in Figure 4.12), a formation of metallic copper and a strong decline in CuO intensity is observed. A reference pattern for metallic copper was added as a line diagram below. Hereby, an *in situ* activation/reduction of pre-catalyst by ethanol in combination with H_2 is demonstrated. Neither hydrogen nor ethanol achieve this alone.

This un-activated pre-catalyst achieves 99.8 % butanol yield which is comparable to a prior activation although this fact should not be over interpreted since a complete conversion of reactants could in one case occur after 30 min reaction time and in the other after 60 minutes which would appear to be the same for the observer after stopping the reaction at 60 minutes. Nonetheless these experiments demonstrate the beneficial effects of ethanol and its mechanism of action, which is the *in situ* reduction of Cu^{2+} to Cu(0), which improves the catalysis. Assuming the oxidation step to Cu^{2+} is a requirement for leaching of copper, it would also explain the reduction in leached copper. For aluminum however, it is unclear as to why its leaching is reduced that drastically.

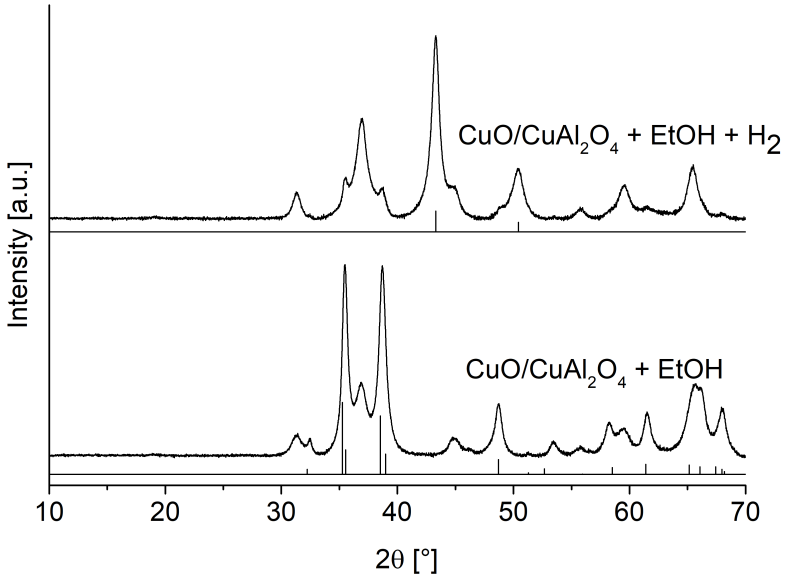

Figure 4.12: Phase composition of pre-catalysts ($CuO \cdot CuAl_2O_4$) exposed to reaction conditions with and without hydrogen and ethanol as an additive. XRD references for metallic copper (top) and CuO (bottom) are shown [120 °C, 750 RPM, 1 h].

4.3 Conclusions

The effects of carboxylic acids on copper aluminate spinel catalysts ($CuO \cdot CuAl_2O_4$) were investigated in the liquid phase hydrogenation of butyraldehyde in hexane (120 °C, 60 bar H_2, 750 RPM). Carboxylic acids were found to inhibit the catalysis by competitive adsorption on active centers, thereby slowing down the reaction. The initial drop in activity can be used to determine adsorption strength. The deactivation did not coincide with phase changes measured after catalysis with the exception of acetic acid, where crystalline copper acetate and aluminum acetate hydroxide was detected. Thus, the strong deactivation for acetic acid could be attributed to large scale restructuring of catalyst surface.

As expected, copper leaching was relatively low for all acids ($C_2 - C_8$) due to the reducing conditions. Octanoic acid had the most copper leached into solution with a maximum of 0.3 wt-% of total copper. The stabilization of $Cu^{1+/2+}$ in solution via shielding of the charge from hydrophobic hexane is probably the most important factor to determine the amount leached.

Most surprisingly, high aluminum leaching was found for all cases except for acetic acid, where aluminum acetate hydroxide precipitated on the catalyst surface. Up to 2.4 wt-% of total aluminum in the catalyst leached in only one hour reaction time. A loss of catalyst stability via erosion of tablets has to be expected and is very likely the reason why industrial copper aluminate tablets suffer from stability losses when exposed to carboxylic acids. It remains unclear why aluminum is leached in such large quantities albeit tension

and charge loss of the cation deficient copper aluminum spinel after activation probably play a major role.

Two methods to prevent the acidic attack on catalysts were found and examined in this work. Silicon promotion can help reduce leaching of copper and aluminum at the cost of catalytic activity. Furthermore, addition of ethanol to the liquid phase or using it as a solvent significantly decreases leaching. If ethanol is used as a solvent, leaching is completely suppressed even if carboxylic acids are present. Simultaneously, ethanol strongly increases catalytic activity via *in situ* reduction of the catalyst in cooperation with H_2.

5 Model Catalysts and Mechanistic Studies

Preface

The active structure and hydrogenation reaction mechanism of copper aluminate and chromite spinel catalysts has received some attention in the past. This is not surprising as copper chromite catalysts have been applied in several different reactions since their discovery in the 1930s. Copper aluminates have been researched in the past because of the importance of Cu-Al catalysts in methanol synthesis. A more recent motivation is the replacing of chromium by less toxic aluminum. Before a detailed overview of mechanistic studies in the literature is given, it can be anticipated that the general functionality of copper spinel catalysts is not solved and merely several suggestions exist. Furthermore, the literature for the interaction of copper and aluminum during catalyst synthesis - especially thermal treatment - and the interaction of such oxides with hydrogen will be summarized, as both parts are crucial in understanding the active structure of copper aluminate catalysts.

5.1 Mechanistic Studies of Hydrogenation Reactions on Copper Spinels in the Literature

Two steps are essential for a successful hydrogenation. First of all the H−H bond has to be activated. Most authors report a splitting of said bond on the catalyst surface. Atomic hydrogen is obtained. Sometimes a heterolytic dissociation into H^+ and H^- is reported. Secondly, activated hydrogen has to be brought into contact with the unsaturated substrate. The vast majority of liquid phase hydrogenations follow a Langmuir-Hinshelwood type mechanism, where both substrates (hydrogen and the unsaturated compound, e.g. C=C) adsorb on active centers, subsequently react and desorb. So how does copper spinel achieve these features?
Bechara et al. and Jalowiecki et al. investigated the reaction mechanism of copper chromite in the hydrogenation of dienes [5, 24]. They found, what they call, an 'occluded hydrogen' species (H·) to take part in the hydrogenation. Unfortunately they were not able to further determine the exact species of said occluded hydrogen. However, they were able to pinpoint cuprous ions in octahedral positions of the spinel to be the active sites for the hydrogenation reaction. Cr^{3+} on the spinel surface was an active center

for isomerization reactions of the diene. Metallic copper particles on the spinel surface did not participate in the hydrogenation reaction according to the authors. In a follow-up investigation, these authors used deuterium tracer analysis to figure out the reaction netwok and intermediates in the hydrogenation of 1,3-pentadiene and isoprene [75]. Based on their analysis, they proposed an allylic carbanion as the major intermediate, which required the occluded hydrogen to be hydridic and a proton to complete the reaction. Hubaut, Daage and Bonelle expanded their research to include α, β-unsaturated aldehydes [14]. They reported a 'considerable enhancement of the 1,4-addition process' due to stronger adsorprtion of the more polar reactants, which according to them is consistent with copper hydride chemistry. In a comparison between Cu-Cr and Cu-Al oxidic catalysts, the latter being calcined at 800 °C thus containing CuO and $CuAl_2O_4$, they did not find any differences in reaction mechanisms in the hydrogenation of allylic alcohols [76]. The selectivities towards isomerization reactions varied to a degree because of the differences in acidity between Al^{3+} and Cr^{3+}. These catalysts were further characterized by Bechara et al. with XPS in the reduction with H_2 and CO [25]. A reduction of copper in tetrahedral positions of the spinel was reported to form metallic copper particles on its surface. Cu^{2+} in octahedral positions was reduced to Cu^{+}, which was stabilized in octahedral positions according to the authors. Further, they reported catalytic activity in the hydrogenation of dienes to be proportional to Cu(I) in octahedral positions, which was also observed for Cu-Cr catalysts according to the authors.

Another group that investigated copper chromite and copper aluminate spinel catalysts originally as methanol synthesis catalysts put a lot of emphasis on the active structure of both spinels and their interaction with hydrogen. For copper chromite Krieger et al. found two different hydrogen species within the spinel after reduction/activation [77]. They found both atomic hydrogen and protons within the activated spinel lattice. Atomic hydrogen was located in octahedral positions. Protons, that exchanged copper ions to offset the charge loss, formed OH bonds. Metallic copper grew epitaxially on the spinel surface. According to the authors, a reduction of the copper chromite spinel at 590 K resulted in the following sum formula: $Cu^{0}_{0.513}/[Cu^{2+}_{0.341}][H^{+}_{0.30}]_4[Cu^{+}_{0.073}H_{0.315}]_2[Cr^{3+}]_2O_4$. Figure 5.1 shows a representative image of the activation of copper chromite as proposed in a follow-up study by Plyasova et al. [34]. It is important to note that the reduction of the spinel is reversible. Upon loss in hydrogen partial pressure, they observed metallic copper to be re-oxidized by protons from the spinel lattice. The cupric ions then migrate back into the spinel and hydrogen gas leaves the solid [34]. Simentsova et al. investigated the mechanism of reduction and found that two reactions account for most of the reduction of Cu(II) [42]. First of all a surface reduction of spinel was proposed as H_2 + $Cu(II)_{(s)}$ + $O_{(s)} \rightleftharpoons {Cu_{(s)}}^{0} + H_2O$, which then turns into a surface and bulk reduction of Cu(II) that does not involve oxygen: $H_2 + Cu(II)_{(s,b)} \rightleftharpoons {Cu_{(s)}}^{0} + 2\,{H_{(b)}}^{+}$.

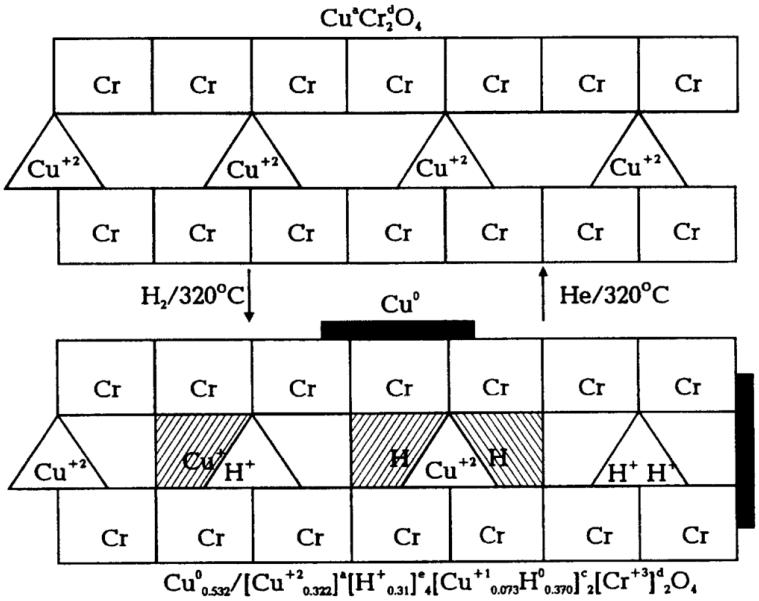

Figure 5.1: Reversible interaction of copper chromite with hydrogen according to Plyasova et al. [34].

Khasin et al. calculated the adsoprtion enthalpy of hydrogen on activated copper chromite spinels [78]. With 70-80 kJ/mol on metallic copper centers (on spinel) regardless of coverage they found higher values than those calculated for copper metal films (40-50 kJ/mol). They see this as evidence, that the spinel phase clearly affects the properties of the epitaxially bound copper particles. Plyasova et al. further investigated the interactions of hydrogen with copper aluminate spinel catalysts [33] and apart from the growth of metallic copper particles not occurring epitaxially did not find any differences between the aluminate and chromite spinel. Yurieva (sometimes written Yur'eva) investigated the reaction mechanisms of acetone and CO hydrogenations on copper chromite and $Cu/ZnO/Al_2O_3$ [23, 79]. Based on the observations of her group on activated spinels that were summarized above, she proposed a reaction mechanism for the acetone hydrogenation as shown in Figure 5.2. In the activation step, Cu(II) is reduced from the spinel and forms metallic copper on the now cation-deficient spinel that is stabilized by the incorporation of protons. A pi-complex between the carbonyl group from acetone and Cu(0) is formed when acetone is adsorbed. Then, two electrons are transferred from the metallic copper center. The cupric ion migrates back into the spinel after two protons are added to acetone from the spinel itself. Therefore, the activated spinels were attributed to be a 'solid protonic medium'. Metallic copper centers are regenerated with hydrogen gas.

In contrast to the hydrogenation of acetone, the hydrogenation of CO/CO_2 exhibits a Cu^+ active center according to Yurieva (comp. Fig. 5.3). After the reduction of copper chromite, the reduced, cation-deficient spinel is obtained just as before. In the first reaction cycle, the CO_2 hydrogenation to methanol leaves behind an oxidized surface (Cu^+-O-Cu^+) that acts as an adsorption site and active center for subsequent CO hyd-

rogenations.

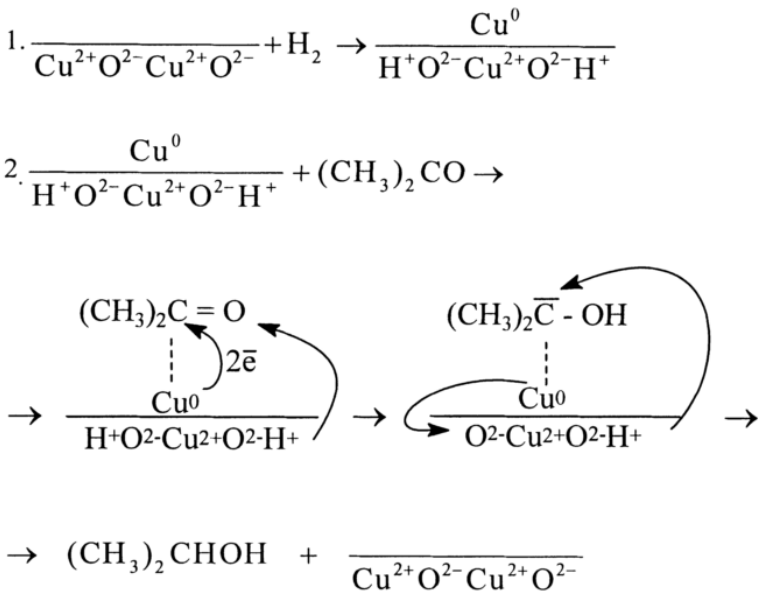

Figure 5.2: Reaction mechanism for the hydrogenation of acetone with Cu^0 active centers as proposed by Yurieva [79].

Yurieva et al. conclude that copper chromite and $Cu/ZnO/Al_2O_3$ interact similarly with hydrogen even though the final mechanism is slightly different (Cu(0) vs. Cu(I) active centers).

Nonetheless this leaves two mechanistic descriptions for hydrogenations on copper chromite that are quite different from eachother. On the one hand Yurieva proposes Cu(0) as an active center, on the other hand Hubaut et al. (see above) proposed Cu^+ to be the active center in the hydrogenation of dienes and carbonyls. Both describe the reduction of the spinel with hydrogen in the same manner, i.e. reduction of copper and incorporation of protons to offset the charge. However, Hubaut et al. proposed the stabilization of Cu^+ in octahedral sites, which then is the catalytically active site. Metallic copper did not take part in the reaction.

The reduction of the spinel itself and the resulting activated spinel structure appears to be key for which reaction mechanism is occurring. The question, whether the mechanism suggested by Hubaut et al. [76] is occuring, really is a binary one. Either cuprous ions are formed during reduction/activation and the reaction itself or they are not. In the latter case of course they could not be the active center. Therefore, further studies are necessary to understand the catalytic mechanism of hydrogenations on copper spinels and to clear up which of the two suggested mechanisms is more likely to occur.

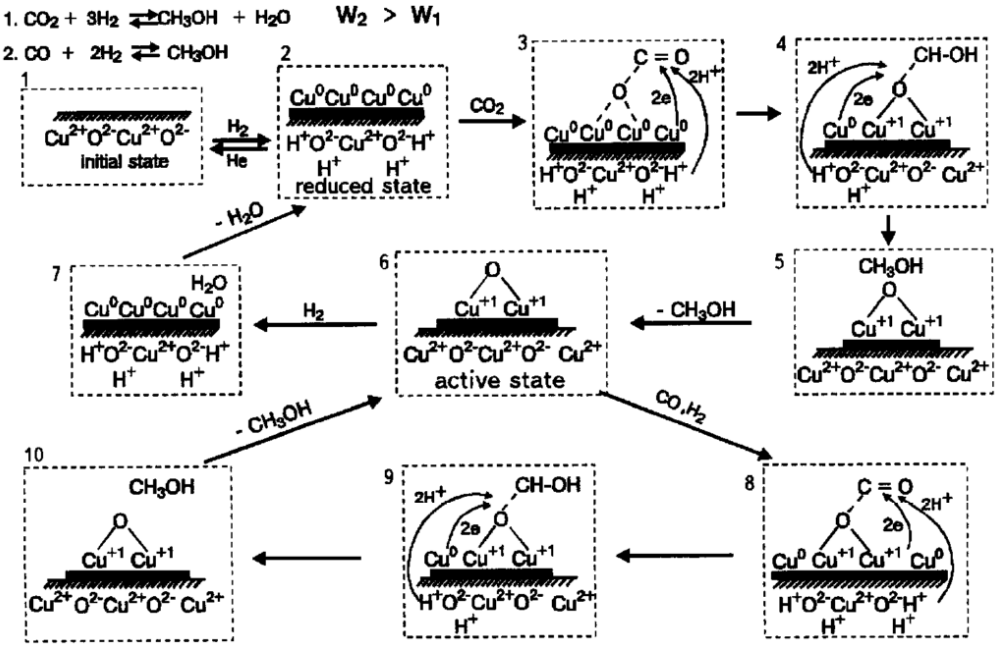

Figure 5.3: Hydrogenation of CO/CO_2 on reduced $Cu/ZnO/Al_2O_3$ catalysts to methanol with oxidation step to Cu^+ according to Yurieva et al. [23].

5.1.1 Activation/Reduction of Bulk Cupric Oxides

Since the activation of the spinel seems to be the major issue to determine which of the two proposed reaction mechanism is possible, a look into the reduction of cupric oxides and ions under relevant conditions may give further insight.

The reduction of copper oxide with hydrogen is an integral part in the activation of copper-based catalysts. It is usually achieved in flow conditions with diluted hydrogen at elevated temperatures ($\geq$180 °C). The reduction can generally follow two different paths. Either it could be sequential via Cu_4O_3 and/or Cu_2O or directly go to metallic copper.

In a recent paper by Rodriguez et al., the authors claim that the reduction is not sequential under reaction conditions similar to process conditions in many industrial applications. By time resolved XRD (1-3 min) they could show that no Cu_2O phase was observed between 150-300 °C with a flow rate of 20 mL/min of a 5 %/95 % H_2/He mixture. They did however, see an induction period after which the process became autocatalytic. To identify possible amorphous phases during said induction period, the authors used X-ray absorption spectroscopy which revealed no other species than Cu(II). Cu(I) as an intermediate was only observed with drastically reduced flow rates (1 mL/min). Reoxidation occurred via Cu_2O [53].

With Rietveld analysis the same authors could show that the CuO lattice expands right before its reduction. They suggest that CuO thereby does not undergo a sequential reduction and instead the reduction occurs at the Cu/CuO interface. This is in line with the observation of an induction period followed by an autocatalytic reduction. The authors used DFT studies to explain their findings especially with regards to the different paths between reduction (with abundant H_2) and oxidation of copper. The direct reduction to

metallic copper was attributed to the high differences in lattice parameters between CuO and Cu_4O_3 thus requiring relatively high energy of activation. Cu_2O can theoretically be reached but the systems reacts faster with hydrogen than reaching an intermediate that can react to Cu_2O, mostly due to the high differences in geometry between CuO and Cu_2O. For the calculations the authors used a CuO lattice with up to 50 % oxygen vacancies to mimic processes during reduction [80].

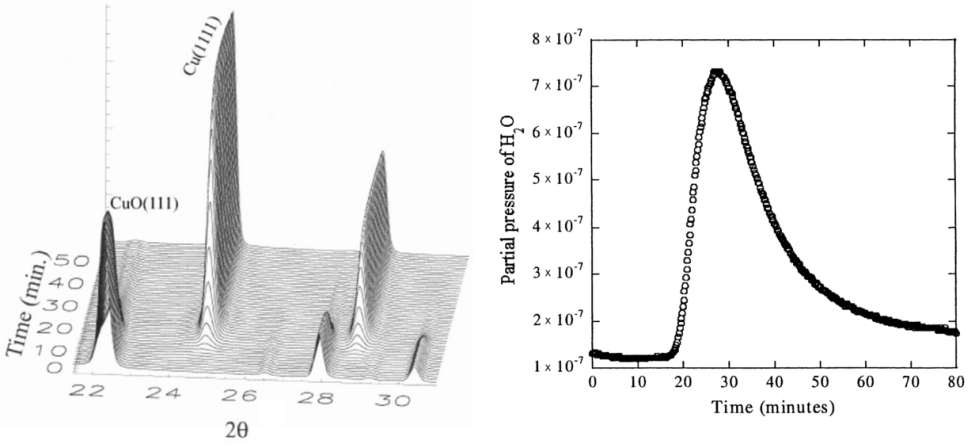

Figure 5.4: *in situ* XRD (left) and water evolution (right) measured by Rodriguez et al. during the reduction of cupric oxide [53]

The induction period was observed as early as 1921 by Pease and Taylor who studied the conversion of CuO in hydrogen above 150 °C. They could eliminate the induction period by the addition of metallic copper [81].
Fleisch and Mains investigated the reduction of cupric and cuprous oxide by UV radiation and hydrogen atoms generated by UV radiation at room temperature. They also found that CuO reduction proceeded directly to metallic copper and that the reduction of CuO is faster than that of Cu_2O. Reoxidation by air at room temperature produced Cu_2O [82].
Poulston and co-workers used XPS and XAES to study the effect of annealing and hydrogen reduction on Cu, Cu_2O and CuO surfaces. A fully oxidized surface was reduced over ten minutes in 10^{-5} mbar hydrogen at 420 K. During subsequent annealing the oxidized surface was recovered [83].

Supported Cupric Oxides and Biphasic Systems

Most copper catalysts are not limited to CuO but contain either mixed metallic (Cu + M) phases or the aforementioned mixed phases with an excess of Cu as copper oxide. Therefore the reduction behavior of a chosen set of components will be presented in this section.
Fernandéz-Garcia and co-workers investigated the reduction of Cu(II) in copper supported on alumina. The first significant observation they made, was that depending on the pH at which the copper solution is impregnated onto alumina, different copper phases are obtained. In a basic milieu the authors found copper to be impregnated as CuO/Al2O3

whereas an acidic solution only yielded copper aluminates. Their copper aluminates underwent a two-step reduction where a stable Cu(I) aluminate was formed, which was only reduced further after Cu(I) migrated to the surface [84]. Two very interesting observations in this publication are that the copper aluminates (acidic impregnation) are not fully reduced up to 800 K. A fraction of roughly 30 % remains as Cu(I) in $CuAlO_2$. Lastly, the authors offer a peak regression analysis for their TPR experiments in which their copper aluminates are reduced before CuO. As shown later in this chapter, this is somewhat surprising as the general consensus appears to be for CuO to be reduced earlier than copper aluminates. The conditions in which all of these XANES measurements were made, mention a stable 10 % H_2 in He atmosphere. According to Rodriguéz et al. (see above, [53]), the mechanism for Cu(II) reduction is heavily reliant on flow conditions so the findings by Fernandéz-Garcia [84], which likely suffer from a lack of sufficient H_2 flow, find Cu(I) species to be stable intermediates in the reduction of Cu(II).
The reduction behavior of the Cu-Cr system was investigated by Apai et al. [85]. The authors found CuO and Cr_2O_3 to form from the respective citrate complexes after vacuum drying at 150 °C. Calcination at 650 °C in air yielded mostly CuO and $CuCr_2O_4$ and higher temperatures made the formation of $CuCrO_2$ favorable. The copper chromite spinel phase was reduced directly to metallic copper at 270 °C (60 mL/min), whereas $CuCrO_2$ which did not undergo further reduction.
Detailed descriptions of the interactions of copper chromite with hydrogen have been published by Yurieva and co-workers (see above). The kinetics of copper chromite reduction were reportedly similar to pure CuO. After an induction period the rate increased to a maximum rate when approximately 50 % of copper was already reduced to Cu(0) [86].
Fierro et al. investigated the reducibility of CuO-ZnO systems [87]. They found CuO could be reduced to metallic copper using 40 mL/min, 6 % H_2 in Helium. ZnO promoted the reducibility of CuO, which can be seen as a decrease of T_M in the TPR-profiles.
In summary, the general consensus appears to be a direct reduction from Cu(II) to Cu(0) with excess hydrogen for cupric oxides. Reaching Cu(I) intermediates can be achieved when hydrogen supply is limited. This issue becomes more complex when the cupric ions are built into other frameworks such as copper aluminate spinels. The groups of Hubaut and Yurieva agree that Cu(II) is first reduced from tetrahedral positions. At higher temperatures, copper is reduced from octahedral positions within the spinel. The main difference between both groups is that Yurieva et al. did not have tools such as XPS to verify or even observe the occurence of Cu(I). Therefore, their proposed mechanism makes perfect sense with respect to the data they were able to obtain. Hubaut et al. then added experiments with XPS. Thus, they were able to detect Cu(I) and quantify its amount which correlated to the catalytic hydrogenation activity of their catalyst [25]. From today's point of view, both mechanisms contradict each other but they are the best each group could come up with. While XPS is considered a surface sensitive technique, the mean free path of photoelectrons is still around 1-2 nm within a solid. Thus, it will detect multiple layers beneath the surface as well. Merely detecting the presence of Cu(I) does

not make it the active center although the correlation of Cu(I) to catalyst activity is a good indicator. Therefore, the mechanistic discussion for these kinds of spinel catalysts is not concluded as of today.

5.1.2 Cu-Al Interactions During Thermal Treatment

Thermal treatment of catalyst precursors will define the proximity and atomic environment of copper, aluminum and oxygen within the solid. Since these pre-catalyst structures heavily influence reduction behavior, this step is crucial in obtaining a desired structure for an active catalyst. Here, a short compilation of relevant literature will give insights into parameter influence and the resulting structures.
Depending on calcination temperature, a variety of copper and aluminum oxides can be obtained. Industrial copper aluminate catalysts are usually calcined between 300 and 900 °C. Below 600 °C, CuO and Al_2O_3 are the typical products, whereas increasing temperature will give the mixed oxide with spinel structure $CuAl_2O_4$ [39, 40]. At temperatures above 1100 °C, a delafossite-like layered structure of $CuAlO_2$ is obtained [54, 88]. In all of those phases the local geometry and coordination of copper is different. CuO consists of Cu(II) with square-planar coordination of oxygen. In Cu_2O and $CuCrO_2$/$CuAlO_2$ copper exhibits linear O-Cu-O bridges. The partially inverse spinel features Cu(II) in tetrahedral and octahedral coordination of oxygen. Spinel formation is solely a solid-state reaction between CuO and Al_2O_3, that has two reaction regimes. The first one being rather fast, whereas the second is limited by the diffusion of reactants through product phase [88]. Luo et al. demonstrated the solid-state reaction by using impregnated CuO/Al_2O_3 precursors that formed the spinel at temperatures of 700 °C and higher [21]. Since γ-Al_2O_3 is a defect spinel structure, where Al^{3+} is located in tetrahedral and octahedral positions with some of them left blank to satisfy the stoichiometry [89], a diffusion of Cu^{2+} into the γ-Al_2O_3 lattice at lower temperatures appears possible and was demonstrated by Friedman et al. for low concentrations of Cu(II) [90]. They measured an uptake of up to 4 wt-% Cu per 100 m^2/g for γ-Al_2O_3. It remains questionable whether this kind of copper could be catalytically active either as proposed by Hubaut or Yurieva et al. [14, 79]. Presumably it would react quite similar to the spinel ($CuAl_2O_4$) with hydrogen and thus offer a similar reactivity although the density or amount of possible active centers would be lower.

5.1.3 Motivation

The literature offers two fundamentally different reaction mechanisms for hydrogenations on copper spinels. This discrepancy has to be cleared up to enable a complete optimization of catalysts in the future. For example, does one have to maximize the copper metal surface, the metal to cation-deficient spinel interface or is only the activated spinel phase important for the catalysis?
Furthermore, the thermal treatment yields the oxidic pre-catalyst that can then be activated with H_2 to give a functioning catalyst. It is obvious that the interactions of copper

and aluminum during thermal treatment cannot be neglected. Some important studies (see above) already yielded interesting results, but they should be expanded with the sole purpose of having catalytic functionality in the hydrogenation of aldehydes in mind. Therefore, this chapter will give a detailed account of model catalysts. Their activity in the hydrogenation of butyraldehyde and their physico-chemical properties were thoroughly investigated.

5.2 Results and Discussion

5.2.1 A Challenge: Obtaining Phase-Pure $CuAl_2O_4$ via Co-Precipitation

Obtaining phase pure and stoichiometric copper aluminate ($CuAl_2O_4$) is quite difficult and was only partially achieved in this work. The motivation to obtain said spinel is quite obvious, as all prior work (see Chapters 2-4) hints towards the importance of the spinel phase. Some mechanistic studies in the literature go as far as calling metallic copper obsolete for the hydrogenation to proceed [25]. Copper aluminate synthesis can proceed via sol-gel [38], co-precipitation [19], thermal decomposition [33], combustion [91] or solid-state [39] routes. The co-precipitation route would be preferable for catalyst manufacturers, as it can be started from cheap precursors and has relatively low investment cost. However, most sources that chose this route use an excess of copper to obtain a $CuO \cdot CuAl_2O_4$ pre-catalyst. Phase pure spinel has not been reported via co-precipitation. The difficulty in this route lies in the formation of copper oxide (CuO) as a by-product (see Figure 5.5).

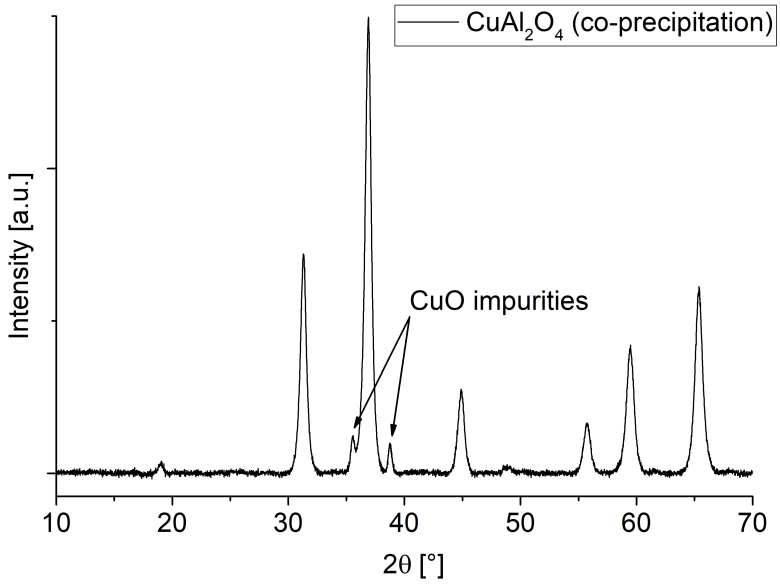

Figure 5.5: $CuAl_2O_4$ spinel after co-precipitation (pH = 6.5) and calcination at 800 °C for four hours.

Varying calcination temperature and duration did not help remove these impurities. Instead

other methods had to be identified to help remove excess copper oxide at least for the sake of obtaining pure $CuAl_2O_4$. These minor CuO impurities are probably not worth the effort to be removed by catalyst manufacturers.
In a first set of experiment, the impurities were attempted to be removed by leaching with nitric acid, hydrochloric acid and ammonium carbonate (comp. Fig. 5.6). Nitric acid and hydrochloric acid achieve complete removal of copper oxide after 30 minutes in an ultrasonic bath. Ammonium carbonate certainly reduces the amount of copper oxide but does not fully remove it within 30 minutes. However, the leached compositions show, that nitric and hydrochloric acid both leach significant fractions of the spinel itself (see Figure 5.7).

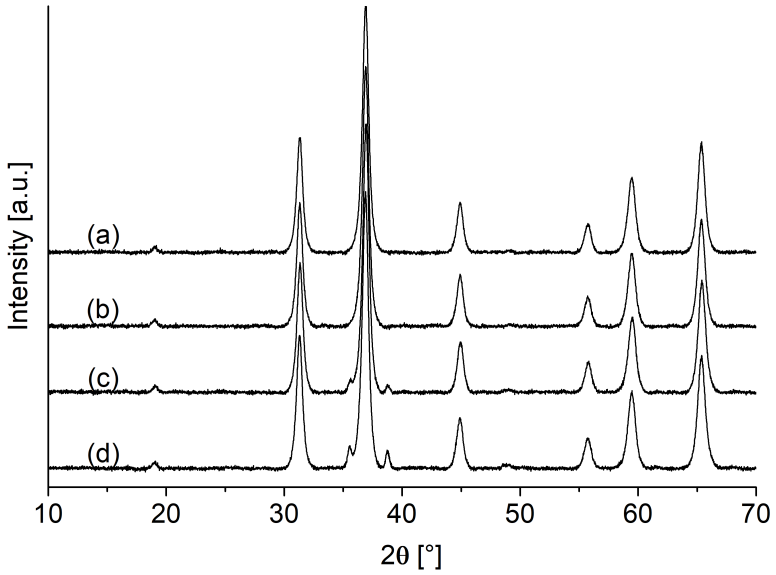

Figure 5.6: Leaching attempts to obtain pure $CuAl_2O_4$ at room temperature in ultrasonic bath with (a) HNO_3 (b) HCl (c) NH_4CO_3 (d) reference spinel wiht impurities after co-precipitation

Since ammonium carbonate showed a higher selectivity in copper oxide dissolution, a follow-up study with modified leaching times was conducted to obtain copper oxide free spinel, without actually leaching the spinel phase (data not shown). The best results were obtained for two hour leaching times in an ultrasonic bath. Phase pure copper aluminate spinel was obtained in this fashion according to its X-ray diffraction pattern. The phase-pure spinel was dissolved and analyzed via ICP-OES to determine its elemental composition (see Table 5.1). From ICP-OES analysis, it becomes quite obvious that a spinel obtained in this fashion suffers from a lack of copper and higher aluminum values. Either copper is partially substituted in the spinel or an amorphous alumina phase forms as a byproduct.

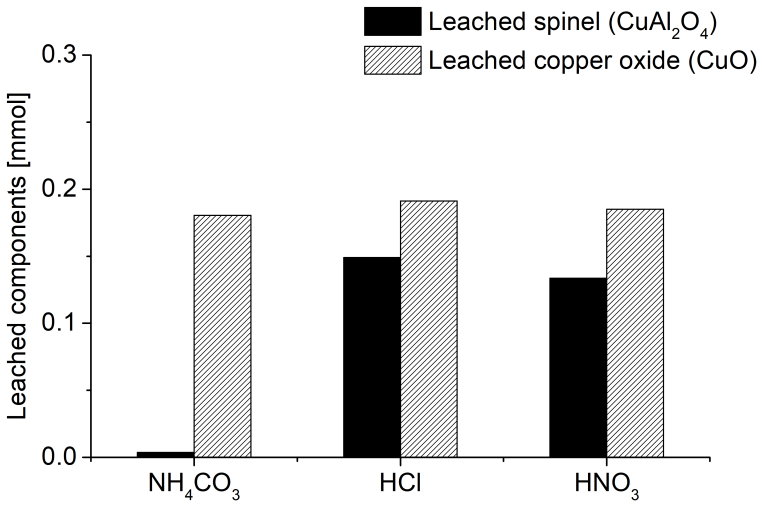

Figure 5.7: Cu and Al leaching followed with ICP-OES after cleaning procedure to obtain pure spinel. Leached fractions calculated from molar ratios of leached elements (determined by ICP-OES).

Another way to interpret these results is, that nitric and hydrochloric acid do not dissolve the spinel itself but CuO and amorphous alumina, which could have been misinterpreted as spinel, since ICP-OES can only give the amount of each element leached. With this in mind, a phase pure, stoichiometric copper aluminate spinel via co-precipitation seems possible. However, this study focussed on a less aggressive leaching method with ammonium carbonate. Other leaching strategies should be investigated in a follow-up study.

Table 5.1: Theoretical and measured Cu and Al contents for the $CuAl_2O_4$ model

Element	Theoretical [wt-%]	Found [wt-%]
Cu	35.0	26.6
Al	29.7	32.4

Nonetheless, according to its XRDs, the bulk-phase is purely copper aluminate spinel and thus it can be said, that a pure spinel phase was obtained via the co-precipitation route (with some Cu missing). Small copper oxide impurities will remain if this copper aluminate is not leached in an extra step. Of course this would increase synthesis cost for manufacturers but the leaching step is worth its effort since it drastically increases catalytic activity as is shown in the next section.

5.2.2 Catalytic Study of Model Compounds

While supported copper catalysts have been investigated with respect to their catalytic activity in a variety of reactions, this section shall follow three general ideas to emphasize and investigate the importance of the support and metal-support interactions in these

types of catalysts. First of all, with supported catalysts in an optimal case a diluted active phase can be created. The bulk copper aluminates $CuO \cdot CuAl_2O_4$ contain up to 50 wt-% copper of which most is inactive bulk material. Many chemical characterization tools can only average over all copper centers and thus give a false idea what the active surface component may be, because the signals will be caused by the 99 % bulk copper.
The second idea is to follow the effect of thermal treatment especially with regards to spinel formation and its impact on catalytic activity. A few studies about the behavior of Cu and Al in close proximity during thermal treatment were already reviewed in the introduction of this chapter. The experiments conducted in this work were intended as a more in-depth study to investigate structure-activity relationship with regards to spinel formation.
Lastly, for a more general study of spinels as support or active phase in this reaction type, copper was impregnated on different aluminate spinels. A migration of copper into the spinel lattice during thermal treatment could lead to functioning pre-catalysts.
Table 5.2 summarizes all model compounds that were synthesized and tested for this study. They can be categorized in bulk catalysts ($CuO \cdot CuAl_2O_4$), spinel ($CuAl_2O_4$), alumina supported ($Cu@Al_2O_3$), spinel supported ($Cu@MgAl_2O_4$, $ZnAl_2O_4$ and $CuAl_2O_4$) and silica supported ($Cu@SiO_2$) catalysts. As it can be seen, most of the model catalysts are active catalysts and thus could help understand active structure and reaction mechanism. The standard catalyst ($CuO \cdot CuAl_2O_4$) yields 52.8 % butanol in the test reaction. The test reaction is the liquid-phase hydrogenation of butyraldehyde to butanol in hexane at 120 °C and 60 bar hydrogen (see Chapter 7). As demonstrated in Chapter 2.3.3, promotion with magnesium enhances catalytic activity to 68 %. Interestingly, the pure $CuAl_2O_4$ spinel trails behind the standard catalyst by only 5 %. When impregnated with copper nitrate (calculated as 10 % Cu after reduction) activity of the spinel can be increased, based on thermal treatment temperature, up to 66.1 %, which makes it equally active as the magnesium promoted ($CuO \cdot CuAl_2O_4$) catalyst, surpassing the unpromoted standard composition. The total amount of copper in this catalyst is with roughly 30 %, much lower than the 40 - 48 % of the standard catalyst. 10 % copper on alumina was much less active. However, when one considers that this catalyst only has a quarter of the total copper compared to the standard catalyst, achieving up up to 17.3 % yields is more than expected per copper atom (expected $\frac{52.8}{4} = 13.2$ %).
10 % $Cu@Al_2O_3$ with citrate as a modifier to obtain higher dispersion of CuO deactivates the catalyst quite significantly compared to a regular impregnation with 3 - 12.3 % yields. A catalyst with 1 % Cu, synthesized via equilibrium adsorption, on alumina barely shows any activity, similar to a 10 % $Cu@SiO_2$ catalyst. Using spinel supports other than copper aluminate did not result in active structures.

Table 5.2: Model catalysts and their respective activity compared to a standard $CuO \cdot CuAl_2O_4$ catalyst.

Catalyst	Calc. Temp. [°C]	Calc. Time [h]	Butanol Yield [%]
$CuO \cdot CuAl_2O_4$ (standard)	800	2	52.8
$CuO \cdot CuAl_2O_4$ 6 % Mg	800	2	68
$CuAl_2O_4$	800	8	47.2
$CuAl_2O_4$ not leached	800	8	33
10 % Cu@$CuAl_2O_4$	400	4	66.1
10 % Cu@$CuAl_2O_4$	600	4	58.1
10 % Cu@$CuAl_2O_4$	800	4	41.8
10 % Cu@Al_2O_3	400	4	15.2
10 % Cu@Al_2O_3	600	4	12
10 % Cu@Al_2O_3	800	4	10.3
10 % Cu@Al_2O_3	400	12	17.3
10 % Cu@Al_2O_3	600	12	16.3
10 % Cu@Al_2O_3	800	12	16.2
10 % Cu@Al_2O_3, citrate	400	4	12.3
10 % Cu@Al_2O_3, citrate	600	4	6.5
10 % Cu@Al_2O_3, citrate	800	4	3
33 % Cu@Al_2O_3	400	4	9.5
33 % Cu@Al_2O_3	600	4	10.9
33 % Cu@Al_2O_3	800	4	13.6
1 % Cu@Al_2O_3	400	4	2.5
10 % Cu@SiO_2	400	4	2.5
10 % Cu@$ZnAl_2O_4$	400	4	0.6
10 % Cu@$ZnAl_2O_4$	600	4	2.5
10 % Cu@$ZnAl_2O_4$	800	4	0.2
10 % Cu@$MgAl_2O_4$	400	4	0
10 % Cu@$MgAl_2O_4$	600	4	0
10 % Cu@$MgAl_2O_4$	800	4	0

In the next sections, the model catalysts will be presented grouped by support or synthesis route, to investigate possible structure-activity relationships.

$CuAl_2O_4$ and 10 % Cu@$CuAl_2O_4$, 4h

The first model catalysts presented here are based on the copper aluminate spinel (see above). A TPR profile for $CuAl_2O_4$ is shown in Figure 5.8. It reveals four different reducible species and is the first TPR published on pure copper aluminate spinel. Multiple peaks are to be expected. The spinel consists of two different copper species (Cu_{Td}^{2+} and Cu_{Oh}^{2+})[Td=tetrahedral positions and Oh=octahedral]. At higher temperatures, lattice oxygen is affected/reduced. The cation deficient spinel (Cu^{2+} migrated to the sur-

face) will disintegrate at higher temperatures to form γ-Al_2O_3. An exact identification of peaks cannot be done on the basis of TPR. Since a reduction of spinel phase at 300 °C yields metallic copper on the spinel surface, the first peak can be attributed to the reduction of Cu^{2+} from the spinel phase. It is likely that at least parts of the higher temperature peak are also based on copper reduction.

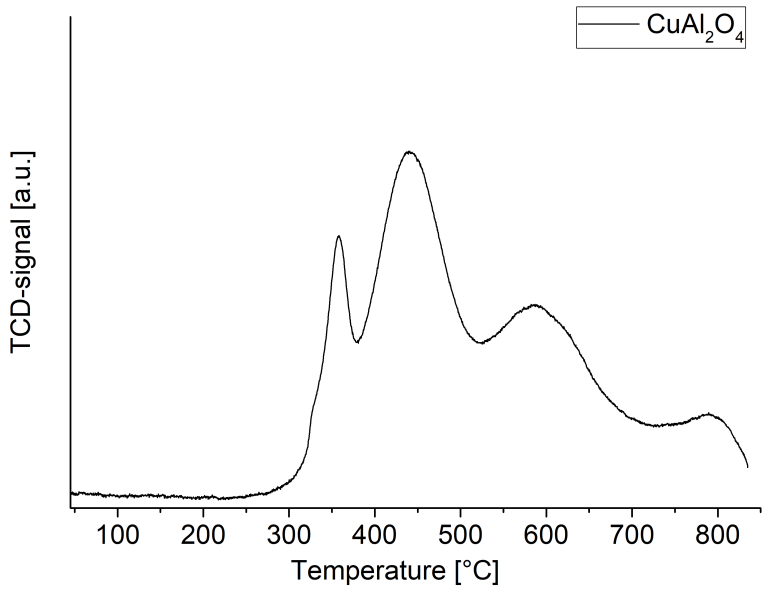

Figure 5.8: Temperature programmed reduction (TPR) of pure $CuAl_2O_4$ in 2.5 % H_2 in argon.

Such a spinel is very active in catalysis (47.2 % yield) only trailing behind the catalyst ($CuO \cdot CuAl_2O_4$) by 5 %. At this point it shall be emphasized, that spinel ($CuAl_2O_4$) as a model compounds refers to the leached spinel after removal of copper oxide impurities. The leaching procedure is crucial to activate the spinel phase apparently since an before leaching this catalyst only yields about 33 % butanol (Tab. 5.2). So this leached spinel has every prerequisite to form an active catalyst after reduction which underlines the importance of the spinel phase. One could argue that the actual catalyst performs even better with only 50 % spinel content, which is to be expected for an optimized system. However, the spinel itself being this good at drastically reduced copper content, which is very relevant in terms of price, can be a good starting point for catalyst optimization in addition to the fact that this work identified the importance of the spinel phase for the catalysis. The question what actually makes pure spinel such a well performing catalyst after activation remains. As was suggested by Plyasova et al. and confirmed by this work, cupric ions are reduced from the spinel phase and form metallic copper particles on the spinel surface [33]. Thus, the activated spinel contains metallic copper, spinel with cation vacancies (filled with protons to offset charge loss), an interface between metallic copper and activated spinel phase and cupric/cuprous copper ions. It is also possible, that the spinel structure influences how metallic copper particles grow on its surface, leading to an increase/maximization of catalytically active Cu^0 faces.

All of these factors can play a role in the catalytic mechanism. Due to the fact that copper aluminate spinel performs well and other catalysts which also contain metallic copper do not (as we shall see later) the spinel can be attributed a crucial part in the reaction mechanism. If the reaction was catalyzed by an interface between Cu^0 and spinel/activated spinel (as suggested by Yurieva [79]), an increase in this interface would lead to higher yields. Of course this increase in interface would be intrinsically tied to higher metallic copper surfaces, assuming all metallic copper particles are in contact with the spinel. To check this hypothesis, the leached spinel phase was impregnated with a copper nitrate solution to obtain 10 % Cu@$CuAl_2O_4$ catalysts. It was attempted to obtain different interface sizes by variation of calcination temperature. The XRD patterns for each catalyst can be found in Fig. 5.9. As expected, all of these model catalysts consist of copper aluminate spinel and copper oxide. No additional phases were detected. The crystallite sizes for copper oxide particles grow between 400 and 600 °C calcination temperature (15.95 nm (400 °C), 20.01 nm (600 °C), 19.03 nm (800 °C)). If one proposes, that copper oxide particle size is a good indicator for metallic copper particles after reduction, then the 10 wt-% Cu@$CuAl_2O_4$ catalyst would be expected to show the best catalytic yields, even better than the pure spinel ($CuAl_2O_4$) due to an increased interface. The catalytic results prove this model, as the 400 °C variant has the highest yield with 66.1 %. At 600 °C, the model catalyst exhibits 58.1 % yield which is further reduced at 800 °C down to 41.8 %. Thus, the catalytic results of these model catalysts support the hypothesis of a larger interface between Cu^0 and activated $CuAl_2O_4$ being crucial for the catalytic mechanism.

To get a better idea of the influence of copper oxide on spinel, the TPR profiles are plotted in Figure 5.10. The pure spinel (orange) was already shown in Figure 5.8 and is displayed as a reference. All catalysts retain the high temperature reduction profile of the pure spinel phase. This indicates that the high temperature reduction is independent of copper reduction and, as described in the literature, connected to lattice disintegration and transformation into γ-Al_2O_3.

At lower reduction temperatures, these samples have two prominent reduction peaks. The first and larger one sits at T_M = 226 °C and the second peak being located at 274 °C with small variations in between calcination temperatures. Compared to the pure spinel, the reduction peak at 350 °C vanishes, likely merging with the lower reduction species. This is a common phenomenon for copper catalysts. Copper species that become reduced act as a catalyst to reduce other copper species. This means copper oxide on the surface of spinel is reduced earlier and catalyzes the 'spinel' reduction. A $CuO \cdot CuAl_2O_4$ pre-catalyst for example only exhibits one large reduction peak (sometimes with a small shoulder, comp. Figure 2.4). As it is demonstrated in the next subsection (10 wt-% Cu@Al_2O_3), there is a high probability that the higher reduction temperature peak (274 °C) is connected to bulk copper oxide, whereas lower reduction species is finely dispersed copper oxide and copper spinel species in combination or as a reduction 'network'. This lower reduction species increases with calcination temperature. High dispersion would ultimately cause a high interface between metallic cop-

per and activated spinel, which would benefit catalysis as per the hypothesis explained above. However in this case the higher calcination temperatures decrease catalytic activity. An effect of a second calcination on the already present spinel phase is very likely. For example, its surface or pore structure could collapse, which, albeit copper/spinel interface appearing maximized, would reduce active surface and thereby catalysis. Also, the 10 wt-% Cu@$CuAl_2O_4$ sample with 41.8 % yield is by no means inactive.

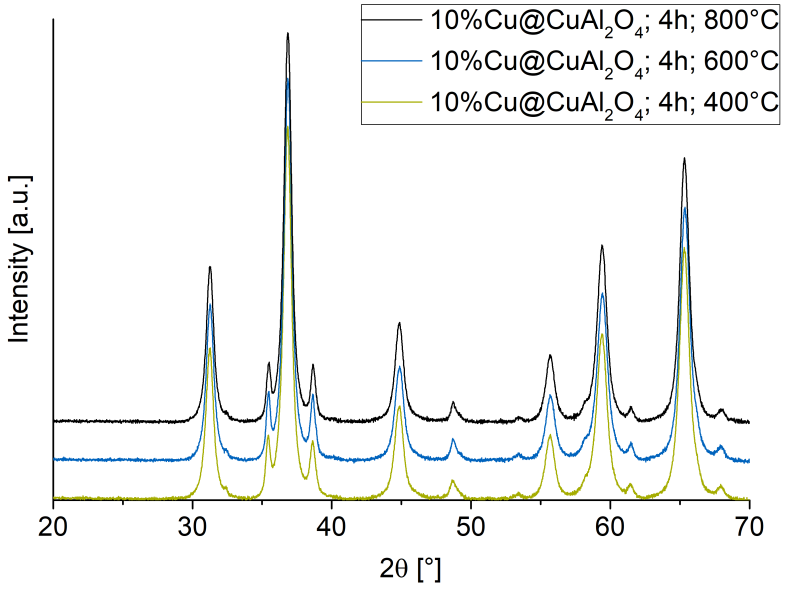

Figure 5.9: XRD patterns for 10 % copper on $CuAl_2O_4$ synthesized by incipient wetness impregnation after drying and calcination at temperatures of 400 - 800 °C.

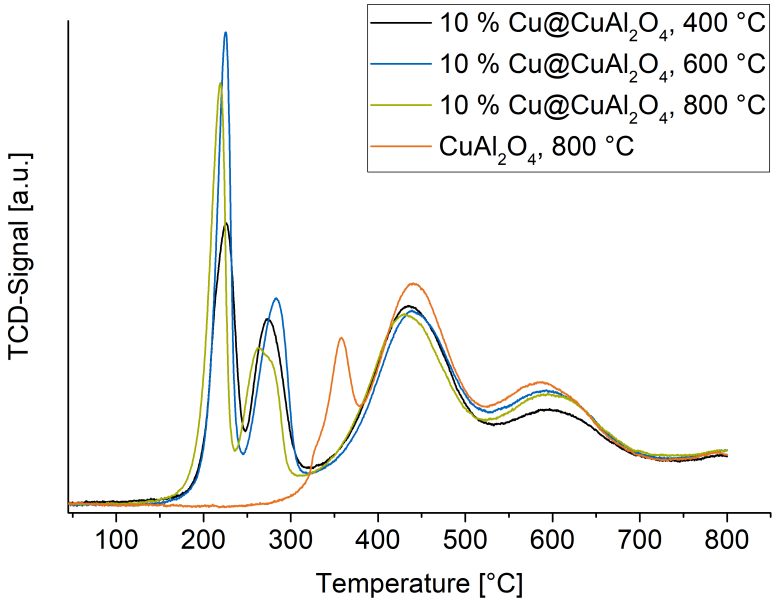

Figure 5.10: TPR profiles for 10 % copper on $CuAl_2O_4$ synthesized by incipient wetness impregnation after drying and calcination at temperatures of 400 - 800 °C compared to a pure $CuAl_2O_4$ spinel (orange).

To summarize this section, three findings should be highlighted. First of all, the pure spinel $CuAl_2O_4$ after reduction/activation contains all features necessary for an excellent catalyst. This again emphasizes the strong influence of the 'support' on the catalysis, which shall be investigated further with the model compounds described below. Secondly, due to these experiments a reaction mechanism involving the interface between metallic copper and activated spinel (similar to examples from the literature) is very likely. An explanation could be that an effective reaction mechanism involves both the metallic copper (as for example an electron reservoir) as well as Cu^{2+} (and/or Cu^{+}) in close proximity under reaction conditions, in particular Cu^{2+}/Cu^{+} in direct contact with Cu^{0} particles, which can only be stabilized by or in spinel type structures. Thirdly, which is also further proof for the interface theory, the strong interdependence of copper oxide and spinel during their respective reduction was demonstrated with the lowering of reduction temperatures and merging of reduction peaks.

10 - 33 % Cu@γ-Al_2O_3, 4 - 12 h

The second group of model catalyst to be presented in this series is the 10 wt-% copper supported on γ-alumina (synthesized by impregnation). Phase compositions are shown in Figure 5.11. As it can be seen, the diffractogram confirms two crystalline phases, namely copper oxide and γ-Al_2O_3 at 400 °C calcination temperature (green). When the sample is calcinated at 600 and 800 °C instead two phenomena occur simultaneously. On the one hand, the reflex intensity of copper oxide decreases and with it the peak integral, which indicates that less crystalline copper oxide is present. This is somewhat counter-intuitive, as usually particle growth is expected which would lead to a decrease in peak full width at half maximum (FWHM) usually accompanied by an increase in intensity to keep integral size the same for constant amounts of CuO that agglomerate. Since some copper oxide particles might be too small or X-ray amorphous at low calcination temperatures, an increase in peak integral might occur at the same time. The opposite is observed here. On the other hand, the peak shapes of γ-Al_2O_3 at 37 ° and 60.5 ° change. It could be interpreted as a sum peak of alumina and the spinel that is forming. Due to its amorphous nature its impossible to verify the spinel formation. However, the spinel formation under these conditions albeit with more copper was demonstrated in the literature [21].
Due to this uncertainty, the new phase will be more generically called copper-alumina mixed oxide. Catalysis results show an activity loss for this group of model catalyst at higher calcination temperatures, i.e. when the copper alumina mixed oxide forms (see Table 5.2). The new mixed oxide (comp. black line in Fig. 5.11) that could have been mistaken as pure spinel ($CuAl_2O_4$) does not share all spinel reflexes however, at least at the angles they would be expected. For example, a broad peak grows around 31.5 °, whereas the spinel peak would be expected at 31 °. The same is true at higher angles e.g. 60.5 ° instead of 59.5 °. The spinel peak at 56 ° is absent entirely. A shift in peaks is indicative of different lattice parameters, which can be caused by a variety of

reasons such as exchanging cupric ions with protons as observed during activation (see Chapter 2.3.1). Hereby, it is possible that the pure spinel has not actually formed and instead a copper alumina mixed oxide, that could have grown on the surface of alumina, is observed.

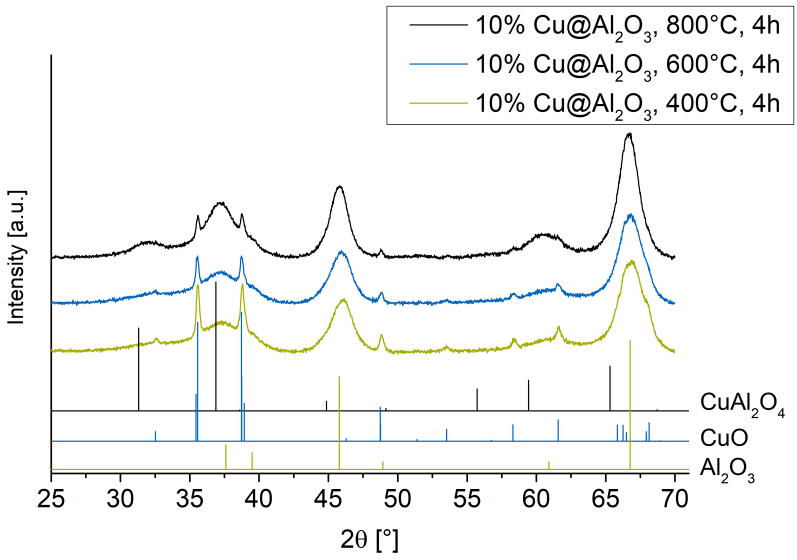

Figure 5.11: 10 wt-% copper on γ-Al_2O_3 synthesized by incipient wetness impregnation after drying and calcination at temperatures of 400 - 800 °C, 4h.

The migration of cupric ions into alumina has been demonstrated by Friedman et al. [90]. XRD and catalysis results here are indicative of such an intermediate phase before the spinel develops, which does not share the same catalytic features as the spinel. It should also be mentioned here, that 10 wt-% copper of course is not enough for a pure spinel to form. By the work of Hu et al., spinel formation has two distict kinetic regimes [88]. The first one was proposed to be rather fast and the second one controlled by diffusion - in other words transport limitations - of reactants. It is possible, that a four hour calcination duration stopped the spinel formation in this transition phase. Experiments with longer calcination durations were therefore conducted (see Figure 5.12).
Qualitatively the increase in calcination duration does not affect the resulting phases. A minor CuO fraction and the Cu-Al mixed oxide with shifted spinel peaks are still the results on top of γ-Al_2O_3. At 400 °C, larger copper oxide crystallites are found, whereas the 800 °C sample barely contains any copper oxide. The 'spinel peak' at 37 ° is more pronounced in this sample as well. The copper alumina mixed oxide exhibits the very same peak shift that was observed in the four hour samples. However, catalysis activity increases compared to the four hour samples at equivalent temperatures. For twelve hour calcination duration all samples have a similar catalysis performance (ca. 16.5 %). These findings increase the likelyhood of the transition phase in the slower kinetic regime, discussed by Hu et al. for copper aluminate spinel formation, that is inhibiting catalysis [88]. For further information to distinguish copper species, temperature programmed reduction profiles are shown in Figure 5.13.

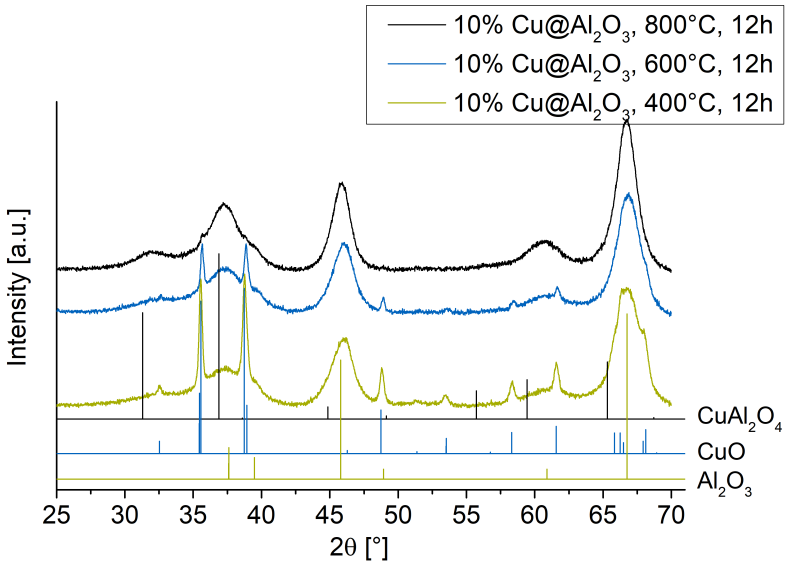

Figure 5.12: Increased calcination time (12 h) for 10 wt-% copper on γ-Al_2O_3 synthesized by incipient wetness impregnation.

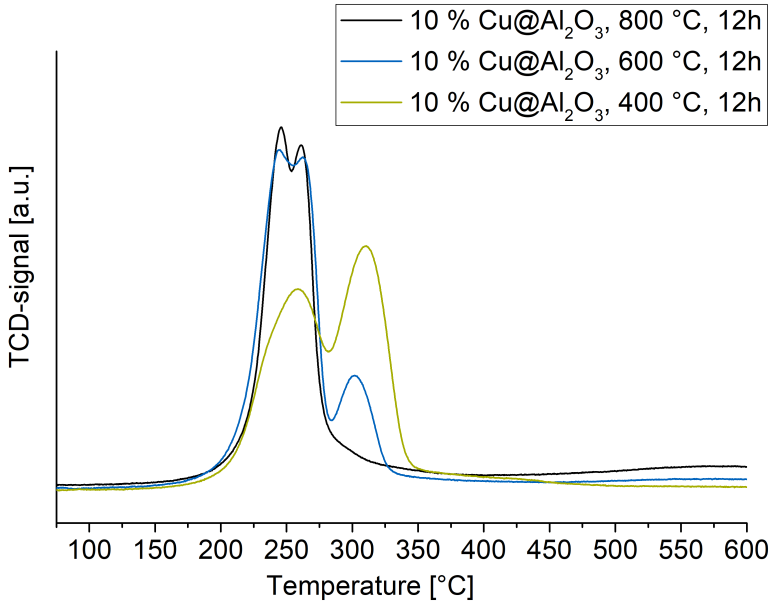

Figure 5.13: Temperature programmed reduction profiles for 10 wt-% copper on γ-Al_2O_3 synthesized by incipient wetness impregnation after calcination (12 h) at temperatures of 400 - 800 °C.

The low calcination temperature sample exhibits two distinguished peaks of maximal hydrogen consumption at 257 and 310 °C. With higher calcination temperature that high temperature peak decreases and finally vanishes. Simultaneously, the low temperature peak splits into a double peak at 246 and 260 °C with a larger integral size. Based on a calibration of TCD-signal to hydrogen consumption with standards such as CuO, the hydrogen consumption can be quantified and calculated into fractions of total Cu(II) reduced to Cu(0). This method neglects possible Cu(I) formation and hydrogen absorption effects

but acts as a decent indicator of total reducible species. The results are shown in Table 5.3. Apparently, higher calcination temperature leads to a loss of reducible species. In our model perspective low calcination temperatures lead to formation of CuO supported on alumina, which is easily and fully reduced unless particle sizes become large enough to enable core-shell-like mechanisms where transport of H_2O from the particle core is inhibited and thereby further reduction stopped. On the other hand, $CuAl_2O_4$ and mixed Cu-Al oxides presumably retain some cupric or cuprous ions to offset the charge or simply because migration to the surface to form metallic copper is not possible due to lack of available paths.

Table 5.3: Reducible species for 10 wt-% copper on γ-Al_2O_3 (12 h) calculated from TPR integrals against a calibration.

Catalyst	Calcination Tempearture [℃]	Reducible Cu [%]
10 % Cu@γ-Al_2O_3	400	97.8
10 % Cu@γ-Al_2O_3	600	92.1
10 % Cu@γ-Al_2O_3	800	72.7

Therefore, these findings are in perfect agreement with the suggested phase development during thermal treatment. Next, distinguishing copper species based on TPR and XRD results is generally possible. While X-ray diffractograms are only showing crystalline phases - anything amorphous or nanocrystalline will remain hidden - TPR does not distinguish between different species because the detector can only follow hydrogen consumption (or specifically the loss of thermal conductivity). Nonetheless, with XRD we were able to follow the reduction of crystalline CuO when temperatures during thermal treatment were raised (see Figs. 5.12 and 5.13). At the same time, the second, high-temperature peak (310 ℃) in the TPR disappears. Thus, this higher temperature reduction can be attributed to be bulk copper oxide. The lower reduction peak is very likely more finely dispersed copper oxide and possibly reducible species from the spinel or mixed Cu-Al oxide that forms. The 20 % loss in reducible species for Cu@γ-Al_2O_3, as discussed above, must also be part of this mixed oxide phase that cannot have access to hydrogen.

Luo et al. investigated calcination behavior of 33 wt-% copper on γ-Al_2O_3 [21]. Since the 10 wt-% Cu samples did not yield a clean spinel phase, as a peak shift was observed, or in other words, differing lattice parameters, the results by Luo et al. were reproduced as a reference sample (see Fig. 5.14). In contrast to Luo et al., our samples yielded much less spinel phase at 800 ℃ and 33 % Cu. Nonetheless, the spinel formation - without peak shifts - is observed. From a qualitative point of view, in all Cu@Al_2O_3 samples a reduction in crystalline, bulk CuO is found at higher temperatures and either spinel or spinel/mixed Cu-Al oxide with slightly varying lattice parameters is obtained.

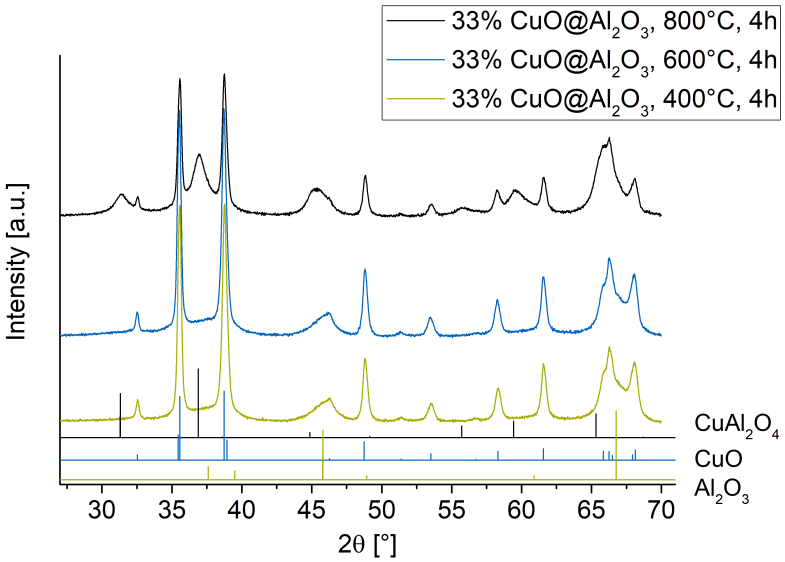

Figure 5.14: Phase composition in relation to calcination temperature for 33 % copper on γ-Al_2O_3 synthesized by incipient wetness impregnation after Luo et al. [21].

If one looks at the copper oxide crystallite sizes of all supported alumina cataylsts (see Table 5.4), the largest crystallites are found in 10 % Cu with a calcination duration of four hours. Around 800 °C, the CuO peaks are too small for an evaluation. Interestingly, the twelve hour calcination samples exhibit smaller crystallite sizes than the four hour samples. Moreover, higher temperatures decrease particle sizes (24 vs 18 nm). This is indicative for a solid state reaction taking place, with the result being either spinel or mixed-oxide phase that is visible at higher temperatures (800 °C). This hypothesis was also supported by the TPR experiments, where a distinct reduction in high temperature peaks showed the removal of bulk CuO. In the 33% Cu samples, the crystallite sizes are not affected by thermal treatment temperature. Likely, there is bulk CuO in excess which reacts to form spinel and leaves behind unreacted CuO. The CuO integral sizes are drastically reduced at 800 °C for the 33 % Cu sample (comp. Fig. 5.14), which is proof for this hypothesis of bulk CuO reacting to form spinel.

Table 5.4: Copper oxide crystallite sizes in nm for $Cu@Al_2O_3$ samples.

Calc. Temp. [°C]	10 % $Cu@Al_2O_3$ (4h)	10 % $Cu@Al_2O_3$ (12h)	33 % $Cu@Al_2O_3$
400	27.3	24.3	20.5
600	27.6	18.2	21.8
800	-	-	21.7

From a catalytic point of view, the 33 % samples perform worse than all 10 % Cu on alumina samples (max. 13.5 % yield), even though the amount of copper is tripled. The crystallite sizes of copper oxide are smaller, thus copper metal surface after reduction should be higher in the 33 % sample. Within the 33 % series, the highest calcination temperature, where spinel formation is observed, performs better than those at lower

calcination temperatures. In the 10 % samples this trend is reversed. How do these results fit into the models by either Bechara et al. or Yurieva et al. [23, 24]? This question is very complex to answer based on our experimental data. Friedman et al. showed a migration of curpric ions into a γ-Al_2O_3 lattice at 500 °C [90]. According to them, cupric ions were predominantly found in tetragonally distorted octahedral positions of the γ-Al_2O_3 defect spinel structure. Beyond 600 °C they observed a kinetically limited transformation to copper aluminate spinel. All of our model compounds therefore contain structural features that can be catalytically active according to both models. Since, we were not able to distinguish between $Cu^{1+/2+}$ within the spinel, it cannot be said with certainity which model is more accurate according to these data. Nonetheless, both options shall be discussed. From the γ-Al_2O_3 support series, it is quite obvious that metallic copper surface is not the active component by itself. The 33 % series hints to the importance of copper aluminate spinel as pre-catalyst. Its formation improves catalysis. On the other hand, the 10 % samples are rather active from the beginning, where bulk phases only consist of copper oxide and alumina. The TPR results confirm a rather large component to be X-ray amorphous however. It is possible that these species are the curpic ions inside of the γ-Al_2O_3 structure, which would react after either mechanism after reduction, depending on which reduction product is obtained. If the amorphous component is CuO, metallic copper would form during reduction supported on alumina. A reaction mechanism after Yurieva et al. would be possible which would need a large interface between metallic copper and support for maximized reaction speed. A finely dispersed copper oxide or copper ions in alumina are detected via TPR that would be able to act as a center for the catalytic cycle of $Cu^0 \rightleftharpoons Cu^{2+}$ after activation.
To summarize this section, it can be said that copper supported on alumina yields an active catalyst after reductive treatment. Its activity heavily depends on thermal treatment temperature and duration. Higher temperatures, unless calcination duration is increased, seem to stall at a phase composition of a spinel or mixed oxide with slightly modified lattice parameters, that lacks in activity compared to pure spinel or supported copper on γ-Al_2O_3. Increasing calcination duration can offset this negative effect to a certain degree, although from a phase composition perspective it cannot be said why, since the phase composition (the bulk phases) remain the same independent of calcination duration. However, it seems imperative for the catalysis that copper migrates into the alumina lattice as a function of time.

10 % Cu@γ-Al_2O_3, Citrate Modifier

During catalyst synthesis, one tries to avoid agglomeration of particles to maximize catalyst surface. One tool to achieve this are modifiers that increase the steric hindrance of metal ions during impregnation for example. For copper, a common modifier is citrate. In the experiments described above, the formation of bulk and disperse CuO was already established with XRD and TPR experiments. But how do the model catalysts perform, if there is no bulk copper oxide in the first place? X-ray diffraction patterns for 10 %

Cu@γ-Al_2O_3 with citrate as a modifier can be found in Figure 5.15. The absence of crystalline copper oxide is obvious right away compared to not using citrate (see above) and thus the finely dispersed (X-ray amorphous) copper oxide synthesis on alumina was achieved. Increasing calcination temperatures to 800 °C, features the same 'spinel' pattern with shifted peaks, i.e. slightly different lattice parameters. Thus, this change in phases occurs regardless of copper oxide crystallite size. In terms of catalysis, this model compound is performing worse than a 10 % variant without modifier. Using citrate, dispersion of copper, if being in either octahedral positions within an alumina lattice or amorphous copper oxide particles on the surface, an increase in catalytic activity would be expected regardless of which mechanism that was suggested in the literature is used for this consideration.

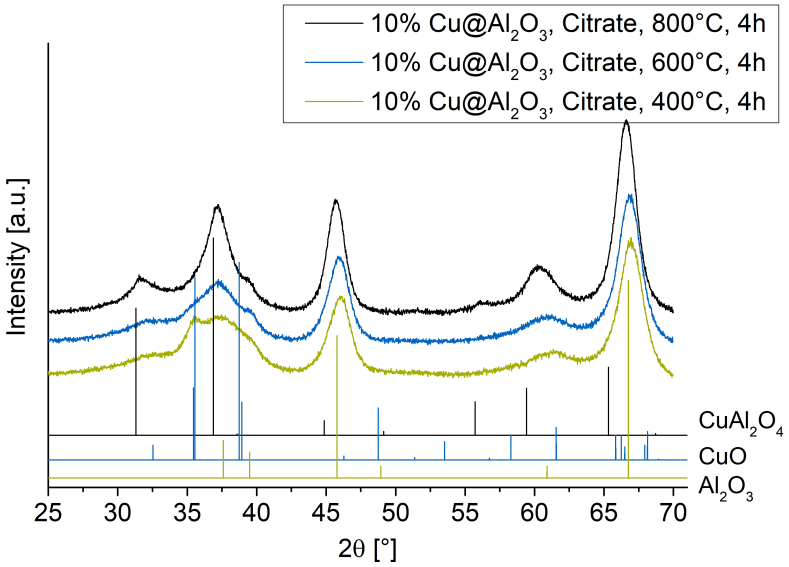

Figure 5.15: Phase composition for 10 % copper on γ-Al_2O_3 with citrate as a modified synthesized by incipient wetness impregnation after drying and calcination (400 - 800 °C)

The TPR results, exemplary shown for the 600 °C sample (see Figure 5.16), confirm that there is mostly one reducible species with a very small high temperature shoulder. At higher temperatures (800 °C), the mixed oxide or spinel with shifted peaks phase forms again (comp. Fig. 5.15), which we could already attribute to losses in activity. The diluted copper migrating deeper into the alumina lattice or a transition phase formation before actually forming the spinel at the cost of active centers is likely the cause. It remains an open question however, why the 400 °C citrate sample, albeit its high dispersion, performs worse than an unmodified one with bulk copper oxide (12.3 vs. 15.2 %). As reported by Friedman et al. the copper uptake of alumina is limited at low temperatures. If the samples are close to saturation, a higher dispersion of copper oxide would not influence catalysis. A 3 % difference in a batch autoclave reaction can be artificial. The harsh losses in activity during thermal treatment can be explained by the way copper aluminate forms. After the experiments presented above, bulk copper oxide appears to

be a requirement for the actual spinel formation. If the amount of bulk CuO is low, fewer spinel centers will be formed, which is detrimental for the catalysis. By varying the length of thermal treatment this can likely be offset to some degree. Also, it is possible that finely dispersed CuO clusters or even atomic Cu does not interact in the same manner with alumina as bulk copper oxide particles in general. The reduction profiles, instead of the large double peak at low temperatures, only have one copper species with a small bulk fraction at higher temperatures, which would support this hypothesis.

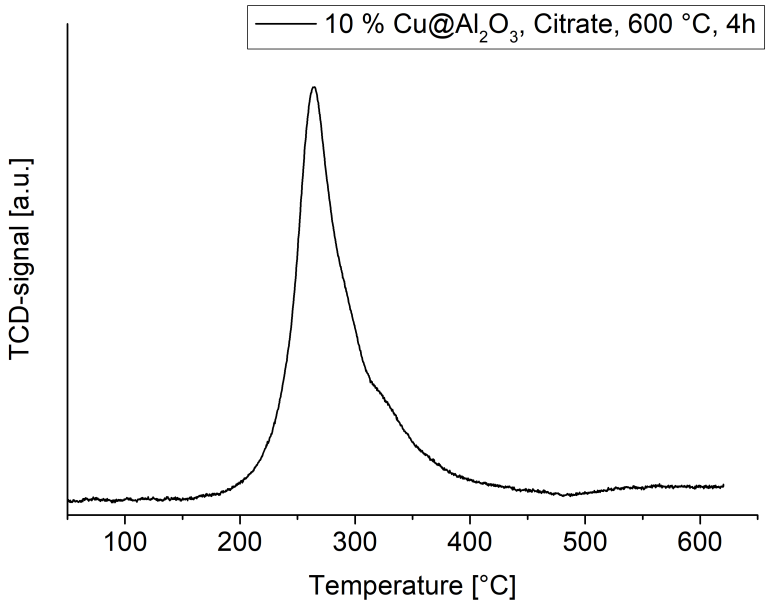

Figure 5.16: TPR profile for 10 % copper on γ-Al_2O_3 with citrate as a modified synthesized by incipient wetness impregnation after drying and calcination (600 °C)

To conclude, the citrate experiments were successful in creating very dispersed copper oxide species with particles sizes that were X-ray amorphous. The finely disperse copper yielded the same copper alumina mixed oxide that was previously observed and suffered from even higher activity losses at high calcination temperature. Thus, bulk copper oxide could be a valuable, necessary phase in catalysts which do not contain bulk copper aluminate spinel.

Inactive Model Compounds: Cu@SiO_2 and Copper Supported on Other Spinels

A look into inactive structures can help understand which structural features are necessary for the catalysis. Three model compounds can be considered inactive with respect to their copper content, namely SiO_2, 10 wt-% Cu@$MgAl_2O_4$ and 10 wt-% Cu@$ZnAl_2O_4$. All three model compounds show their expected phase compositions after drying and calcination, which are CuO, SiO_2, $ZnAl_2O_4$ and $MgAl_2O_4$. This is unaffected by calcination temperature. After reduction, CuO particles will convert to metallic copper but these model compounds are inactive in catalysis further evidencing the concept, that metallic copper surface alone is not enough for an active catalyst. Furthermore, the required

proximity of Cu^{2+} can possibly not be stabilized. For zinc aluminate spinels copper was not found to migrate into the spinel [92] in contrast to magnesium aluminates [93]. Silica as an inert support also does not allow ion diffusion into its lattice. From these findings one would expect these model compounds with the exception of magnesium to be inactive. However, exchange of magnesium by copper only occurs at temperatures around 1000 °C.

5.2.3 Copper Metal Surface: A Measure for Catalytic Activity?

All of the model compounds contain copper in oxidic form prior to activation and catalysis. A reduction to metallic copper is achieved in hydrogen flow. Metallic copper clusters and particles will grow on top of the support, regardless if it is copper aluminate spinel, alumina or silica. This was demonstrated in the literature (e.g. [33]) and in this work (e.g. 2.3.1). One way of attempting to solve the mechanism is to investigate the interaction of hydrogen and metallic copper. In contrast to group X metals (Ni, Pd, Pt), which dissociatively adsorb hydrogen even at room temperature, the capabilities of copper to do so remains questionable. Gudkov et al. reported a dissociative adsorption of hydrogen on copper based on the rate they were able to measure in the hydrogenation of butyraldehyde [26]. The capability of metallic copper to dissociatively adsorb hydrogen was reported to be dependent on particle sizes and its index faces [94–96]. The energy barrier for the adsorption is significantly higher on copper than on noble metals such as Pt [97]. Based on the literature, copper may dissociatively adsorb hydrogen and could act as an active center by itself. A mechanism completely different from Bechara and Yurieva et al. would be possible and would look much more like a hydrogenation on platinum catalysts albeit needing higher activation energies. Thus, larger metal surfaces and smaller particles should benefit the catalysis that was investigated in this work. If a standard $CuO \cdot CuAl_2O_4$ catalyst is promoted with manganese, this exact feature is achieved. Manganese retains copper within the spinel structure during reduction but keeps metal surfaces the same, i.e. causing metallic copper particles to be smaller. Therefore, if above considerations were true, the catalysis should be improved if more manganese was present (see Figure 5.17).
The opposite is observed here, as increasing manganese content, which replaces copper and retains more copper in the spinel phase after reduction, thus resulting in smaller Cu^0 particles to keep metal surface the same, perform a lot worse. A 0 % Mn sample achieves roughly 55 % yield, whereas 4 % Mn decrease activity to 21 % with copper surface being constant around 9 m^2/g. Mn does affect the spinel formation however. Known as a redox catalyst, it is very likely that manganese affects redox properties of the activated spinel and thereby inhibits catalysis. Of course other interferences are possible and cannot be excluded.

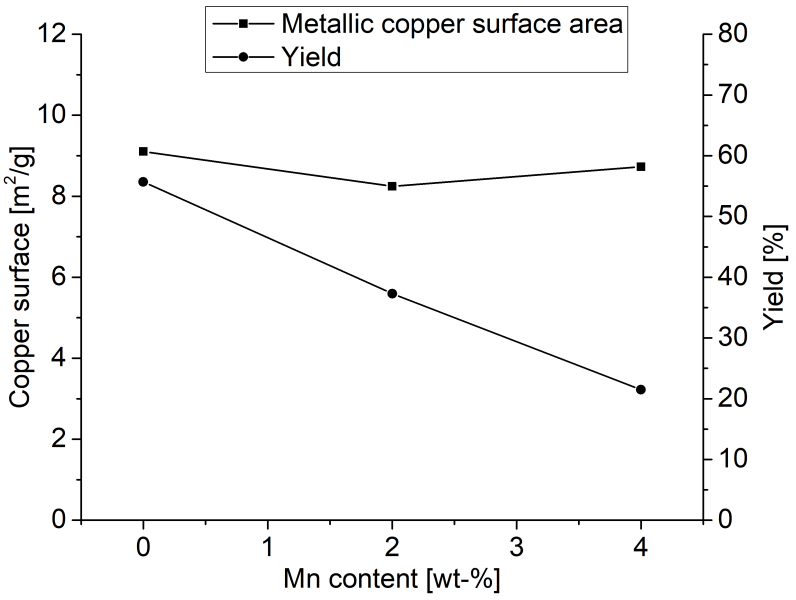

Figure 5.17: Copper surface measured by N_2O-chemisorption and catalytic yield in the hydrogenation of butyraldehyde [120 °C, 60 bar H_2] against manganese content in a standard $CuO \cdot CuAl_2O_4$ catalyst.

Still, the fact that metallic copper surface cannot be used as a prediction how well a catalyst performs proves that the reaction mechanisms is different from what is usually considered for hydrogenation mechanisms: the dissociative adsorption and subsequent addition of hydrogen to the unsaturated molecule. Therefore, the mechanisms suggested by Bechara and Yurieva et al. that involve the spinel phase are more likely.

5.2.4 Partial Conclusions: Catalysis

- Copper spinel formation proceeds from bulk copper oxide
- As a result of high calcination temperatures finely dispersed copper oxide or reducible species inside of the spinel/Al lattice are stabilized.
- At lower copper contents (10 %), a spinel-like mixed oxide forms with slightly shifted lattice parameters, because the copper amount is too low for pure spinel formation.
- This mixed oxide negatively affects catalytic activity unless calcination is prolonged.
- Dissociative adsorption of hydrogen on copper is unlikely to be part of the reaction mechanism.
- Catalysts consisting of copper aluminate spinel ($CuAl_2O_4$) exhibit the highest activity, emphasizing how strong of an effect and how important the aluminate spinel phase is for catalysis.

5.3 Al-NMR

The fate of aluminum was followed with ^{27}Al MAS NMR for four different samples. At the bottom of Figure 5.18 the $CuAl_2O_4$ spinel (1) can be seen. It displays a sharp peak at δ = 4.77 ppm and a very broad peak at δ = 117.31 ppm. The pre-catalyst $CuO \cdot CuAl_2O_4$ (2) features peaks at δ = 6.87 ppm and δ = 89.74 ppm. Shielding by copper oxide suppresses signal intensity, which is observed here for the pre-catalyst.

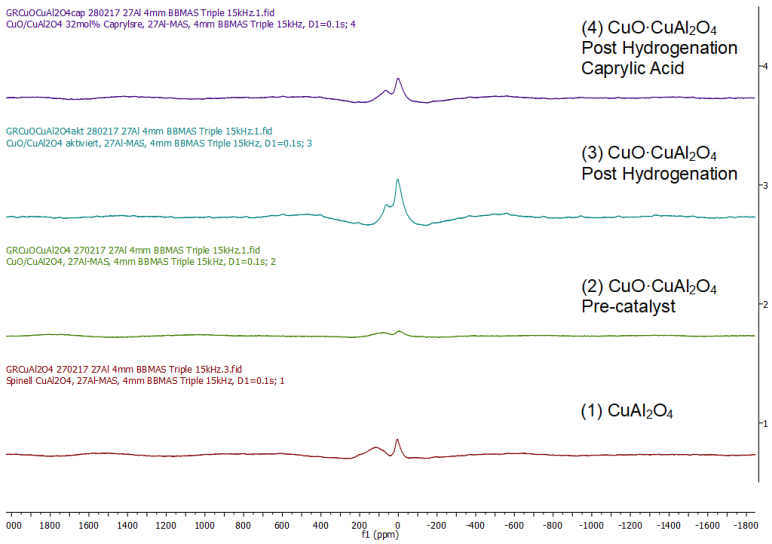

Figure 5.18: ^{27}Al NMR of $CuAl_2O_4$ (1) and $CuO \cdot CuAl_2O_4$ pre-catalyst (2), as well as $CuO \cdot CuAl_2O_4$ catalyst after activation and hydrogenation (3) and the same except after a hydrogenation in the presence octanoic acid (4)

After going through an activation and hydrogenation, the catalyst (3) features a large peak at δ = 1.2 ppm and a broader peak at 64.4 ppm. If octanoic acid was added to the reaction (4), the peaks shift again to δ = 1.5 ppm and 69.5 ppm.
In the spinel ($CuAl_2O_4$ (1)) two different alumina species are detected. One would expect two peaks for octahedral and tetrahedral positions in the spinel. The higher chemical shift belongs to tetrahedral aluminum, whereas octahedral Al is the larger peak at 4.77 ppm. From elemental analysis, we know this copper aluminate spinel to be copper deficient (comp. Section 5.2.1) with the only crystalline phase present being from the spinel phase. Thus, excess aluminum must have formed X-ray amorphous alumina or could be incorporated into the spinel. This could explain the higher chemical shift for tetrahedral aluminum in this case. For example, literature values for $MgAl_2O_4$ and $ZnAl_2O_4$ are δ = 5 ppm (oct.) and 68.1 ppm (tetr.) [98]. The degree of inversion is of course different between all three of these spinels. Zinc aluminate can be considered a regular spinel and the degree of inversion increases from magnesium aluminate to copper aluminate based on a comparison of these results against the literature. γ-Al_2O_3 as a defect spinel structure shows the same features with peaks at 5 and 65 ppm for octahedral and tetrahedral Al respectively [99]. Van der Laag and co-workers found the degree of inversion to be dependent on synthesis route and calcination temperature for zinc aluminate [100].

Furthermore, they postulated zinc aluminate and γ-Al_2O_3 to form a solid solution. The same could be true for copper aluminate as presented in this work, which could explain the very broad peak with high chemical shift for tetrahedral aluminum.
Due to the strong shielding in the oxidic pre-catalyst (2), the peak positions should not be overemphasized. They resemble the spinel more closely however. Due to the higher amount of copper a more complete transformation to copper oxide and spinel can be expected. After activation, Cu^{2+} ions leave the spinel lattice according to Plyasova et al. [33]. It is therefore not surprising, that an activated catalyst (3), after the hydrogenation, has very similar Al-NMR signals to γ-Al_2O_3, namely at 1.2 and 64.4 ppm. When exposed to acid, a very small peak shift is observed (4), that is likely connected to the removal of aluminum from the catalyst surface via leaching (see Chapter 4). Although unsaturated aluminum on the catalyst surface could artificially increase what is interpreted as degree of inversion [100]. It appears from the change in peak ratio that octahedral aluminum is leached more readily than tetrahedral aluminum.

5.4 *In Situ* Infrared Spectroscopy

With infrared spectroscopy and probing molecules such as CO, the activated structure of the catalyst, which still remains uncertain to a degree, was investigated. Prior work by Hierl et al. on $CuAl_2O_4$ structures found copper as Cu(II) and Cu(0) after reduction with hydrogen [101]. The absence of Cu^+ was excluded because according to the authors it cannot be stabilized due to electric neutrality reasons. Distinguishing between Cu^+ and Cu^{2+} species is difficult with CO as a probing molecule. Table 5.5 summarizes the most important Cu-CO species.

Table 5.5: Cu-CO Infrared-Bands as Reported in the Literature.

Structure	Wavenumber [cm^{-1}]	Reference
CO (gas)	2178, 2115	[102]
Cu^0-CO	2100	[101]
Cu-CO^+	2170	[103]
$Cu_{tetr.}{}^{2+}-CO$	2118	[101]
$Cu_{oct.}{}^{2+}-CO$	2135	[101]

In Figure 5.19 the interaction of CO with reduced $CuAl_2O_4$ spinel can be seen. The time in minutes denotes the time passed after starting the CO flow (1 % CO in He, 5 mL/min). It is obvious, that instantly CO starts interacting with the reduced spinel surface by the shift in peaks and also the inversion of peak intensity from gaseous CO to the observed species. A large band is observed at 2109 cm^{-1} with a second peak at 2137 cm^{-1}.

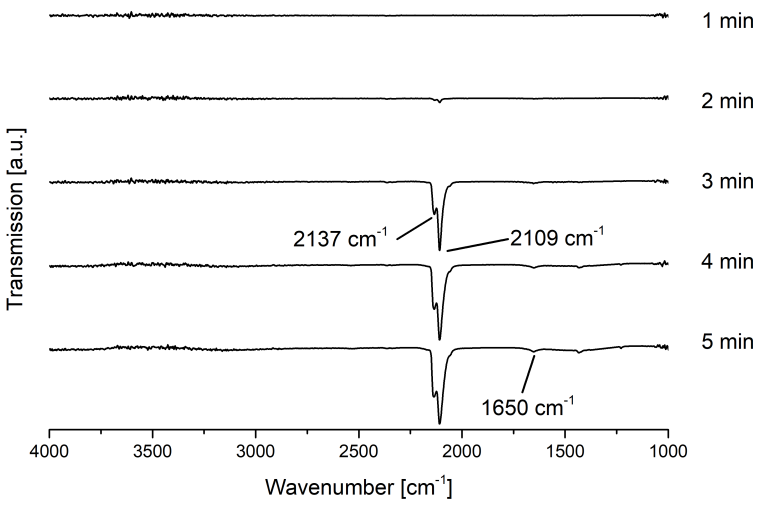

Figure 5.19: Infrared spectra of CO interaction with activated (reduced at 300 °C in H_2) $CuAl_2O_4$ at room temperature with background removal (self supporting spinel tablet in 100 % helium).

According to the literature, these peaks belong to a chemisorption on metallic copper and cupric ions in octahedral positions albeit it could also be cuprous ions according to Hierl et al. [101]. Thus, the IR results confirm that the activated spinel not only has metallic copper on its surface but also $Cu^{1+/2+}$ in octahedral positions. Cu^+ is explicitly mentioned here because several sources cited in this work find Cu(I) and thus the reasoning by Hierl et al. to exclude Cu^+ from spinel positions has to be questioned. Both hydrogenation mechanisms in the literature require these species to function [25, 79]. Unfortunately we are unable to distinguish between cuprous and cupric ions at this stage. The time interval from 10 to 60 minutes CO flow at room temperature is shown in Figure 5.20. The merging of both previously reported peaks is observed to form a broader peak with a shoulder at 2103 cm^{-1}. This shows that gaseous CO chemically alters the catalyst surface over time at room temperature.

In this case, the formation of carbonates and/or bicarbonates is observed with its peak centered at 1640 cm^{-1}. To proof this, the sample was flushed with helium and subsequently heated up. All peaks disappeared over time and an evolution of CO_2 was observed (data not shown). Unfortunately, due to its deep black color, this observations could not be made for the $CuO \cdot CuAl_2O_4$ pre-catalyst after activation and CO treatment.

In summary, the *in situ* IR-spectroscopy experiments showed metallic copper as expected but also oxidized species on the surface, which reacted with CO to form carbonates over time. These findings are in agreement with the literature. The distinguishing of $Cu^{1+/2+}$ with this technique is quite difficult, thus it does not help to determine which reaction mechanism (Bechara or Yurieva) is more likely.

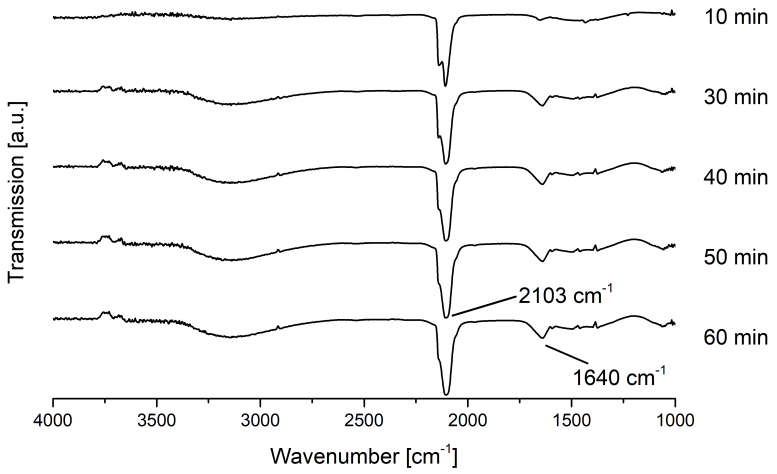

Figure 5.20: Infrared spectra of CO interaction with activated (reduced at 300 ℃ in H_2) $CuAl_2O_4$ at room temperature with background removal (spinel tablet in 100 % helium)

The strong peak at 2137 cm^{-1} hints to Cu^{2+} which would support Yurieva's mechanism. The (bi)carbonate formation is a very interesting observation in this regard, as it supports a reduction of cupric ions to metallic copper. The resulting CO_2 could then react with surface hydroxyl groups to form bicarbonates. This must be the case, otherwise the carbonate peaks would appear faster. Instead, the carbonate peak and the Cu^0-CO (2103 cm^{-1}) band become larger while simultaneously the $Cu^{2+}-CO$ (2137 cm^{-1}) band decreases.

5.5 EPR

With electron paramagnetic resonance (EPR) spectroscopy the evolution and location of Cu^{2+} ($3d^9$, s = $1/2$) species can be followed. Cuprous ions and metallic copper are EPR-silent as diamagnetic species. Paramagnetic species, such as cupric ions, can become EPR-silent depending diamagnetic dilution. Closely packed paramagnetic species such as Cu(II) in bulk copper oxide can experience antiferromagnetic spin-spin interactions and thus extinction of the EPR-visible speciies [104]. The pre-catalyst ($CuO \cdot CuAl_2O_4$) consists of at least three different copper(II) species and possibly more, namely cupric ions in bulk copper oxide and cupric ions in tetrahedral and octahedral spinel lattice positions. Possible other species are isolated Cu(II) species on the outermost surface of either phase and Cu(I) ions in any position. In EPR spectroscopy, only the isolated Cu(II) species on either the catalyst surface or within the spinel would become visible. To illustrate this the X-band EPR spectrum of pure spinel is compared to the oxidic pre-catalyst in Figure 5.21. The spinel (red) exhibits an EPR spectrum described by an axially symmetric spin-Hamiltonian, where $g_{||}$ is larger than $g_{\perp}$. The large hyperfine coupling (I = $\frac{3}{2}$) in $g_{||}$ (z-direction) is consistent with an axial distortion of an octahedron

or tetrahedron in that direction. For a partially inverse spinel, where Cu^{2+} is located in both tetrahedral and octahedral environments, this can be expected. The very small hyperfine coupling in $g_{x,y}$ direction, where the electron is more dislocated between Cu and four equatorial oxygen ligands, i.e. in an x^2-y^2 magnetic orbital fits well into this model.

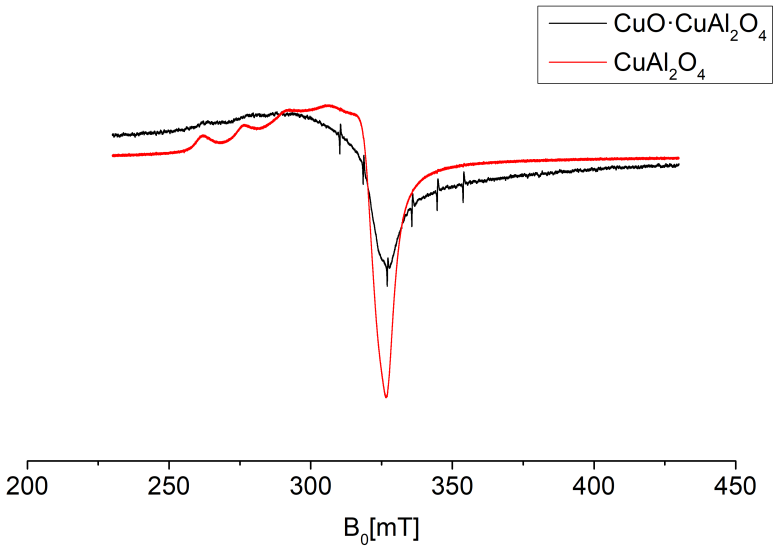

Figure 5.21: X-band EPR spectra of pre catalyst $CuO \cdot CuAl_2O_4$ (black) and copper aluminate spinel $CuAl_2O_4$ (red) at room temperature without treatment.

In contrast to the spinel, the pre-catalyst which contains up to two times more copper (ca. 50 %) has a smaller integrated intensity for the Cu^{2+} signal due to antiferromagnetic coupling. As described above, this effect makes large fractions of Cu(II), i.e. in bulk CuO EPR-silent. Furthermore, the hyperfine coupling of the signal is barely resolved. It is possible that excess copper oxide on the spinel surface lead to a strain and deformation of the spinel unit cell in z-axis and thereby influence the hyperfine coupling. However, the first two peaks for the hyperfine coupling in the $g_{||}$ part are resolved albeit at a slightly higher g-value. Their hyperfine-tensor A appears to be the same as the spinel's and thus a deformation along the z-axis is unlikely. Nonetheless, these experiments confirm the presence of spinel in the pre-catalyst in particular with regards to the cupric ion environment.

During reduction/activation of the spinel the migration of Cu(II) from the spinel to form metallic copper at the outermost surface was proposed and shown by Plyasova et al. [33] and confirmed in this work for example in TPR experiments and *in situ* XRD. *In situ* X-band EPR experiments (comp. Fig. 5.22) further are in good agreement with this hypothesis.

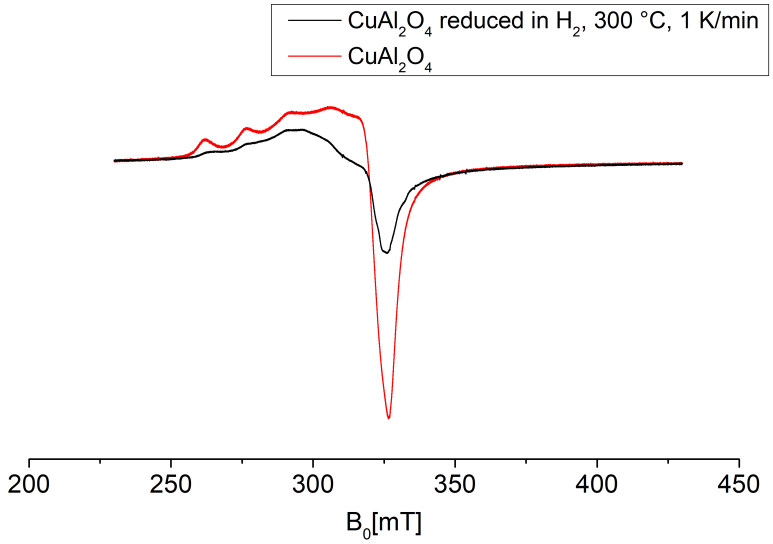

Figure 5.22: X-band EPR spectra of $CuAl_2O_4$ (black) and its reduced state (red) at room temperature. The spinel was reduced with hydrogen at 1 K/min up to 300 °C with a holding time of one hour.

The red graph depicts the spinel without treatment as discussed above. Upon reduction in hydrogen (black graph), the integrated intensity becomes much smaller due to reduction of Cu^{2+} from the spinel itself. As we know from other experiments, metallic copper forms on the surface. A possible formation of Cu(I) cannot be seen in EPR spectroscopy. These experiments confirm that not all Cu(II) is reduced from the spinel phase.

5.5.1 The Fate of Cu^{2+} during Thermal Treatment - An EPR Story

A possible exchange of copper into spinel supports was investigated with copper supported on zinc and magnesium aluminate spinels as this exact exchange or migration of copper into the alumina(te) lattice appears to be a requirement for any of the proposed reaction mechanisms. 10 % copper supported on magnesium aluminate was calcined at different temperatures and measured by X-band EPR (see Fig. 5.23). Already in the impregnated sample, after drying at 120 °C, isolated Cu(II) species can be seen, which must be copper nitrates bound to the spinel surface. After calcination at 400 °C these isolated species remain present. Values of g and hyperfine coupling do not change, which is quite interesting and could be a sign for strong metal support interactions considering that copper nitrates will have transformed into cupric oxide species at this temperature of which the bulk is EPR-silent (see above). When the temperature is increased up to 800 °C, an EPR spectrum closely related to the copper aluminate spinel is obtained.

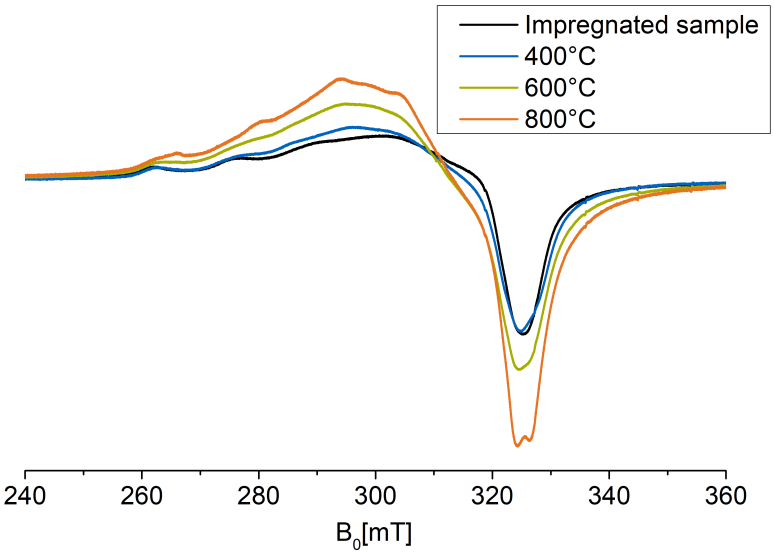

Figure 5.23: Effect of calcination temperature on X-band EPR spectra of 10 wt-% Cu supported on $MgAl_2O_4$ collected at -120 °C.

The single EPR peak for $g_\perp$ splits into a double peak, which is caused by the strong temperature dependance for these samples and often observed in copper EPR spectra. Thus, it is in agreement that copper migrates into the magnesium aluminate spinel substituting for magnesium ions. This exchange occurs only at 1000 °C and above for the bulk phases according to the literature, i.e. magnesium oxide formation detectable by XRD. The same effects can be observed for zinc aluminate (comp. Fig. 5.25) although its integral sizes remain much smaller across all samples. Although a total quantification is impossible with this method, a relative quantification works.

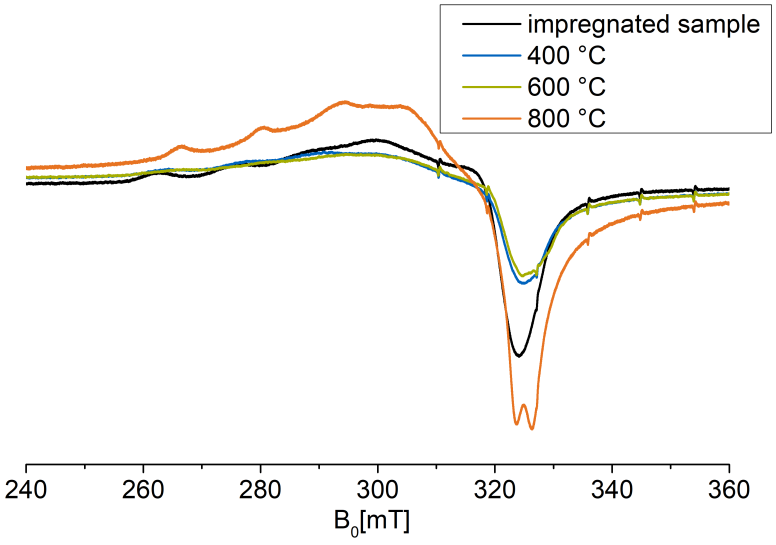

Figure 5.24: Effect of calcination temperature on X-band EPR spectra of 10 wt-% Cu supported on $ZnAl_2O_4$ vs. the impregnated precursor, collected at 13.5 °C.

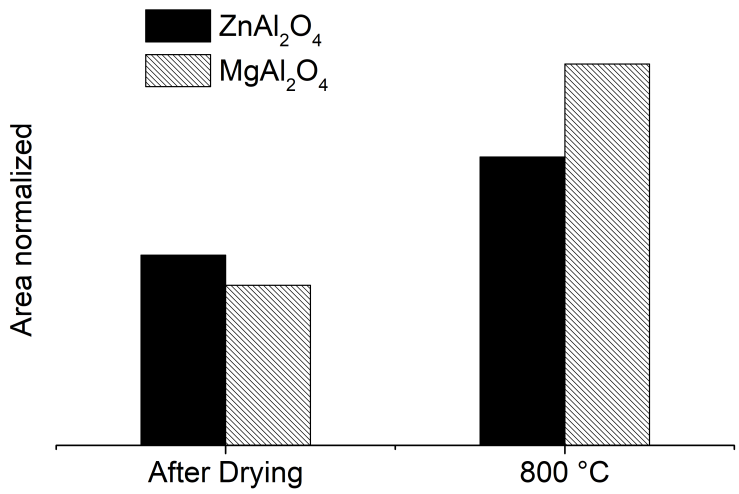

Figure 5.25: Normalized integrals of X-band EPR spectra of 10 % Cu supported on $ZnAl_2O_4$ and $MgAl_2O_4$ collected at 13.5 °C in relation to calcination temperature to visualize relative amounts of Cu(II).

Therefore it can be said that the magnesium aluminate support stabilizes these isolated copper(II) species better that later become spinel-like Cu(II). Up to 25 % more Cu(II) is detected in the $MgAl_2O_4$ sample at 800 °C calcination temperature. Since these catalysts are both completely inactive after activation, these samples prove that a simple exchange/migration of copper into the spinel lattice does not yield active catalysts. Rather these Cu(II) ions must be reduced to create the lattice defects, that are filled with protons (according to Yurieva et al. [23]) which can take part in the reaction. Or in other words the zinc and magnesium spinels are not transformed into solid Brønsted acids, which are capable of achieving the catalysis.
The cause of this is rather speculative at this point. Copper ions, if entering the zinc or magnesium spinel, should be close to the surface and thus should be reducible. This reduction would then yield the spinel defects or interface that acts as an active center. Regardless of what the true inhibitor is however, these experiments show again, how important the reduction of the spinel phase is for the catalysis, underlining why pure $CuAl_2O_4$ is among the best catalysts tested.

5.5.2 EPR Study of Acidic Attack and Spent Copper Aluminates

The spent catalysts were collected after the liquid-phase hydrogenation of butyraldehyde and subsequently measured by EPR against the oxidic pre-catalyst (comp. Fig. 5.26). The spectra are not surprisingly still representative for axial symmetric paramagnetic centers with $g_{\parallel} > g_{\perp}$. Strong antiferromagnetic coupling of close-proximity paramagnetic Cu^{2+} leads to the very low resolution, line broadened spectrum of $CuO \cdot CuAl_2O_4$ (black). During reduction, copper oxide becomes metallic copper and cupric ions leave the spinel phase (as shown above). This leads to reduced antiferromagnetic coupling and larger

integrated intensities, which could be falsely interpreted as more Cu(II) species. This phenomenon is certainly a weakness of EPR spectroscopy when neglected.

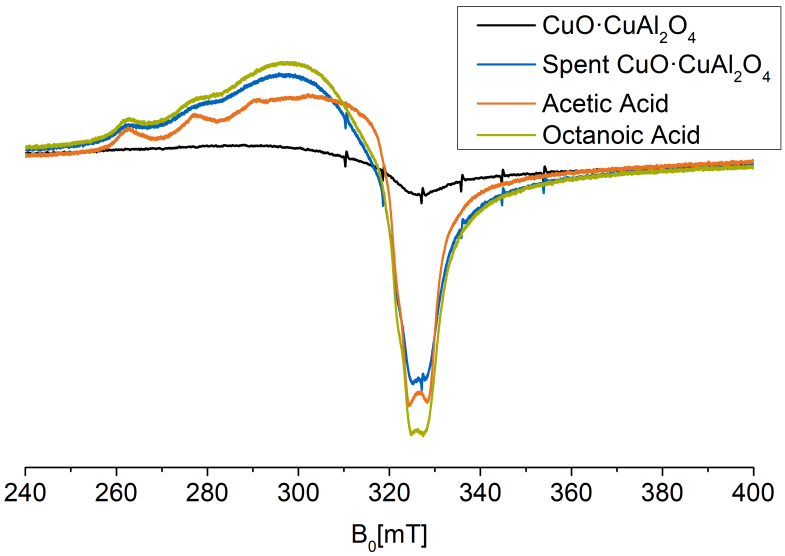

Figure 5.26: X-band EPR spectra of $CuO \cdot CuAl_2O_4$ pre-catalyst (black) and spent catalyst (blue) after the liquid-phase hydrogenation of butyraldehyde (120 °C, 60 bar H_2, 1 h) with the effect of acetic acid (orange) and octanoic acid (green) on catalysts, recording temperature 13.5 °C

Just like the activated spinel (see Fig. 5.22) the spent catalyst and similarly the octanoic acid exposed sample, lose resolution in the parallel part due to evolution of a species with a large peak around 300 mT. Thus, an effect of octanoic acid on Cu(II) species can be excluded. Acetic acid on the other hand prevents the formation of the Cu(II) species, that is responsible for this broad peak. From XRD patterns of spent catalysts, we know that copper acetate (and aluminum acetate hydroxide) is formed during the reaction. This leads to the conclusion, that the 'broad-peak' Cu(II) species is a surface species.
To further investigate this hypothesis, the EPR spectra of spent catalyst was adjusted in intensity to compare spectral features qualitatively to copper aluminate spinel and activated spinel (see Figure 5.27). As it can be seen, two different spectra are obtained. The black and blue curves for the spinel and its activated form were already discussed above (comp. Fig. 5.22). During reduction, Cu^{2+} is migrating from its tetrahedral and octahedral positions to the surface to form Cu^0. Without enhancement this is reflected in a reduction in integrated intensity, i.e. less Cu(II) is detected. Furthermore, the sharp separation of $g_\perp$ and $g_\parallel$, in oxidized state located at 320 mT, turns into two broad peaks at 295 and 310 mT. According to the findings by Plyasova et al. the blue EPR spectrum must be representative of the minimal amount of Cu^{2+} that is left in the spinel after reduction [33]. For the spent catalyst (green) a very similar spectrum is obtained compared to the activated catalyst. The broad peak at 300 mT is further losing resolution in $g_\parallel$. On the other hand, $g_\perp$ retains the double peak already seen for the activated spinel but its peak is broadened. This loss in resolution and the broadening of peaks is caused by

the paramagnetic centers being closer together thereby influencing each other. For this to occur, Cu(II) centers have to migrate during catalysis, i.e. an enrichment of Cu(II) close to the spinel surface would be possible considering the mechanism suggested by Yurieva does exactly that [79].

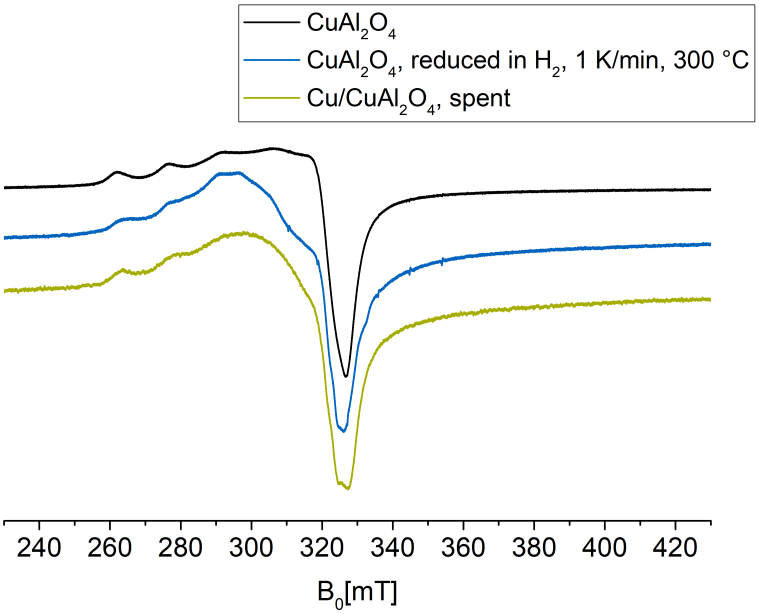

Figure 5.27: X-band EPR spectra of $CuAl_2O_4$ spinel (black), activated (H_2, 300 °C) spinel (blue) against spent catalyst (orange).

In summary, EPR spectroscopy showed that organic acids do not alter Cu(II) species in the spinel during catalysis. An exception to this rule is acetic acid, which causes large restructuring of the catalyst surface and ultimately formation of aluminum and copper acetates. It was demonstrated, that Cu(II) is reduced from the spinel itself using *in situ* EPR spectroscopy. For copper on other spinel supports (zinc and magnesium aluminate), it appeared that copper was replacing both zinc and magnesium in the spinel. However, all of these types of model catalysts were inactive, showing that Cu(II) in a spinel position is not the only requirement for the precursor to turn into a working catalyst upon activation. Unfortunately, using EPR spectroscopy it was not possible to help identify parts of the reaction mechanism, for example the formation of Cu(II) during the reaction although spent catalyst appeared to exhibit some form of Cu(II) enrichment in the spent catalyst.

5.6 Mechanistic Considerations from Literature to This Work

In the literature, two different reaction mechanisms were suggested for the hydrogenation of dienes and aldehydes on copper aluminate spinel catalysts. Both (Bechara et al. and Yurieva et al.) agree that during reduction/activation of the spinel catalyst ($CuAl_2O_4$) cupric ions from the spinel lattice are reduced. Yurieva describes hemispherical, metallic copper particles on the catalyst surface. Protons, reaction product from copper

reduction, migrate into the spinel lattice to offset the charge. Bechara et al. were not able to observe the proton migration as they did not conduct neutron scattering experiments. They focussed on the oxidation state of copper itself. After reduction in vacuo and in hydrogen, Bechara et al. found residual Cu^+, which they claimed to be located in octahedral positions of the spinel lattice. Quantification of said Cu(I) and its correllation to catalytic activity in the hydrogenation of dienes made them propose cuprous ions as the active center. XPS on copper catalysts and its interpretation is a difficult task and sometimes leaves room for interpretation that could be misinterpreted as fact. The photoelectron spectrum and its satellite peak is a nice tool for determination of curpic ions and their local geometry. For cuprous ions and copper metal separation the Auger electron spectrum has to be consulted and most likely fitted for quantification. This is exactly where the lines between fact and interpretation become blurred. Furthermore, determination of local geometry for curpous ions based on these data might not be possible at all. If one considers the quick reoxidation of copper surfaces in only a few ppm O_2, which are most definitely present unless the experimental setup is an *in situ* apparatus, these XPS results could be entirely false. However, if reoxidation occurs, the Cu^+ integrals in the photoelectron spectrum are usually larger. Nonetheless, the determination and quantification of cuprous ions in their respective local geometry has to be questioned and with it the proof for their mechanism. Regardless, all suggested reaction mechanisms shall be contrasted and evaluated within the data obtained in this work.
The oxidic pre-catalyst consists of cupric oxide and copper aluminate spinel. The partially inverse nature of the copper aluminate spinel was confirmed with solid state MAS aluminum-NMR. During reduction treatment, we could show with *in situ* XRD and *in situ* EPR, that not only copper oxide forms metallic copper but also cupric ions from the spinel phase itself. Residual Cu^{2+} is left within the spinel phase. Upon reduction of the spinel, the spinel lattice stays intact albeit experiencing a lattice contraction. The charge must be offset by protons. No other source of positive charge is available. *In situ* IR experiments confirmed the existence of surface-accessible Cu^0 and Cu^{2+} in octahedral positions of the spinel, which is likely the Cu(II) that is leached during acidic attack of the spinel. Cuprous ions were not detected in our experiments. Distinguishing between $Cu^{0/1+/2+}$ species even via XPS is a very difficult task. Preliminary XPS results and *in situ* XAS results (not shown) confirm the presence of Cu^+ and Cu_2O respectively. The re-oxidation ($Cu^0 \longrightarrow Cu_2O$) occurs rapidly after exposure to very low quantities (ppm) of oxygen. Thus, the presence of Cu(I) does not necessarily support the mechanism proposed by Bechara et al. as we will see below [24]. Bechara et al. claim that metallic copper is not involved in the catalysis as they were able to correlate their activity to the amount of Cu(I) ions in spinel positions. Our experiments clearly establish the opposite regarding metallic copper. For identical chemical compositions, i.e. unpromoted $CuO \cdot CuAl_2O_4$ catalysts, the copper surface area is clearly an indicator how well the catalyst performs (see Figure 5.28). This is a very strong argument against the mechanism by Bechara et al. that, as it was established above, already rests on a questionable argumentation.

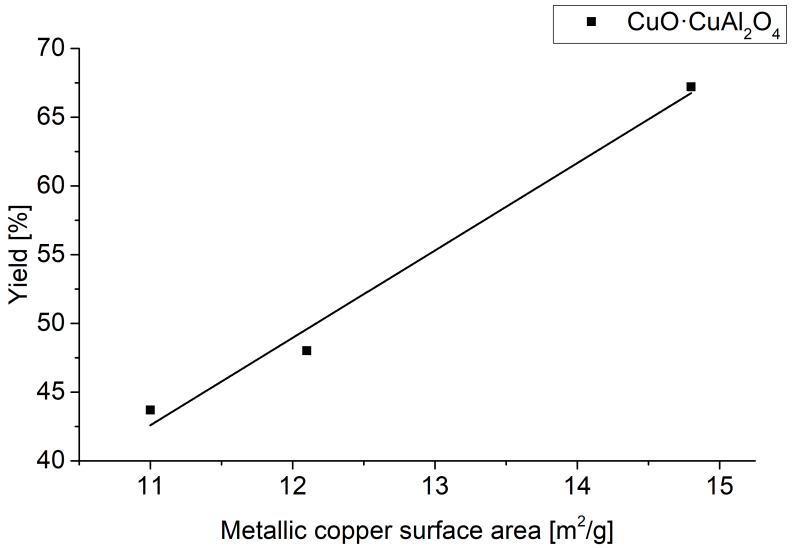

Figure 5.28: Correlation between copper metal surface area and catalytic yields for identical chemical compositions $CuO \cdot CuAl_2O_4$ [120 °C, 60 bar H_2, 750 RPM, 1 h].

However, our results also show that the activated spinel phase takes a crucial part in the catalysis. Its destruction, i.e. by sodium (comp. Chapter 3) renders the catalyst inactive. Slight modification of the spinel phase, i.e. via manganese promotion, heavily inhibits the catalysis albeit exhibiting large copper surface areas (see Section 5.2.3). Only a reaction mechanism based on an interface between copper metal and activated spinel phase can account for all of these observations, where modification of either phase affects the catalysis because its modification of course will also influence the interface. For example, for identical chemical compositions, a larger metallic copper surface area has to stem from smaller copper crystallites (because total copper is constant), which are in direct contact with the activated spinel phase. Hereby, the interface between both phases, which is ultimately responsible for the catalysis, will also be larger.
Yurieva et al. have suggested a mechanism that features an underlying interface between activated spinel and metallic copper [23], which is in good agreement to our results. However, Yurieva suggests the migration/movement of copper ions at a catalytically relevant rate (comp. Fig. 5.2). At reaction temperatures of only 120 °C this appears at least unlikely. Instead, the distinctive feature of the spinel could be understood as the stabilization of multiple oxidation states of copper in close proximity and its Brønsted acidity. Of course, the capability of metallic copper to activate hydrogen by itself cannot be neglected and can certainly be a contribution to the observed reaction rates. The autocatalytic progress of copper oxide temperature programmed reductions shows this. A third variant, where Cu^{2+} does not play an active role in the catalysis and is only residual Cu^{2+} stabilizing the activated spinel is also possible. One has to imagine a metallic copper and activated spinel interface. The metallic copper particles act as a valence band and supply of electrons similar to what Yurieva proposed. The hydrogenation then takes place with protons from the activated spinel and two electrons from the metallic

copper electron pool from its valence band. Now the particle has a partially positive charge but instead of a cupric ion migration into the spinel (as suggested by Yurieva et al.) the electrons are recharged by hydrogen from feed which become protons in the activated spinel, thereby completing the catalytic cycle. In this fashion the rather unrealistic migration/movement of cupric ions on catalytically relevant rates is removed from the equation but the interface where metallic copper connects to the activated spinel can be considered to be the active center. Of course more complex mechanisms with Cu^{2+}-Cu^0 pairs in close proximity to defect spinel (occupied by protons) positions should not be disregarded. Based on the data obtained in this work, this distinction cannot be made. Nonetheless, the necessity for the spinel and the interface was proven with many different experiments directly and indirectly over the course of this work. The inactivity of all catalysts not comprised of spinel or at least defect spinel (such as γ-Al_2O_3) structures heavily supports this model.
In summary, an interface based reaction mechanisms has to be suggested with respect to all experiments conducted in this project, where metallic copper and activated spinel form an active center/area in close proximity.

5.7 Conclusions

In this section, the strong influence of the support on metallic copper was demonstrated for the hydrogenation of butyraldehyde. Metallic copper supported on copper aluminate spinel and defect spinel structures such as γ-Al_2O_3 were identified as core structures for active catalysts.
During thermal treatment, it was shown that copper migrates into the alumina lattice and forms spinel phase at temperatures above 600 °C if sufficient copper is present. A mixed Cu-Al phase in copper deficient systems was observed. By combination of TPR and XRD, the spinel formation was shown to proceed from bulk copper oxide. High calcination temperatures result in finely dispersed CuO species on spinel, i.e. the spinel has an effect on copper oxide crystallite sizes. The partially inverse nature of copper aluminate spinel was demonstrated with ^{27}Al MAS NMR.
An activated/reduced spinel was shown to feature cupric ions and metallic copper on its surface with CO-chemisorption and *in situ* IR. The catalysis data of a wide variety of model catalysts combined with all characterization, supports the reaction mechanism to be interface based between metallic copper and activated spinel similar to what Yurieva et al. have proposed [23]. Since their migration of copper ions on catalytic rates seems unlikely due to the size of copper ions, interface based models without the necessity for this step were suggested. However, the data collected here do not allow for a more exact determination.

6 Global Conclusions and Outlook

Copper aluminates ($CuO \cdot CuAl_2O_4$) are chromium-free hydrogenation catalyst alternatives that could replace copper chromites ($CuO \cdot CuCr_2O_4$). In this work, copper aluminates were investigated regarding their synthesis conditions (e.g. precipitation parameters, sodium poisoning), effect of promoters for catalytic activity, activation and catalysis conditions, as well as stability against organic acids under reaction conditions. In the last chapter, a contribution to the controversially discussed reaction mechanism was made.
Sodium has been identified as a threat to all types of copper-aluminum catalysts that are calcined at higher temperatures, since its high affinity to the alumina phase will result in layered, delafossite-like $NaAlO_2$ instead of the desired catalyst phases (e.g. $CuAl_2O_4$). Even small amounts of sodium were found to strongly influence reduction behavior as 1 % Na^+ shifted reduction temperature of $CuO \cdot CuAl_2O_4$ to higher temperatures by 100 K. The disintegration of copper aluminate spinel into copper oxide and amorphous alumina was demonstrated for the first time.
When exposed to carboxylic acids under hydrogenation conditions (120 °C, 60 bar H_2, 750 RPM, 1 h), copper aluminates suffer from deactivation and leaching. Carboxylic acids inhibit catalysis via competitive, reversible adsorption on active sites. Cu^{2+} is leached from the spinel phase but overall copper leaching was low, never exceeding 0.2 wt-% for the catalyst as expected for reducing conditions. However, aluminum leaching is a point of concern. Up to 2.4 wt-% of total aluminum was leached, which will result in stability losses of shaped catalysts, where leaching as a surface phenomenon will attack the (oxo)bridging aluminum between primary particles. The cause of aluminum leaching is likely connected to the strain put onto the lattice due to activation of the spinel, where Cu^{2+} ions are removed from spinel positions, leading to a lattice contraction. These results warrant further research regarding the leaching mechanism and underlying equilibria. Since the solvent is hexane, standard protonation-deprotonation reactions are rather difficult to implement per se. Maybe surface hydroxyl-groups play an important part in the dissolution mechanisms, because the acids have to be de-protonated before they can offset the positive charge of cupric ions to form soluble (in hexane) complexes. On the other hand, the activated spinel acts as a solid Brønsted acid and is thus able to store protons. Two methods to improve catalyst stability were identified. The promotion with silicon stabilizes copper aluminate catalysts at the cost of activity. Co-feeding of ethanol reduces leaching, while simultaneously increasing catalyst activity. The mechanism of both could be connected to the *in situ* reduction of catalyst but is far from being understood. Future experiments should look into solubility of cupric complexes in these solvent mixtures and effects of polar components (such as EtOH) on catalyst surfaces

immersed in nonpolar solvents such as hexane.
Two types of reaction mechanisms have been suggested in the literature. The first one resolves around Cu(I) in spinel positions being the active site, whereas the second identified activated copper aluminates as Brønsted acids, that supply protons and metallic copper on the surface supplying the electrons to complete the hydrogenation. Results of this work support the second mechanism because clear correlations between metallic copper surface area and the properties of spinel to catalytic activity were shown. Many experiments, such as sodium poisoning, i.e. destruction of the spinel leading to catalyst inactivity, directly or indirectly showed the importance of the spinel phase in proximity to metallic copper. For identical chemical compositions, a clear correlation between metallic copper surface area and catalytic activity was found. Not only is the surface area of the metal increased but due to smaller copper crystallites to achieve this higher surface, the interface between spinel and copper will also be larger. A simple experiment proved that Cu^0 surface area alone does not define an active catalyst. For example, the promotion with manganese, which affects the spinel phase without affecting the surface area of metallic copper, leads to drastic decreases in catalytic activity. Many of the model catalysts investigated in this work further support the necessity for metallic copper being in contact with activated copper aluminate spinel, since the inactive model catalysts, while featuring metallic copper surface area, did not consist of spinel structures (including defect spinels such as γ-Al_2O_3). Nonetheless, many of the experiments here are not able to distinguish between copper ions in different positions on a molecular level. Bulk methods such as XRD of course show the activated spinel and metallic copper but they cannot see cupric ions on the surface for example. Distinguishing $Cu^{1+/2+}$ with CO-chemisorption coupled with *in situ* IR did not show any Cu(I) but the Cu(I)-CO band is located right in the middle of those from metallic copper and cupric-CO bands, which are the majority species and thus can overshadow Cu(I). Conclusive XPS results were not obtained in time to be included here. However, even in methods such as XPS the separation of cuprous and cupric ions is rather difficult and requires complex evaluation of its data (Photoelectron and Auger spectra). Another option to probe Cu(I) is the low temperature chemisorption with NO at 80 K used in zeolithe analysis for example. This would definitely be an important follow-up experiment. Nonetheless, the catalysis data overwhelmingly points towards an interface-type mechanism. The elucidation of the exact mechanism must be a next task. *In situ* vibrational spectroscopy could be an important tool to observe intermediates and thus solve reaction networks. Observing how and where the reactants adsorb on the activated catalyst could also be an important step in further clarifying the reaction mechanism.

Zusammenfassung und Ausblick

Kupferaluminate ($CuO \cdot CuAl_2O_4$) sind Chrom-freie Katalysatoralternativen, die Kupferchromite ($CuO \cdot CuAl_2O_4$) ersetzen könnten. Im Rahmen dieser Arbeit wurden Kupfera-

luminate bezüglich ihrer Synthesebedingungen (z.B. Fällungsparameter, Natriumvergiftung), Promotoreneffekte für katalytische Aktivität, Aktivierungs- und Katalyseparameter sowie Stabilität gegen organische Säuren untersucht. Das letzte Kapitel widmet sich der Aufklärung des Reaktionsmechanismus, welcher in der Literatur kontrovers diskutiert wird.

Es lässt sich festhalten, dass Natrium zu einem Problem für alle Arten von Kupfer-Aluminium basierten Katalysatoren wird, die bei höheren Temperaturen calciniert werden. Anstelle der Katalysatorphasen (z.B. $CuAl_2O_4$) bilden sich Delafossit-artige Schichtstrukturen ($NaAlO_2$). Sogar kleinste Mengen an Natrium wirken sich sehr stark auf das Reduktionsverhalten von Kupfer aus. 1 wt-% Natrium verschiebt die Reduktionstemperatur um 100 K zu höheren Temperaturen. Die Zersetzung von Kupferaluminatspinell in Kupferoxid und amorphes Alumina wurden zum ersten Mal gezeigt.

Organische Säuren bewirken eine Desaktivierung und das Leachen von Bestandteilen des Katalysators unter Hydrierbedingungen (120 °C, 60 bar H_2, 750 RPM, 1 h). Die Desaktivierung beruht auf der kompetitiven, reversiblen Adsorption der Säuren auf aktiven Zentren. Kupferleaching wurde aus Spinellpositionen beobachtet. Der Anteil ist mit maximal 0.2 Gew.-% bezogen auf den Kupfergehalt sehr gering. Aluminium auf der anderen Seite leacht mit bis zu 2.4 wt-% des gesamten Aluminiums. Darauf lassen sich die Stabilitätsprobleme dieses Katalysatortyps zurückführen, da z.B. in Formkörpern so die Aluminium-Sauerstoffverbrückungen zwischen Primärpartikeln aufgelöst werden und die Formkörper an Integrität verlieren. Das Aluminiumleaching lässt sich auf die Gitterkontraktion durch das Herauslösen von Kupfer(II)-Ionen bei der Aktivierung des Spinells zurückführen und die damit einhergehende Spannung des Gitters. Diese Ergebnisse sind überraschend und ebnen den Weg für weitere Untersuchungen bezüglich des Leachingmechanismus. Im Lösemittel Hexan sind simple Protonierungs-Deprotonierungs-Gleichgewichte schon nicht mehr einfach darzustellen. Die Säuren müssen jedoch deprotoniert werden, damit die Ladung von Kupfer(II)-Ionen des gelösten Komplexes im unpolaren Lösemittel Hexan ausgeglichen werden können. Möglicherweise spielen Oberflächenhydroxylgruppen hier eine entscheidende Rolle. Außerdem ist der Spinell bekannt als Brønsted-Säure und kann in diesem Rahmen Protonen aufnehmen. Zwei Methoden zur Stabilisierung der Katalysatoren wurden gefunden. Zum einen kann durch Siliziumpromotierung das Leaching auf Kosten der Aktivität reduziert werden, zum anderen kann Ethanol dem Feed beigesetzt werden und das Leaching unterdrücken bei gleichzeitiger Steigerung der Aktivität. Die positiven Eigenschaften von Ethanol könnten mit der *in situ* Reduktion des Katalysators zusammenhängen. Die genaue Wirkung ist jedoch nicht verstanden. Weitere Experimente sollten die Löslichkeit von Kupfer(II)-Komplexen in diesen Lösemittelgemischen untersuchen. Des Weiteren ist der Effekt von polaren Komponenten (EtOH) auf Katalysatoroberflächen in unpolaren Lösemitteln wie Hexan interessant.

Die Literatur schlägt zwei Arten von Reaktionsmechanismen für Hydrierungen auf dieser Art Katalysator vor. Der Erste benennt Cu(I) in Spinellumgebung als aktives Zentrum, wohingegen ein anderer Mechanismus den aktivierten Spinell als Brønstedsäure iden-

tifiziert, die Protonen und metallisches Kupfer Elektronen für die Hydrierung liefert. Die Ergebnisse dieser Arbeit unterstützen den zweiten Mechanismus, da sehr klare Zusammenhänge zwischen metallischer Kupferoberfläche und den Spinelleigenschaften zur katalytischen Aktivität aufgezeigt wurden. Ebenso bestätigen viele Experimente die entscheidende Rolle des Spinells z.B. die Vergiftung mit Natrium, die den Spinell zerstört und zu inaktiven Katalysatoren führt. Weiterhin wurde für identische chemische Zusammensetzungen ein klarer Zusammenhang zwischen metallischer Oberfläche und Aktivität gefunden, was deutlich zeigt, dass metallisches Kupfer nicht vernachlässigt werden kann. Trotzdem reicht metallische Kupferoberfläche alleine nicht, wenn der Spinell z.B. durch Promotierung mit Mangan verändert wird. Bei gleichbleibender Kupferoberfläche aber chemischer Modifikation des Spinells bricht die katalytische Aktivität ein. Viele der Modellkatalysatoren, die im Rahmen dieser Arbeit synthetisiert und getestet wurden, zeigen wie wichtig die Grenzfläche zwischen metallischem Kupfer und aktiviertem Spinell ist, da alle inaktiven Modellkatalysatoren zwar metallische Kupferoberflächen aber keine aktivierten Spinell- bzw. Defektspinellstrukturen aufwiesen. Dennoch muss an dieser Stelle auf die schwierige Unterscheidbarkeit zwischen Kupfer in verschiedenen Oxidationsstufen und Koordinationsgeometrien hingewiesen werden. Viele Methoden wie XRD bestätigen zwar die Anwesenheit von aktiviertem Spinell und metallischem Kupfer, aber sind im Prinzip gar nicht in der Lage Cu(I) auf molekularer Ebene sichtbar zu machen. *In situ* IR mit CO-Chemisorption als eine der wenigen Methoden, wo dies möglich ist, zeigt zu großen Teilen die CO-Banden für metallisches Kupfer und oktaedrisch koordiniertes Cu(II). Eine mögliche Cu(I)-CO Bande würde genau zwischen den beiden anderen Banden liegen und so von den Mehrheitsspezies überlagert werden. Hier könnte die Chemisorption bei 80 K mit NO und *in situ* IR, wie sie bei der Zeolithanalytik praktiziert wird, weiterhelfen. Auch stellt XPS eine Alternative dar zur Unterscheidung der Kupferspezies. Die Experimente sind zu diesem Zeitpunkt leider noch nicht abgeschlossen. Es muss auch darauf hingewiesen werden, dass selbst mit einer Methode wie XPS die Unterscheidung der Kupferspezies und Lokalgeometrien sehr komplex ist. Trotzdem deuten die katalytischen Untersuchungen alle auf einen Grenzflächen-basierenden Reaktionsmechanismus zwischen metallischem Kupfer und aktiviertem Spinell hin. In einem nächsten Schritt muss der Mechanismus noch genauer aufgeklärt werden. *In situ* Schwingungsspektroskopie könnte hier eine wichtige Methode zur Feststellung möglicher Intermediate sein, womit ein Reaktionsnetzwerk aufgeklärt werden könnte. In einem weiteren Schritt sollte untersucht werden, wo und wie die Reaktanten auf der Katalysatoroberfläche adsorbieren, denn diese Adsorption stellt höchstwahrscheinlich einen grundlegenden Schritt für den Reaktionsmechanismus dar.

7 Experimental

All chemical substances, unless stated otherwise, were obtained at analytical grade from Sigma-Aldrich, Merck Millipore or VWR. Gases were supplied by Westfalen and unless stated otherwise had a purity of 5.0. All substances will be stated with a complete description, sorted by methods in which they were applied (s. below).

7.1 Synthesis

7.1.1 Bulk Catalysts - Copper Aluminate (ca. 10 g)

Copper aluminate ($CuO \cdot CuAl_2O_4$) catalysts were synthesized via co-precipitation of their respective metal nitrates with soda. A metal nitrate feed solution was prepared by dissolving 36.44 g $Cu(NO_3)_2 \cdot 3\,H_2O$ and 56.58 g $Al(NO_3)_3 \cdot 9\,H_2O$ in 250 mL deionized H_2O. 2M Na_2CO_3 solution is used as base. For the co-precipitation, 500 mL deionized water are filled into the precipitation vessel and heated to the desired temperature (usually 50 °C) with a water bath. Stirring was set to 400 RPM with a (KPG) stirrer. The feed and soda solutions are pumped into the precipitation vessel with peristaltic pumps (medorex) for 20 minutes. Pump rates are set and calibrated to 5 mL/min. Pump rate of the base was manually adjusted to account for varying acidity of promoter salts when necessary. The pH was kept constant at 6.5. The precipitates were aged for 1 h at precipitation temperature. Afterwards, the precipitates were filtered and washed by redispersing in deionized water until the spent wash fluid had a conductivity $\leq$ 0.5 mS. The solids obtained in this fashion were dried at 120 °C over night and subsequently calcined at 750 °C for 2 h (2 K/min). Catalyst attributed were verified with XRD for phase compositions, N_2O-chemisorption for copper surface areas, TPR for reduction behavior and BET for catalyst surface area.

7.1.2 Bulk Catalysts - Copper Aluminate (ca. 2 g)

Small synthesis batches were in principle conducted as the large ones described above (s. Section 7.1.1). The pH was automatically controlled by a Metrohm *736 GP Titrino*. To keep precipitation times constant, feed/pump rates were reduced to 1 mL/min and only 100 mL deionized water was provided to the precipitation vessel (Erlenmayer flask with baffles). Otherwise the procedure was the same as described above.

7.1.3 Promoter Addition to Copper Aluminate Catalysts

The promoter screening for copper aluminate catalysts $CuO \cdot CuAl_2O_4$ was exclusively conducted in the smaller precipitation setup after the procedure described above. The promoters were dissolved in deionized water and added to the metal nitrate solutions. Insoluble promoter salts that needed other treatments are listed below.

Table 7.1: Promoters and treatment conditions for their dissolution

Promoter substance	Treatment
$Mg(NO_3)_2 \cdot 6\,H_2O$	Dissolve in H_2O
$Ca(OH)_2$	Dissolve in HNO_3
$Sr(NO_3)_2$	Dissolve in H_2O
$Ba(NO_3)_2$	Dissolve in H_2O
V_2O_5	Dissolve in H_2O_2
Sc_2O_3	Dissolve in HNO_3, up to 4 weeks
$Cr(NO_3)_3 \cdot 9\,H_2O$	Dissolve in H_2O
$Mn(NO_3)_2 \cdot 4\,H_2O$	Dissolve in H_2O
$Fe(NO_3)_3 \cdot 9\,H_2O$	Dissolve in H_2O
$Co(NO_3)_2 \cdot 6\,H_2O$	Dissolve in H_2O
$Ni(NO_3)_2 \cdot 6\,H_2O$	Dissolve in H_2O
$Zn(NO_3)_2 \cdot 6\,H_2O$	Dissolve in H_2O
Y_2O_5	Dissolve in HNO_3
$ZrO(NO_3)_2 \cdot xH_2O$	Dissolve in HNO_3
Nb_2O_5	see below
Mo powder	Dissolve in HNO_3
$(NH_4)_6H_2W_{12}O_{40}$	Dissolve in H_2O
$(NH_4)ReO_4$	Dissolve in H_2O
$La(NO_3)_3 \cdot 6\,H_2O$	Dissolve in H_2O
$Ce(NO_3)_3 \cdot 6\,H_2O$	Dissolve in H_2O
Pr_6O_{11}	Disperse in H_2O, dissolve in HNO_3
Nd_2O_3	Disperse in H_2O, dissolve in HNO_3
$Sm(NO_3)_3 \cdot 6\,H_2O$	Dissolve in H_2O
Gd_2O_3	Dissolve in HNO_3
Tb_4O_7	Disperse in H_2O, dissolve in HNO_3 (ultrasonic bath, 70 °C)
$Er(NO_3)_3 \cdot 9\,H_2O$	Dissolve in H_2O
Tm_2O_3	Disperse in HNO_3, ultrasonic bath for 3 days (70 °C)

Nb_2O_5

1 g Nb_2O_5 was pestled with 2 g KOH, filled into a porcelain crucible and melted with a bunsen burner. After slowly cooling to room temperature, the niobates are leached with 50 mL DI water at 50 °C. The addition of oxalic acid leads to a white precipiate

that readily dissolves to form oxalates. The Nb content can be measured by gravimetric analysis via precipitation with dilute nitric acid.

7.1.4 Synthesis of Phase Pure Copper Aluminate Spinel via Precipitation

Phase pure copper aluminate spinel $CuAl_2O_4$ was obtained via co-precipitation similar to the procedure for bulk catalyst described above (see Section 7.1.1). A feed solution would consist of 18.22 g $Cu(NO_3)_2 \cdot 3\,H_2O$ and 56.58 g $Al(NO_3)_3 \cdot 9\,H_2O$ dissolved in deionized water (to account for molar ratio Cu:Al = 1:2). The co-precipitation was conducted exactly as described above, including the washing and drying steps. Calcination procedure was modified to 800 °C and 5 K/min. This calcinced spinel will contain residual CuO, thus will not be phase pure. A leaching step to remove CuO will yield the final product. Nitric acid, hydrochlorid acid and ammonium carbonate are all tools to achieve this. A mild procedure, which does not affect the spinel/alumina phase, is the leaching with ammonium carbonate. 300 mg of the precipitated spinel with copper oxide impurities is added to a saturated $(NH_4)_2CO_3$ solution (11 mL) and put into an ultrasonic bath for two hours. Afterwards, it is stirred at 50 °C for 30 minutes, filtered and washed with 100 mL deionized water. The leached spinel has to be dried at 120 °C over night to obtain the final product, which is a phase pure spinel ($CuAl_2O_4$) according to XRD. However, copper content is less than stoichiometric (ca. 25 wt-% instead of 33 wt-%).

7.1.5 Supported Catalysts by Incipient Wetness Impregnation

Supported catalysts such as 10 wt-% Cu@$CuAl_2O_4$, $ZnAl_2O_4$, $MgAl_2O_4$, Al_2O_3, SiO_2 were synthesized via incipient wetness impregnation (IWI). In a first step, the pore volume of the support has to be determined by measuring the uptake of water. Copper amount (e.g. 10 %) is calculated based on the reduced state, i.e. not as copper oxide. A solution to account for the amount of copper needed was prepared by dissolving an appropriate amount of $Cu(NO_3)_2 \cdot 3\,H_2O$ in deionized water. The necessary amount of copper nitrate solution (depending on pore volume of the support) was added to the support with Eppendorf pipettes. The impregnated solids were agitated with a Heidolph shaker to obtain a homogeneous mixture. After drying at 120 °C over night, the impregnated samples were calcined for 4 - 12 h at 400 - 800 °C with heating rates of 5 K/min.

7.1.6 Impregnation with Citrate Modifier

The incipient wetness impregnation was conducted as described above (see Section 7.1.5). Citrate was added to the copper nitrate solution, before impregnation. 4.1 g citric acid (19.5 mmol) were added to 2.21 mL of a 75 % copper nitrate solution (9.42 mmol) ($\geq$ 2 eq.). Deionized water was added and mixture heated until citric acid was complete dissolved. The total volume was adjusted to 5.05 mL with deionized water and added to 5.4 g γ-Al_2O_3. Drying and calcination procedures were described above.

7.2 Catalysis

7.2.1 Activation Procedure

Prior to the catalytic reaction, these types of catalysts need to undergo activation/reduction in hydrogen. 350 - 700 mg of catalyst are filled into a U-shaped reactor. The exact amount going into the autoclave has to be determined by weighing the residue after filling activated catalyst into the autoclave (see below for catalyst transfer). The reactor is flushed with argon (Westfalen, 5.0) for five minutes after which the gas is switched to hydrogen (Westfalen, 5.0) (40 mL/min). Heating was commenced at a set heating rate. Upon reaching the final temperature, it was held for 1 h. Heating conditions for copper chromites were 15 K/min to 180 °C and for copper aluminates (and all other catalysts) 1 K/min to 300 °C. The oven was removed and the reactor flushed with argon to instantly stop the activation procedure.

7.2.2 Catalyst Inert-Transfer

After the reactor was cooled to room temperature and flushed with argon, the argon supply is closed and the reactor is closed. It is then transported into an argon chamber, where the bottom of the autoclave is already filled with the reactants (see below). The bottom half of the autoclave and the reactants are flushed/de-gassed with argon for at least 5 minutes before the activated catalyst is added to the reactants under Schlenk conditions. The autoclave is assembled and flushed with argon for the entirety of the transfer and several minutes after to keep oxygen out. Many experiments were conducted to verify that this Schlenk transfer is working and reproducible as the exposure of the catalyst to air drastically reduces catalytic activity, which was confirmed by deliberately exposing activated catalyst to air for varying amounts of time as a reference.

7.2.3 Liquid-Phase Hydrogenation

The liquid-phase hydrogenation of butyraldehyde was chosen as the test reaction for all catalytic experiments conducted within this thesis. It was used to benchmark promoter effects, synthesis parameters, sodium poisoning, carboxylic acid poisoning and for the determination of the reaction mechanism.
A 300 mL stainless steel autoclave by Parr has been used as a reaction vessel equipped with a glass inlet. Stirring was supplied by a propeller type impeller at 750 RPM. The liquid phase composition for the reaction was as follows: 100 mL hexane as solvent, 1.2 g n-dodecane as internal standard for gas chromatography and 8 g butyraldehyde as reactant. Before the reduced catalyst was added, the liquid phase was de-gassed with argon (Westfalen, 5.0) for 5 minutes. After closing the autoclave, it was pressurized with 60 bar hydrogen (Westfalen, 5.0) and subsequently heated to 120 °C. After reaching the desired temperature, the stirring was commenced and the reaction time started. After 1 hour, the reaction was quenched by stopping the stirring and replacing the heater with

an ice bath. When the autoclave core reached 17 °C, the pressure was released. The autoclave was opened and a liquid sample taken for product analysis with gas chromatography. If samples for ICP-OES (leached metals) had to be taken, they were taken first and rapidly filtered from spent catalyst to avoid oxidative leaching processes falsifying results.

Reproducibility

Experimental reproducibility is an important factor in sciences as the data obtained lays the foundation for the discussion and future experimental strategies. Autoclave experiments such as the test reaction of this thesis when coupled to an 'outside' activation treatment are particularly vulnerable to handling errors.
In the early stages of this work, reproducing experiments was found to be an issue as the activated catalysts were transferred without Schlenk technique and likely suffered partial re-oxidation. With the implementation of Schlenk technique, after purposely deactivating the catalysts in air confirmed this to be the problem, we were able to achieve yields in repeated experiments with only minor differences in the first decimal position after the comma.
Due to the long activation period for copper aluminate catalysts, no more than one experiments were conducted daily. Nonetheless roughly 500 catalysis experiments were conducted over the course of this work that are the foundation for this discussion. Many issues, such as varying the solvent supplier because suddenly analysis pure hexane led to Tishchenko and Aldol condensation side reactions, were fixed and repaired to achieve such a high quality in reproducibility. The large promoter screening further supports this.

7.3 Characterization

7.3.1 Gas Chromatography

Liquid-phase composition was determined by gas chromatography using a *HP6890* gas chromatograph by Hewlett Packard equipped with a HP-1 methyl siloxane capillary column (60 m length, 0.25 mm diameter, 0.25 mm film thickness) and a flame ionization detector (FID). The oven program started at 40 °C with a hold time of four minutes which was then heated to 280 °C with 30 K/min. Helium was used as a carrier gas with 1.2 mL/min and the chromatograph was set to operate at constant pressure. For component identification and quantification, n-dodecane was used as an internal standard. With calibration standards, the characteristic retention times and response factors were determined. The relationship between response factors (f_x), mass of substances (m) and gc area/integral (A) referenced to the internal standard is shown exemplary in equation 7.1.

$$f_x = \frac{A_{standard} * m_{product}}{A_{product} * m_{standard}} \tag{7.1}$$

This method easily quantifies product/reactant mass which can be transformed into yields/conversions and of course can be used to verify carbon balance.

7.3.2 ICP-OES

Optical emission spectroscopy with an inductively coupled plasma was used to determine metal contents of both solids and liquids. While analysis parameters are the same for both types of samples, sample preparation varied quite drastically to achieve for example a complete dissolution of solids or remove organics (s. below) from liquid samples. The analysis was conducted on an Agilent *700 Series* ICP-OES equipped with an autosampler. Emission wavelengths used for quantification were verified to be free of overlaps or other disturbing influences and are shown in Table 7.2.

Table 7.2: Elements and wavelength used for quantification via ICP-OES analysis.

Element	Wavelength [nm]
Cu	324.751
Al	394.401
Mn	294.921
Na	–

Solid Samples

Solid oxidic samples such as $CuAl_2O_4$ were digested with potassium disulfate by mixing 100 mg of the substance to be analyzed with 2 g $K_2S_2O_7$ and heating to red heat in a porcelain crucible. The melt was allowed to cool and added to a solution of 2 mL conc. H_2SO_4 in 100 mL DI water. The solution was heated until the solidifed melt was dissolved entirely. The crucible was removed and washed multiple times to transfer all of the metal ion containing solution into the beaker. The solution was transferred into a 1 L volumetric flask and diluted to 1 L with DI water after reaching room temperature. The same matrix was used for the calibration standard preparation (from 1000 mg/L ICP grade element standards).

Liquid Samples (Leaching)

Samples to be analyzed for leached components had to be purged from their organic matrix since the ICP was run on 3 % HNO_3. 10 mL liquid phase was filtered through a 0.22 µm syringe filter. The organic phase was removed by slowly heating to 250 °C. 4 mL H_3PO_4 were added to the residue and stirred at 80 °C for 30 minutes. The vials were then put into an ultrasonic bath for another 30 minutes. The solution was diluted to 10 mL with DI water and analyzed by ICP-OES.

7.3.3 XRD

X-ray diffractograms were measured on a *X'Pert Pro* by PANalytic with a Bragg-Brentano geometry using Cu-K_a radiation (45 kV, 40 mA). Scanning step rate was set to 0.24 °/s with a step size of 0.013 °. Particle sizes were calculated with the Scherer equation:

$$\Delta(2\theta) = \frac{K * \lambda}{L * cos\theta} \tag{7.2}$$

with $\Delta(2\theta)$ = full width at half maximum, θ = Bragg angle, K = shape factor (usually 0.89), λ = radiation wavelength (0.15418 nm) and d = particle diameter.

In situ XRD

In situ XRD was performed on an *X'Pert Pro PW 3040/60* by PANalytical with Bragg-Brentano geometry and Cu-K_a radiation (λ = 1.54 Å, 45 kV , 40 mA). The instrument was equipped with a Ni-Kβ filter and a solid state detector (*X'Celerator*). Scanning range was 5 - 70 °2θ with a step size of 0.017 °. The in-situ measurements were conducted in a *HTK 1200* sample chamber by Anton Parr on a special sample holder equipped with heating. Reduction gas (5 % H_2 in N_2) was mixed with Bronkhorst MFCs from the pure gases to obtain a flow of 10 mL/min. Heating rates were set to 2 K/min and samples were allowed to equilibrate after reaching the desired temperatures for 15 minutes.

7.3.4 Al-NMR

^{27}Al MAS NMR spectra (resonance frequency 78.276 MHz) were recorded on a Bruker *Advance* 300 MHz spectrometer. 4 mm ZrO_2 rotors were used at a spinning speed of 10 and 15 kHz with 1000 to 10000 scans with single-pulse technique with a pulse length of 3 ms and a repition time of 2 s. Spectra manipulation was done with *MestreNova*.

7.3.5 Temperature Programmed Reduction (TPR)

Temperature programmed reduction experiments were conducted on an *AutoChem 2910* by micromeritics. TPR parameters were adjusted according to Monti and Baiker [32]. By parameter variation, the proposed relationships by Monti and Baiker were verified for our system. Parameter K, according to Monti and Baiker, was targeted to be between 55 and 140 for heating rates β = 0.1 - 0.3 K/s (comp. Equation 7.3).

$$K = \frac{S_0}{c_0 \cdot \dot{V}} \tag{7.3}$$

S_0: amount of reducible species in µmol
c_0: initial hydrogen concentration in µmol/mL
$\dot{V}$: total gas flow mL/s

20 mg of the sample to be analyzed were fixed in the quartz reactor (ø= 9 mm) with

quartz wool. To account for effects such as varying storage time or air humidity, samples were pre-dried and flushed with helium prior to reduction at 120 °C (10 K/min) for 30 minutes in Helium (15 mL/min). After cooling back to room temperature, the cooling trap was equipped with a LN_2/isopropanol cooling bath before the TPR experiments were started. Heating rate was set to 10 K/min with 75 mL/min 2.5 % H_2 in Argon. TPR experiments were concluded usually at 600 °C and never exceeded 800 °C to avoid damage on the equipment. Removal of hydrogen from the reduction gas was observed with a thermal conductivity detector (TCD) detector. To quantify reducible species, the TCD-signal was calibrated with known quantities of CuO assuming complete reduction.

7.3.6 N_2O-Chemisorption

Surface area of metallic copper was determined with the N_2O pulse chemisorption method (N_2O gas purity 99.5 %, Westfalen) on an *AutoChem 2910* by micromeritics. The loop volume was calibrated with nitrogen gas as well as the pulse size for complete conversion with the aid of manual injections. Prior to chemisorption, 200 mg of the sample were fixed in the U-tube quartz reactor and subsequently flushed with Helium, followed by the activation procedure described above for the catalysts with pre-drying (120 °C, 30 minutes, 10 K/min). Flows were adjusted to 20 mL/min to account for the reduced amount of catalyst. After activation, the cool trap was supplied with liguid nitrogen. It was veryfied, that flowing nitrogen, product of copper oxidation with nitrous oxide, was not affected and only leftover N_2O was removed by the cooling trap. Via the calibrated TCD-integrals, a stoichiometric factor of two and a surface density of copper of $1.47 \cdot 10^{-19}\,\mathrm{m}^{-2}$, the copper surface can be calculated following equation 7.4 [105].

$$M_{surf} = \frac{n(\mathrm{N_2O}) \cdot N_A \cdot f_A \cdot A_{Cu}}{m} \tag{7.4}$$

M_{surf}: surface area of a metal in m^2/g
N_A: Avogadro constant in mol^{-1}
f_A: stoichiometric factor
A_{Cu}: surface space requirements for a copper atom in m^2
m: sample mass in g

7.3.7 In situ IR with CO-Chemisorption

For the infrared spectroscopic measurements, a *FTS-175* by BioRad was used. The gas cell with a tablet holder as well as heating were built and created by the group of Professor Koehler at TUM. A *2416* by Eurotherm was used as a controller for heating. Gas supplies were connected to the cell with Swagelok tubing. Helium, 1 % CO in He and hydrogen gas for the reduction of catalyst tablets were connected and steered by Bronkhorst mass flow controllers with *get red-y* software.

Catalysts were pressed into self-supporting tablets for measurement and cut into smaller pieces to fit into the heating coil, which acted as the top part/cover of the gas cell. After closing of the cell, it was put into the IR spectrometer and connected to the gas supply. The IR was then flushed with N_2 for at least 20 minutes prior to the first measurement. Activation/treatment procedures were set at 5 mL/min gas flows with heating rates of 1 K/min. After activation, the catalyst tablets were cooled to room temperature in helium before CO-adsorption was begun with varying measurement intervals. Any given times (see results chapter) always reference to when a step was begun, i.e. 5 minutes would mean 5 minutes after the CO/He mixture was supplied to the catalyst tablet or 5 minutes after a heating step was commenced.

7.3.8 BET Surface Area

Surface areas were measured by the Brunauer-Emett-Teller method in a *NOVAtouch* by Quantachrome. 200 mg (depending on surface area) were degassed (50 mbar) at 120 °C for two hours. Nitrogen adsorption was conducted and measured at 77 K with a minimum of 5 measurement points (usually 7) with relative pressures between 0.1 and 0.3.

7.3.9 Electron Paramagnetic Resonance (EPR) Spectroscopy

EPR spectra were recorded on a *JES-FA 200* spectrometer by JEOL at X-band frequency (9.25 GHz). Microwave power was set to 5 mW with a modulation amplitude of 0.4 mT, sweep time of 4 min, time constant of 0.1 s, and modulation frequency of 100 kHz. Microwave frequency was measured with a microwave frequency counter Advantest R5372.Analysis temperature was monitored with a *JEOL ES DVT4* controller equipped with a calibrated thermocouple. Low temperature measurements (113 K) were conducted with LN_2 cooling.
For in situ measurements, a capillary reactor as shown in Figure 7.1 was used. Reduction parameters were 20 mL/min H_2 with 1 K/min to 300 °C and a 1 hour isothermal part. The reactor was cooled to room temperature under Argon flow before it was inserted into the EPR spectrometer. A Mn^{2+} (nuclear spin I = 5/2) standard embedded in MgO was used to determine g and A values. Experimental errors are $\Delta g = \pm 0.003, \Delta A = \pm 10^{-4} cm^{-1}$.

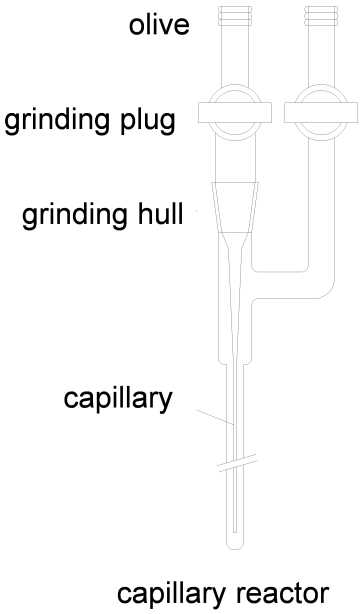

Figure 7.1: Reactor scheme for in situ EPR experiments

Bibliography

[1] D. Sanfilippo and P. N. Rylander, "Hydrogenation and dehydrogenation," *Ullmann's Encyclopedia of Industrial Chemistry*, 2009.

[2] C. Dörfelt, R. Kolvenbach, A. S. Wirth, M. Albert, and K. Köhler, "Catalytic properties of a novel raney-nickel foam in the hydrogenation of benzene," *Catalysis Letters*, vol. 146, no. 12, pp. 2425–2429, 2016.

[3] R. W. Wegman and D. R. Bryant, "Catalysts of Cu-Al-third metal for hydrogenation," Apr. 16 1991. US Patent 5,008,235.

[4] M. Villaverde, N. Bertero, T. Garetto, and A. Marchi, "Selective liquid-phase hydrogenation of furfural to furfuryl alcohol over cu-based catalysts," *Catalysis Today*, vol. 213, pp. 87–92, 2013.

[5] L. Jalowiecki, G. Wrobel, M. Daage, and J. Bonnelle, "Structure of catalytic sites on hydrogen-treated copper-containing spinel catalysts," *Journal of Catalysis*, vol. 107, no. 2, pp. 375–392, 1987.

[6] A. Bialas, P. Niebrzydowska, B. Dudek, Z. Piwowarska, L. Chmielarz, M. Michalik, M. Kozak, and P. Kuśtrowski, "Coprecipitated Co–Al and Cu–Al oxide catalysts for toluene total oxidation," *Catalysis Today*, vol. 176, no. 1, pp. 413–416, 2011.

[7] P. A. Kumar, M. P. Reddy, L. K. Ju, B. Hyun-Sook, and H. H. Phil, "Low temperature propylene scr of NO by copper alumina catalyst," *Journal of Molecular Catalysis A: Chemical*, vol. 291, no. 1, pp. 66–74, 2008.

[8] M. N. Barroso, M. F. Gomez, L. A. Arrúa, and M. C. Abello, "Reactivity of aluminum spinels in the ethanol steam reforming reaction," *Catalysis Letters*, vol. 109, no. 1-2, pp. 13–19, 2006.

[9] H. Adkins and R. Connor, "The catalytic hydrogenation of organic compounds over copper chromite," *Journal of the American Chemical Society*, vol. 53, no. 3, pp. 1091–1095, 1931.

[10] H. Adkins, E. E. Burgoyne, and H. J. Schneider, "The copper—chromium oxide catalyst for hydrogenation," *Journal of the American Chemical Society*, vol. 72, no. 6, pp. 2626–2629, 1950.

[11] J. Jenck and J.-E. Germain, "High-pressure competitive hydrogenation of aldehydes, ketones, and olefins on copper chromite catalyst," *Journal of Catalysis*, vol. 65, no. 1, pp. 141–149, 1980.

[12] S. V. Koritala, E. Selke, and H. Dutton, "Deuteration of methyl linoleate with nickel, palladium, platinum and copper-chromite catalysts," *Journal of the American Oil Chemists Society*, vol. 50, no. 8, pp. 310–316, 1973.

[13] D. Liu, D. Zemlyanov, T. Wu, R. J. Lobo-Lapidus, J. A. Dumesic, J. T. Miller, and C. L. Marshall, "Deactivation mechanistic studies of copper chromite catalyst for selective hydrogenation of 2-furfuraldehyde," *Journal of Catalysis*, vol. 299, pp. 336–345, 2013.

[14] R. Hubaut, M. Daage, and J. Bonnelle, "Selective hydrogenation on copper chromite catalysts IV. hydrogenation selectivity for α, β-unsaturated aldehydes and ketones," *Applied Catalysis*, vol. 22, no. 2, pp. 231–241, 1986.

[15] P. Gallezot and D. Richard, "Selective hydrogenation of α, β-unsaturated aldehydes," *Catalysis Reviews*, vol. 40, no. 1-2, pp. 81–126, 1998.

[16] G. Bacchini, "Market overview and new applications for oleochemicals in asia," presentation, OFI Hyderabad, Desmet Ballestra, 2016.

[17] K. Noweck and W. Grafahrend, "Fatty alcohols," *Ullmann's Encyclopedia of Industrial Chemistry*, 2006.

[18] G. Kale, "Thermal decomposition of $CuCrO_4 \cdot 2\,CuO \cdot 2\,H_2O$ and phase relations in the Cu-Cr-O system," *Journal of materials science*, vol. 30, no. 6, pp. 1420–1424, 1995.

[19] J. Chen, "Preparation and use of non-chrome catalysts for Cu/Cr catalyst applications," Sept. 24 2002. US Patent 6,455,464.

[20] L. Patron, V. Pocol, O. Carp, E. Modrogan, and M. Brezeanu, "New synthetic route in obtaining copper chromite i. hydrolysis of some soluble salts," *Materials research bulletin*, vol. 36, no. 7, pp. 1269–1276, 2001.

[21] M.-F. Luo, P. Fang, M. He, and Y.-L. Xie, "In situ xrd, raman, and tpr studies of CuO/Al_2O_3 catalysts for CO oxidation," *Journal of Molecular Catalysis A: Chemical*, vol. 239, no. 1, pp. 243–248, 2005.

[22] K. Turner, M. Sharif, J. Scarlett, A. B. Carter, and G. Webb, "Process for producing a hydrogenation catalyst of copper chromite," July 9 1991. US Patent 5,030,609.

[23] T. Yurieva, L. Plyasova, O. V. Makarova, and T. Krieger, "Mechanisms for hydrogenation of acetone to isopropanol and of carbon oxides to methanol over copper-containing oxide catalysts," *Journal of Molecular Catalysis A: Chemical*, vol. 113, no. 3, pp. 455–468, 1996.

[24] R. Bechara, G. Wrobel, M. Daage, and J. Bonnelle, "Selective hydrogenation of dienes on copper chromite catalysts ii. structure-activity relationships and catalytic sites," *Applied catalysis*, vol. 16, no. 1, pp. 15–27, 1985.

[25] R. Bechara, A. Aboukaïs, and J.-P. Bonnelle, "X-ray photoelectron spectroscopic study of a Cu–Al–O catalyst under H_2 or CO atmospheres," *Journal of the Chemical Society, Faraday Transactions*, vol. 89, no. 8, pp. 1257–1262, 1993.

[26] B. S. Gudkov, V. I. Yakerson, A. N. Subbotin, and V. M. Kogan, "Dissociative adsorption of hydrogen on copper and the mechanism of butyric aldehyde hydrogenation," *Mendeleev Communications*, vol. 4, no. 4, pp. 143–144, 1994.

[27] R. Rao, A. Dandekar, R. Baker, and M. Vannice, "Properties of copper chromite catalysts in hydrogenation reactions," *Journal of Catalysis*, vol. 171, no. 2, pp. 406–419, 1997.

[28] R. Pillai, "A study of the preactivation of a copper chromite catalyst," *Catalysis letters*, vol. 26, no. 3-4, pp. 365–371, 1994.

[29] R. Alsfasser, C. Janiak, T. M. Klapötke, and H.-J. Meyer, *Moderne Anorganische Chemie, 3. Auflage*. Berlin: De Gruyter, 2007.

[30] N. Wiberg, E. Wiberg, and A. F. Holleman, *Lehrbuch der Anorganischen Chemie, 102. Auflage*. Berlin: De Gruyter, 2007.

[31] M. Schneider, K. Kochloefl, and G. Maletz, "Chromium-free catalyst for the hydrogenation of organic compounds," Apr. 4 1995. US Patent 5,403,962.

[32] D. A. Monti and A. Baiker, "Temperature-programmed reduction. parametric sensitivity and estimation of kinetic parameters," *Journal of catalysis*, vol. 83, no. 2, pp. 323–335, 1983.

[33] L. Plyasova, T. Yur'eva, I. Y. Molina, T. Kriger, A. Balagurov, L. Davydova, V. Zaikovskii, G. Kustova, V. Malakhov, and L. Dovlitova, "Dynamics of structural transformations in the reduction of copper aluminate," *Kinetics and catalysis*, vol. 41, no. 3, pp. 429–436, 2000.

[34] L. Plyasova, L. Solovyeva, T. Krieger, O. Makarova, and T. Yurieva, "The nature of hydrogen stabilization in the reduced copper chromites," *Journal of Molecular Catalysis A: Chemical*, vol. 105, no. 1-2, pp. 61–66, 1996.

[35] K. P. de Jong, *Synthesis of solid catalysts*. John Wiley & Sons, 2009.

[36] T. Mimani, "Instant synthesis of nanoscale spinel aluminates," *Journal of alloys and compounds*, vol. 315, no. 1, pp. 123–128, 2001.

[37] M. A. Willard, Y. Nakamura, D. E. Laughlin, and M. E. McHenry, "Magnetic properties of ordered and disordered spinel-phase ferrimagnets," *Journal of the American Ceramic Society*, vol. 82, no. 12, pp. 3342–3346, 1999.

[38] J. J. Vijaya, L. J. Kennedy, G. Sekaran, M. Bayhan, and M. A. William, "Preparation and voc gas sensing properties of Sr(II)-added copper aluminate spinel composites," *Sensors and Actuators B: Chemical*, vol. 134, no. 2, pp. 604–612, 2008.

[39] D. W. Susnitzky and C. B. Carter, "The formation of copper aluminate by solid-state reaction," *Journal of materials research*, vol. 6, no. 9, pp. 1958–1963, 1991.

[40] E. Pierron, J. Rashkin, and J. Roth, "Copper oxide on alumina: I. xrd studies of catalyst composition during air oxidation of carbon monoxide," *Journal of Catalysis*, vol. 9, no. 1, pp. 38–44, 1967.

[41] B. Chen, U. Dingerdissen, J. Krauter, H. L. Rotgerink, K. Möbus, D. Ostgard, P. Panster, T. Riermeier, S. Seebald, T. Tacke, *et al.*, "New developments in hydrogenation catalysis particularly in synthesis of fine and intermediate chemicals," *Applied Catalysis A: General*, vol. 280, no. 1, pp. 17–46, 2005.

[42] I. Simentsova, A. Khasin, and T. Yurieva, "Character of hydrogen interaction with copper chromite," *Reaction Kinetics and Catalysis Letters*, vol. 58, no. 1, pp. 49–56, 1996.

[43] A. Khasin, T. Yur'eva, L. Plyasova, G. Kustova, H. Jobic, A. Ivanov, Y. A. Chesalov, V. Zaikovskii, A. Khasin, L. Davydova, *et al.*, "Mechanistic features of reduction of copper chromite and state of absorbed hydrogen in the structure of reduced copper chromite," *Russian Journal of General Chemistry*, vol. 78, no. 11, pp. 2203–2213, 2008.

[44] M. Selim and N. Youssef, "Thermal stability of CuO-Al_2O_3 system doped with sodium," *Thermochimica acta*, vol. 118, pp. 57–63, 1987.

[45] E. Ligner, F. Meunier, A. Travert, S. Maury, and N. Cadran, "Dramatic promotion of copper–alumina catalysts by sodium for acetone trimerisation," *Catalysis Science & Technology*, vol. 4, no. 8, pp. 2480–2483, 2014.

[46] S. Koritala, "Selective hydrogenation of soybean oil: Vii. poisons and inhibitors for copper catalysts," *Journal of the American Oil Chemists Society*, vol. 52, no. 7, pp. 240–243, 1975.

[47] S. A. Kondrat, P. J. Smith, J. H. Carter, J. S. Hayward, G. J. Pudge, G. Shaw, M. S. Spencer, J. K. Bartley, S. H. Taylor, and G. J. Hutchings, "The effect of sodium species on methanol synthesis and water–gas shift Cu/ZnO catalysts: utilising high purity zincian georgeite," *Faraday Discussions*, vol. 197, pp. 287–307, 2017.

[48] Y. Du, C. Wang, Q. Lv, L. Deng, and D. Che, "Influence of sodium on deactivation and regeneration of scr catalyst during utilization of zhundong coals," *Asia-Pacific Journal of Chemical Engineering*, vol. 11, no. 6, pp. 973–980, 2016.

[49] F. Figueras, A. Nohl, L. De Mourgues, and Y. Trambouze, "Dehydration of methanol and tert-butyl alcohol on silica-alumina," *Transactions of the Faraday Society*, vol. 67, pp. 1155–1163, 1971.

[50] A. G. Deem and J. E. Kaveckis, "Catalytic poisoning in liquid-phase hydrogenation," *Industrial & Engineering Chemistry*, vol. 33, no. 11, pp. 1373–1376, 1941.

[51] E. Kruissink, H. Pelt, J. Ross, and L. Van Reüen, "The effect of sodium on the methanation activity of nickel/alumina coprecipitated catalysts," *Applied Catalysis*, vol. 1, no. 1-2, pp. 23–29, 1981.

[52] M. Maciejewski, "Somewhere between fiction and reality: the usefulness of kinetic data of solid-state reactions," *Journal of Thermal Analysis and Calorimetry*, vol. 38, no. 1-2, pp. 51–70, 1992.

[53] J. A. Rodriguez, J. Y. Kim, J. C. Hanson, M. Pérez, and A. I. Frenkel, "Reduction of CuO in H_2: in situ time-resolved xrd studies," *Catalysis Letters*, vol. 85, no. 3, pp. 247–254, 2003.

[54] S. Kato, R. Fujimaki, M. Ogasawara, T. Wakabayashi, Y. Nakahara, and S. Nakata, "Oxygen storage capacity of $CuMO_2$ (m= Al, Fe, Mn, Ga) with a delafossite-type structure," *Applied Catalysis B: Environmental*, vol. 89, no. 1, pp. 183–188, 2009.

[55] A. Santos, P. Yustos, A. Quintanilla, G. Ruiz, and F. Garcia-Ochoa, "Study of the copper leaching in the wet oxidation of phenol with CuO-based catalysts: causes and effects," *Applied Catalysis B: Environmental*, vol. 61, no. 3, pp. 323–333, 2005.

[56] A. Santos, P. Yustos, A. Quintanilla, and F. Garcia-Ochoa, "Influence of pH on the wet oxidation of phenol with copper catalyst," *Topics in catalysis*, vol. 33, no. 1, pp. 181–192, 2005.

[57] C. Miro, A. Alejandre, A. Fortuny, C. Bengoa, J. Font, and A. Fabregat, "Aqueous phase catalytic oxidation of phenol in a trickle bed reactor: effect of the pH," *Water Research*, vol. 33, no. 4, pp. 1005–1013, 1999.

[58] H. Kanzaki, T. Kitamura, R. Hamada, S. Nishiyama, and S. Tsuruya, "Activities for phenol formation using Cu catalysts supported on Al_2O_3 in the liquid-phase oxidation of benzene in aqueous solvent with high acetic acid concentration," *Journal of Molecular Catalysis A: Chemical*, vol. 208, no. 1, pp. 203–211, 2004.

[59] P. M. Álvarez, D. McLurgh, and P. Plucinski, "Copper oxide mounted on activated carbon as catalyst for wet air oxidation of aqueous phenol. 1. kinetic and mechanistic approaches," *Industrial & engineering chemistry research*, vol. 41, no. 9, pp. 2147–2152, 2002.

[60] P. M. Álvarez, D. McLurgh, and P. Plucinski, "Copper oxide mounted on activated carbon as catalyst for wet air oxidation of aqueous phenol. 2. catalyst stability," *Industrial & engineering chemistry research*, vol. 41, no. 9, pp. 2153–2158, 2002.

[61] A. Alejandre, F. Medina, P. Salagre, A. Fabregat, and J. Sueiras, "Characterization and activity of copper and nickel catalysts for the oxidation of phenol aqueous solutions," *Applied Catalysis B: Environmental*, vol. 18, no. 3, pp. 307–315, 1998.

[62] Q. Wu, X. Hu, P. L. Yue, X. S. Zhao, and G. Q. Lu, "Copper/MCM-41 as catalyst for the wet oxidation of phenol," *Applied Catalysis B: Environmental*, vol. 32, no. 3, pp. 151–156, 2001.

[63] A. Sadana and J. R. Katzer, "Catalytic oxidation of phenol in aqueous solution over copper oxide," *Industrial & Engineering Chemistry Fundamentals*, vol. 13, no. 2, pp. 127–134, 1974.

[64] D. Mantzavinos, R. Hellenbrand, A. G. Livingston, and I. S. Metcalfe, "Catalytic wet oxidation of p-coumaric acid: partial oxidation intermediates, reaction pathways and catalyst leaching," *Applied Catalysis B: Environmental*, vol. 7, no. 3, pp. 379–396, 1996.

[65] A. Alejandre, F. Medina, A. Fortuny, P. Salagre, and J. Sueiras, "Characterisation of copper catalysts and activity for the oxidation of phenol aqueous solutions," *Applied Catalysis B: Environmental*, vol. 16, no. 1, pp. 53–67, 1998.

[66] A. Alejandre, F. Medina, X. Rodriguez, P. Salagre, Y. Cesteros, and J. Sueiras, "Cu/Ni/Al layered double hydroxides as precursors of catalysts for the wet air oxidation of phenol aqueous solutions," *Applied Catalysis B: Environmental*, vol. 30, no. 1, pp. 195–207, 2001.

[67] A. Fortuny, C. Miró, J. Font, and A. Fabregat, "Three-phase reactors for environmental remediation: catalytic wet oxidation of phenol using active carbon," *Catalysis today*, vol. 48, no. 1, pp. 323–328, 1999.

[68] S. Hočevar, U. O. Krašovec, B. Orel, A. S. Aricó, and H. Kim, "Cwo of phenol on two differently prepared CuO–CeO_2 catalysts," *Applied Catalysis B: Environmental*, vol. 28, no. 2, pp. 113–125, 2000.

[69] K. George and S. Sugunan, "Nickel substituted copper chromite spinels: Preparation, characterization and catalytic activity in the oxidation reaction of ethylbenzene," *Catalysis Communications*, vol. 9, no. 13, pp. 2149–2153, 2008.

[70] E. Vasiliadou and A. Lemonidou, "Investigating the performance and deactivation behaviour of silica-supported copper catalysts in glycerol hydrogenolysis," *Applied Catalysis A: General*, vol. 396, no. 1, pp. 177–185, 2011.

[71] J. Kuusisto, J.-P. Mikkola, P. P. Casal, H. Karhu, J. Väyrynen, and T. Salmi, "Kinetics of the catalytic hydrogenation of d-fructose over a CuO-ZnO catalyst," *Chemical Engineering Journal*, vol. 115, no. 1, pp. 93–102, 2005.

[72] M. N. Santiago, M. Sanchez-Castillo, R. Cortright, and J. Dumesic, "Catalytic reduction of acetic acid, methyl acetate, and ethyl acetate over silica-supported copper," *Journal of Catalysis*, vol. 193, no. 1, pp. 16–28, 2000.

[73] J. Ladebeck and T. Regula, "Fatty methyl ester hydrogenation: Application of chromium free catalysts," *Studies in Surface Science and Catalysis*, vol. 121, pp. 215–220, 1999.

[74] M.-J. Mouche, J.-L. Mermet, M. Romand, and M. Charbonnier, "Metal-organic chemical vapor deposition of copper using hydrated copper formate as a new precursor," *Thin Solid Films*, vol. 262, no. 1-2, pp. 1–6, 1995.

[75] M. Daage and J. Bonnelle, "Selective hydrogenation of dienes on copper-chromite catalysts iii reaction mechanism and nature of the occluded hydrogen species," *Applied catalysis*, vol. 16, no. 3, pp. 355–374, 1985.

[76] R. Hubaut and J. Bonnelle, "Comparative selectivities of two copper-based catalysts: Mixed Cu-Cr and Cu-Al oxides for allylic alcohol reactions in the presence of molecular hydrogen," *Reaction Kinetics and Catalysis Letters*, vol. 47, no. 1, pp. 73–81, 1992.

[77] T. Krieger, L. Plyasova, L. Solovyeva, T. Yur'eva, and O. Makarova, "The structure of copper chromite activated by hydrogen," in *Materials Science Forum*, vol. 228, pp. 627–632, Trans Tech Publ, 1996.

[78] A. Khasin, I. Simentsova, and T. Yur'eva, "Moderate-temperature reduction of copper chromite by hydrogen and hydrogen desorption from the surface of reduced chromite," *Kinetics and catalysis*, vol. 41, no. 2, pp. 282–286, 2000.

[79] T. Yurieva, "Mechanisms for activation of hydrogen and hydrogenation of acetone to isopropanol and of carbon oxides to methanol over copper-containing oxide catalysts," *Catalysis Today*, vol. 51, no. 3, pp. 457–467, 1999.

[80] J. Y. Kim, J. A. Rodriguez, J. C. Hanson, A. I. Frenkel, and P. L. Lee, "Reduction of CuO and Cu_2O with H_2: H embedding and kinetic effects in the formation of suboxides," *Journal of the American Chemical Society*, vol. 125, no. 35, pp. 10684–10692, 2003.

[81] R. N. Pease and H. S. Taylor, "The reduction of copper oxide by hydrogen.," *Journal of the American Chemical Society*, vol. 43, no. 10, pp. 2179–2188, 1921.

[82] T. Fleisch and G. Mains, "Reduction of copper oxides by UV radiation and atomic hydrogen studied by XPS," *Applications of Surface Science*, vol. 10, no. 1, pp. 51–62, 1982.

[83] S. Poulston, P. Parlett, P. Stone, and M. Bowker, "Surface oxidation and reduction of CuO and Cu_2O studied using XPS and XAES," *Surface and Interface Analysis*, vol. 24, no. 12, pp. 811–820, 1996.

[84] M. Fernández-Garcıa, I. Rodrıguez-Ramos, P. Ferreira-Aparicio, and A. Guerrero-Ruiz, "Tracking down the reduction behavior of copper-on-alumina catalysts," *Journal of Catalysis*, vol. 178, no. 1, pp. 253–263, 1998.

[85] G. Apai, J. Monnier, and M. Hanrahan, "Evidence for the stabilization of copper(i) in Cu-Cr oxide methanol catalysts," *Applications of Surface Science*, vol. 19, no. 1-4, pp. 307–314, 1984.

[86] A. Khasin, I. Simentsova, and T. Yurieva, "Interaction of hydrogen with copper chromite surface," *Reaction Kinetics and Catalysis Letters*, vol. 52, no. 1, pp. 113–118, 1994.

[87] G. Fierro, M. L. Jacono, M. Inversi, P. Porta, F. Cioci, and R. Lavecchia, "Study of the reducibility of copper in CuO-ZnO catalysts by temperature-programmed reduction," *Applied Catalysis A: General*, vol. 137, no. 2, pp. 327–348, 1996.

[88] C.-Y. Hu, K. Shih, and J. O. Leckie, "Formation of copper aluminate spinel and cuprous aluminate delafossite to thermally stabilize simulated copper-laden sludge," *Journal of Hazardous Materials*, vol. 181, no. 1, pp. 399–404, 2010.

[89] L. Samain, A. Jaworski, M. Edén, D. M. Ladd, D.-K. Seo, F. J. Garcia-Garcia, and U. Häussermann, "Structural analysis of highly porous y-Al_2O_3," *Journal of solid state chemistry*, vol. 217, pp. 1–8, 2014.

[90] R. M. Friedman, J. J. Freeman, and F. W. Lytle, "Characterization of $CuAl_2O_3$ catalysts," *Journal of Catalysis*, vol. 55, no. 1, pp. 10–28, 1978.

[91] I. Mindru, D. Gingasu, L. Patron, G. Marinescu, J. M. Calderon-Moreno, S. Preda, O. Oprea, and S. Nita, "Copper aluminate spinel by soft chemical routes," *Ceramics International*, vol. 42, no. 1, pp. 154–164, 2016.

[92] M. C. Marion, E. Garbowski, and M. Primet, "Catalytic properties of copper oxide supported on zinc aluminate in methane combustion," *Journal of the Chemical Society, Faraday Transactions*, vol. 87, no. 11, pp. 1795–1800, 1991.

[93] P. Artizzu, E. Garbowski, M. Primet, Y. Brulle, and J. Saint-Just, "Catalytic combustion of methane on aluminate-supported copper oxide," *Catalysis today*, vol. 47, no. 1, pp. 83–93, 1999.

[94] M. Schoenmaker-Stolk, J. Verwijs, and J. Scholten, "The catalytic hydrogenation of benzene over supported metal catalysts.: Ii. gas-phase hydrogenation of benzene over copper-on-silica," *Applied catalysis*, vol. 29, no. 1, pp. 91–105, 1987.

[95] J. Pritchard, T. Catterick, and R. Gupta, "Infrared spectroscopy of chemisorbed carbon monoxide on copper," *Surface Science*, vol. 53, no. 1, pp. 1–20, 1975.

[96] F. Boccuzzi, G. Ghiotti, and A. Chiorino, "Metal-semiconductor interaction: Effect of H_2 chemisorption on the IR transparency of the Cu/ZnO system," *Surface science*, vol. 183, no. 1-2, pp. L285–L289, 1987.

[97] B. Hayden and C. Lamont, "Coupled translational-vibrational activation in dissociative hydrogen adsorption on Cu(110)," *Physical review letters*, vol. 63, no. 17, p. 1823, 1989.

[98] V. Šepelák, I. Bergmann, S. Indris, A. Feldhoff, H. Hahn, K. D. Becker, C. P. Grey, and P. Heitjans, "High-resolution 27Al MAS NMR spectroscopic studies of the response of spinel aluminates to mechanical action," *Journal of Materials Chemistry*, vol. 21, no. 23, pp. 8332–8337, 2011.

[99] M. I. Macedo, C. C. Osawa, and C. A. Bertran, "Sol-gel synthesis of transparent alumina gel and pure gamma alumina by urea hydrolysis of aluminum nitrate," *Journal of sol-gel science and technology*, vol. 30, no. 3, pp. 135–140, 2004.

[100] N. Van der Laag, M. Snel, P. Magusin, and G. De With, "Structural, elastic, thermophysical and dielectric properties of zinc aluminate ($ZnAl_2O_4$)," *Journal of the European Ceramic Society*, vol. 24, no. 8, pp. 2417–2424, 2004.

[101] R. Hierl, H. Knözinger, and H.-P. Urbach, "Surface properties and reduction behavior of calcined $CuOAl_2O_3$ and CuO-$NiOAl_2O_3$ catalysts," *Journal of Catalysis*, vol. 69, no. 2, pp. 475–486, 1981.

[102] U. D. of Commerce, "Nist chemistry webbook," 2009.

[103] J. W. London and A. T. Bell, "Infrared spectra of carbon monoxide, carbon dioxide, nitric oxide, nitrogen dioxide, nitrous oxide, and nitrogen adsorbed on copper oxide," *Journal of Catalysis*, vol. 31, no. 1, pp. 32–40, 1973.

[104] P. W. Park and J. S. Ledford, "The influence of surface structure on the catalytic activity of alumina supported copper oxide catalysts. oxidation of carbon monoxide and methane," *Applied Catalysis B: Environmental*, vol. 15, no. 3, pp. 221–231, 1998.

[105] G. Parris and K. Klier, "The specific copper surface areas in CuZnO methanol synthesis catalysts by oxygen and carbon monoxide chemisorption: Evidence for irreversible CO chemisorption induced by the interaction of the catalyst components," *Journal of Catalysis*, vol. 97, no. 2, pp. 374–384, 1986.